Aleksi Turunen

Investigation of Direct Drive Hydraulics Implemented in Mining Loader

Abstract

The conventional mining loader is a diesel-hydraulic off-road mobile machine that is expected to routinely operate in enclosed areas. Such machines could benefit from more efficient hydraulic solutions. One avenue of improvement lies in electrification, which in itself is advantageous to underground mining machinery that would otherwise require expensive ventilation of their ICE exhaust. The high controllability of brushless DC motors allows direct pump control instead of conventional valve control, eliminating throttling losses. This work investigates the efficiency of such a direct-driven valveless hydraulic system for the front end of a mining loader and compares it to a conventional load-sensing system that was previously installed in the same machine. Economic viability of the described system is analyzed based on a real life working cycle, and the control software implemented as part of the work is described.

The efficiency of the direct-driven system was determined to be superior in all tested cases, increasing from 21% to 53% at high velocity and from 2% to 22% at low velocity and maintaining a very flat efficiency curve over most loads and velocities. The direct drive hydraulic system is capable of energy regeneration, recouping a portion of energy used for lifting thus allowing longer runtimes with a given battery capacity. These advantages were found to be enough to offset the higher up-front cost except for equipment with lower than usual lifespans.

Tiivistelmä

Kaivoslastarit ovat usein dieselhydraulisia työkoneita, jotka monesti toimivat maanalaisissa kaivoksissa. Sähkökäyttöiset toimilaitteet ovat yksi mahdollinen tapa parantaa näiden koneiden energiatehokkuutta, eteenkin suljetuissa tiloissa joissa polttomoottorin pakokaasujen tuulettamisesta aiheutuu huomattavia kustannuksia. Sähkömoottoreiden hyvä hallittavuus mahdollistaa venttiilittömän pumppuohjatun hydraulijärjestelmän, joka ei kärsi venttiilihäviöistä. Tämä työ vertailee pumppuohjattuja suoravetohydraulisia kaivoslastarin toimilaitteita saman lastarin alkuperäisiin kuormantuntevalla säädöllä toteutettuihin, keskittyen hyötysuhteeseen sekä suorituskykyyn. Näin muokatun lastarin taloudellista kilpailukykyä tarkastellaan oikean kaivostyösyklin avulla. Työn osana on myös rakennettu kaivoslastarin toimilaitteinen sähköinen hallintajärkestelmä, jonka rakenne ja toiminta esitetään.

Pumppuohjatun hydraulisen järjestelmän hyötysuhteen havaittiin olevan nostotyössä parempi kaikissa tilanteissa hyötysuhteen noustessa nopeilla liikkeillä 21 prosentista 53:een, ja hitailla liikkeillä 2 prosentista 22:een. Pumppuohjattu hydrauliikka kykenee myös potentiaalienergian talteenottoon, mahdollistaen pidemmän käyntiajat samalla akkukapasiteetilla. Nämä edut ovat taloudellisesti riittäviä kompensoimaan laitteiston korkeamman hinnan lyhytikäistä kalustoa lukuunottamatta.

Acknowledgements

I was recruited to the EL-Zon project by Tatiana Minav after helping with the brake system assembly of a certain hybrid mining loader as part of my summer job. This work is the result.

I would like to thank Antti Sinkkonen, Henri Hänninen, Panu Sainio, professor Matti Pietola and the rest of the talented people of Aalto who have provided invaluable help and an inspiring working environment. I would like to give special thanks to my instructor Tatiana Minav, whose can-do attitude, dedication and ability to pull a team together are unrivaled, as well as my co-worker and friend Tom Sourander, who was always there with me squashing the most baffling issues the prototype mining loader threw at us. Finally, I would like to thank Riikka Soitinaho, whose humor and compassion belie a keen eye and a sharp mind ever ready to help.

Espoo 26.11.2018

Aleksi Turunen

Table of contents

Notation

C_{hyb}	[€]	Capital costs of the hybrid mining loader
C_{conv}	[€]	Capital costs of the conventional option
E_{tot}	[J]	Total cycle energy
F_{cyl}	[N]	Combined force acting on lifting cylinders
P_{in}	[W]	Power input to system (engine)
P_{out}	[W]	Power output (lifting)
R_{conv}	[€/month]	Monthly running costs of the conventional loader
R_{hyb}	[€/month]	Monthly running costs of the hybrid loader
t_{ROI}	[month]	Time to return of investment (payback time) in months
η	[ ]	Efficiency

Abbreviations

BLDC	Brushless direct current (motor)
BMS	Battery management system
CAN	Controller area network
DDH	Direct drive hydraulics
ICE	Internal combustion engine
LHD	Load-haul-dump
PID	Proportional-integral-derivative (controller)
PMSM	Permanent magnet synchronous motor
Pp	Percentage point
ROI	Return of investment
UI	User interface

1 Introduction

Hydraulics are widely used in mobile working machines for their power and utility. Historically, the efficiency of such systems has not always been a priority in their design, with power, working ability and cost being the more pressing concerns. A trend towards increased efficiency in these systems is driving not only innovation of improved hydraulics but also novel solutions for replacing current hydraulic systems. Whether driven by economic, environmental or regulatory pressures, it is clear that there exists considerable demand for solutions that improve upon classic hydraulic systems used in working machines.

In Europe, the first legal measures against emissions of road vehicles were taken in 1970 [1], with the ongoing and increasingly stringent European emissions standards putting hard limits on emissions of new vehicles sold [2]. Similar legislation in other large markets such as China [3] and the US [4] ensue strong interest in emission reductions. Unlike road automobiles, where economic and the aforementioned legal considerations combined with the more limited resources of private owners have long since created a demand for higher efficiencies, off road working machines have traditionally exhibited poor energy efficiency [5].

A method for improving the efficiency of working machines is to apply hybridization, which can combine the different capabilities and strengths of several systems. Working machines employing some form of hybrid technology and/or energy recovery have only recently appeared in the marketplace with offerings from Hitachi[6], Cat[7], Sandvik[8] and Volvo[9] among others, using various technologies ranging from energy recovery based on capacitors and hydraulic accumulators to plug-in electrohydraulics. For example, Hitachi's ZH200-5B excavator uses a capacitor bank charged by swing movement deceleration to assist that movement or general hydraulic power, whereas Cat's 336E H excavator uses a hydraulic accumulator for similar tasks. Sandvik uses a different approach for their DD422iE mining jumbo, with a wholly electric power system but with hydraulic actuators. These systems either use energy regeneration and power assist to allow more efficient ICE operation or eliminate the ICE completely.

In the Tubridi mining loader prototype, diesel-electric hybridization has been proposed to gain advantages of engine downsizing, battery assist and kinetic energy regeneration, much in the same way as modern hybrid passenger vehicles. An electric direct drive hydraulic (DDH) system has been designed and built to power the working implements of the loader. Electric DDH can present an opportunity to realize the benefits of full electric hybridization when more comprehensive energy regeneration and higher efficiency for runtime on batteries is desired, such as in the presented mining loader case.

Using conventional hydraulics in a working machine with a hybrid drivetrain would be wasteful, as battery energy limitations place added emphasis on efficiency. Furthermore, without methods of energy regeneration some of the benefits associated with hybridization are lost. A system suitable for powering working implements while maintaining high efficiency and complementing the hybrid vehicle is needed.

While there has recently been much development in the field of electric working machines, they have mostly been confined to either partial hybridization with limited energy storage and recovery capacities or fully electric vehicles. While these solutions might be adequate for special cases such as excavators and mining jumbos which do not move long distances during their work, machines which do could benefit greatly from full hybridization and energy recovery from all their movements.

The DDH system combines shock- and overload tolerance and compact size of hydraulics with the flexibility and high efficiency of electric drives, being readily suitable to hybrid platforms already equipped with high capacity batteries. Equipping a hybrid working machine with DDH implements could thus be cost efficient as well as increase battery runtime due to better efficiency and energy regeneration. In the presented mining loader case, this would have the additional benefit of completing all or part of the underground working cycle on batteries, reducing the need to ventilate ICE exhaust which is a significant cost in mining operations [10]. The work of a conventional mining loader consists of digging and dumping actions separated by travel between the dumping ground and mine itself. This cycle, consisting of periodic and predictable actions which are partly performed in a poorly ventilated area, lends itself well to the capabilities of hybrid vehicles.

The goal of this this thesis is to assess the feasibility of the DDH system in terms of its efficiency in a synthetic working cycle. To accomplish this goal, the thesis will compare the efficiency of the DDH system with that of the conventional load sensing setup at different velocities and loads, spanning the practical range allowed by the machine specifications. Thermal considerations are not expressly investigated, due to the difficulty of doing so with an immobile full size 14-tonne experimental setup. From these results conclusions are drawn on the suitability of the DDH system for use in off-road working machines in comparison to more traditional load sensing hydraulics. The DDH system is investigated on its own merits, as well as suitability for use in the case of an underground mining loader. Due to their importance in adopting emerging technologies, economic considerations of equipping working machines with the DDH system are also investigated, especially in concert with electric hybridization are investigated since there are notable synergistic benefits to be realized with such an approach.

Feasibility of the DDH system is investigated by determining its ability to do work and the efficiency at which this work is performed. Efficiency is determined with synthetic working cycles, during which the system input and output power is recorded. These cycles are repeated with different weights and velocities to characterize the operating envelope of the DDH units. There are two different cycles, one focuses on comparing the DDH system with the conventional load sensing system, and the other on the DDH system performance with a wider range of parameters. These cycles are discussed further in more detail.

The economic consideration focus on determining the time to return of investment for a hypothetical hybrid mining loader equipped with a DDH powered frontend, and indicating which factors affect it the most. This way, the DDH system is evaluated based on its financial attractiveness.

Since a plug-in hybrid vehicle does by its nature require far more sophisticated electronic and software controls than the original donor vehicle did, such a system is also created and described in this work. The purpose of this control program is to bring together and operate all the sensors, actuators and controllers required for the scope of this work in a safe and operator-friendly manner and allow for the information gathering needed to draw conclusions about the system's capabilities. The resulting software greatly eases logging of all sensor data, troubleshooting any hardware problems and operating the loader itself, while implementing many safety features making the vehicle more fail-safe than fail-deadly in the event of hardware or software failure.

The rest of this thesis is divided into 10 chapters. Chapter 2 reviews the current state of the art, including the methods currently used to improve the efficiency of mobile working machines. Chapter 3 describes the physical test system, with special attention given to the custom manufactured components and their characteristics. This chapter also provides an overview of the most critical components. Chapter 4 details the software control system designed during this work, its purpose, capabilities, limitations and methods of operation. Chapter 5 describes the methods and procedures for measuring, as well as presents the cycle used to simulate normal working conditions. Chapter 6 presents the measurement results. In chapter 7 measurement data is used to determine the performance and efficiency of the proposed system. The chapter also includes comments on the data itself and any anomalies. Complementing the empirical research, the next chapter is about the economic considerations of using the proposed setup with two cases. The first investigates possible generalized economic advantages of using DDH, while the second focuses on those of DDH implemented in a hypothetical mining loader working in a closed mine. Chapter 8 discusses the results. Chapter 9 discusses the main findings and potential advantages of the proposed system, including possible improvements and applications for DDH technology, comparisons to other approaches as well as possible future developments. In addition, it includes a short future outlook section where the possibilities of DDH technology is discussed. Chapter 10 provides a conclusion to the research goals of this paper

During this thesis two conference publications were published:

1. A.Turunen, T.Minav, H.Häninen, M.Pietola, (2018), Experimental investigation of direct drive hydraulic units implemented in a mining loader, GFPS, Samara, Russia, July 2018
2. T. Martinovski, T. Sourander, A. Turunen, T. Minav, M. Pietola, (2018), Control strategy for a direct driven hydraulics system in the case of a mining loader in *IFK*, March 2018, Aachen, Germany.

2 State of the art

This chapter examines the current zeitgeist in increasing the energy efficiency of mobile working machines as well as current and near future alternatives for diesel vehicles with that goal, focusing mainly on LHD's and mining trucks.

Currently there exist two major drives to use other options: economic and legislative. For the economic side, any energy efficient system has the potential to save money through lower energy costs, be they diesel, electric or other. Any technology reducing ICE usage also offers the chance to reduce ventilation costs in addition to the obvious fuel cost savings. These savings can be significant as they cut into what can amount to 40% of the total energy cost of the mine [10] and 60% of the total power consumption [11], [12]. Continuously tightening environmental regulations provide a legal incentive to look at other options then ICE. In the European Union, Stage V regulations for non-road mobile machinery come into effect in 2019-2020. Similar regulations exist abroad with the EPA's Tier IV for the USA, and in China by the China VI standard [13], [14], [3]. These regulations make ICE alternatives more attractive due to the increased cost, complexity and maintenance requirements of compliant engines.

There are also novel, yet unrealized specialized cases such as seabed mining which preclude the use of ICE's. Depending on when and if these materialize, the vehicles used can either drive or benefit from progress made in more conventional mining [15].

A great majority of underground mining vehicles are diesel powered due to the versatility and high autonomy of ICE vehicles [16]. Hydraulics are ubiquitous for powering working implements such as booms, buckets and the arms of a mining jumbo. Their compactness and ability to handle shock loads commonplace in mining make them indispensable. Any significant alternatives could not be found, with the exception of electrical actuators for lighter duty [9]. This is a big part of the DDH value proposition, combining the good practical qualities of hydraulics with the efficiency and controllability of modern electric drives.

Fortunately for those developing alternatives, electric traction technology in mining loaders and trucks is well developed, with both loaders and trucks, especially the larger ones, already using a diesel-electric transmission [17]. There are currently four main types of technologies available for mobile working machines in addition to pure ICE power [18]

- Tethered electric (umbilical cable)
- Battery electric
- Trolley line
- Hybrid electric

Each of these has varying levels of adoption, interest and potential. Paraszczak also mentions fuel cell powered vehicles as an option. Since the characteristics of the technology currently make it more suitable as a component of a hybrid system, and as no major developments relying solely on them was found, this category is ignored [19].

2.1 Tethered electric

Tethered electric vehicles are powered by a trailing cable, allowing unrestricted operating times at the cost of low autonomy and high infrastructure requirements, and are the most common type of non-ICE LHD in use today [18]. According to Jacobs et al, electric

LSH's can reach operating costs 30% lower than their ICE counterparts in underground mines [20]. Due to the longer distances driven by trucks, they are not feasible applications for this technology.

Examples of tethered mining loaders include the Sandvik LH514E and LH625E as well as the Atlas Copco Scooptram EST1030 and EST3.5. The tethered LHD's are common enough to be the default when discussing "electric" LHDs.

2.2 Battery electric

Battery electric vehicles are those that rely completely on their onboard battery storage. Although not traditionally used in mining, there has been interest and research in them for quite some time [21]. These vehicles have higher practical autonomy than tethered vehicles but are still limited by the battery capacity. Furthermore, since their operating time is likewise limited, they often cannot complete a normal 8-12 - hour shift requiring a larger fleet per work done [18]. It must be noted that this 2014 source discounted lithium-ion batteries with their higher energy densities as not yet applicable to vehicles even as they are currently mass produced for commercial road vehicles [22]. In addition, Artisan Vehicles has launched the Z40 battery electric haul truck in 2018, which they promise can complete a full shift on a single charge in "good conditions" as well as using a battery swap system to facilitate longer continuous operation. [23]. While as of now quite unproven, the Z40 is a part of the broader trend of increasing electric vehicle autonomy, and battery electric haulage trucks will most likely find their niche in the near future. Due to the superior energy density of lithium batteries, they are currently the most viable choice for battery electric vehicles requiring good autonomy. This does lead to some concerns about the supply of raw material for widespread adoption as well as the environmental concerns of battery waste. The current state of art in lithium battery recycling allows for a high portion of materials to be reused, including nearly 100% of the lithium and more than 90% of cobalt by weight [24], with the toxic and expensive cobalt being particularly noteworthy. Mass use of lead-acid batteries has resulted in an efficient recycling system for them, and such an industry is growing around nickel-based batteries as large amounts of them reach their end of life. Since resource supply does not seem to be an overt constrain during this century [25], it would be very prudent and advantageous for such a system to be developed for lithium batteries [26].

Examples of battery electric mining loaders include the RDH-Scharf Muckmaster 600EB and 300EB [27], Artisan Vehicles A10 and A3 [28], [29] and the Atlas Copco ST7 Battery. [30] Battery electric haul truck include the early the very recent 2018 Artisan Z40 [23] and the RHD-Scharf Haulmaster 800 [31]. Although not an underground vehicle, the Volvo HX2 with autonomous capability deserves a mention [32].

2.3 Trolley line

Trolley line powered vehicles enjoy similar advantages as those equipped with umbilical cables. In addition, they can cover much greater distances due to not being constrained by the cable reel, at the cost of even higher infrastructure requirements in the form of the trolley line itself. This lends itself much better to mining trucks than to LHD's: the trucks longer driving distance within the mine is achievable, they use the same stretches of trolley-equipped path and do not need to operate long beyond it, unlike LHD's. This technology has found successful applications as early as 1985 in the form of Kiruna

trucks' electric offerings [33], [16]. Although Paraszczak's sources are unverifiable, he claims that experience with these trucks at the Coleman, Creighton and Stillwater mines in Canada and the US have been positive. As reported, electric trolley trucks have significantly higher performance, with electric 50-ton units managing 16 km/h on a 14% grade compared to only 9 km/h of equivalent diesel ones. The faster cycle times result in a smaller fleet for a given volume moved. Some of the referenced fleets include newer Kiruna (now Atlas Copco) designed around 2007 [34]. Trolley line mining vehicles are not limited underground, with Hitachi providing a trolley option for its 386-ton EH-5000 dump truck [35].

Examples include the early DC-powered Kiruna K-1050E and K-635E [36] and the newer AC-powered Atlas Copco (formerly Kiruna/ABB) K-1050ED (now EMT-50) and K-635ED (now EMT-35) [37]. The Hitachi EH-5000 and others of the same product range showcase this technology on a larger scale [35].

2.4 Hybrid

The hybrid drivetrain offers energy saving opportunities mainly through allowing the engine to be sized to run efficiently at average power and "shave the peaks" with some other source of power, as well as kinetic energy recovery. Swing energy recuperation for excavators is currently the most common hybrid use case, which already yields positive economic results [38]. Several commercial excavators are already offering swing energy recovery through hybrid technology using capacitors or hydraulic accumulators [6], [7]. Hybrid technology for traction applications also shows promise of economic viability [39], [40]. Such hybrid drivetrains for traction applications have been researched and developed and even marketed for mining applications [41], [42], but any accounts of such vehicles in use or referenced in real-world operations could not be found.

According to Paraszczak et al, the only completed example of a hybrid mining truck or LDH as of 2014 is a Canadian prototype LHD based on a LT-270 base model. This is a small series hybrid narrow mining LHD under development since 2005, which proved to have good performance characteristics yet below expected energy savings. [43], [18]. However, several other examples do exist: The EJC-90 based diesel-electric hybrid LHD equipped with zonal hydraulics that this work concerns also falls into this category with its intended diesel-electric hybrid drivetrain. Commercial examples are somewhat rare, including the Komatsu Joy-18 and Joy-22 hybrid LHD's [42]. as well as the MES ALHA5140. The former is notably not a battery hybrid, instead using a "kinetic energy storage system" in conjunction with its diesel-electric drivetrain. This is a flywheel/motor system suitable for peak power shaving only. A detailed description of the latter's drivetrain could not be found, but the specifications seem to indicate a diesel-electric battery hybrid with a 700V battery of unknown capacity for storage. [44]. Outside of mining there exist machines such as the Logset 12H hybrid forestry harvester [45] and the Komatsu HB205-1 and Caterpillar 336E H, which use capacitors and hydraulic accumulators respectively to store energy from the swing motion [46], [7].

There is clearly a recent and continuing surge in new unconventional mining vehicle designs. Due to increased stringency of emissions standards and progress of technology, the trend will most likely remain so for the foreseeable future. While the greatest energy savings potential is found in the drivetrain, there is significant room for improvement in the working hydraulics. DDH as discussed in this work are one method of bringing them up to the standard of emerging drivetrain technologies.

3   Hardware description

This section aims to fully describe the hybridized EL-Zon mining loader to the extent as it appears in this work.

A detailed description of the direct drive hydraulic machinery is provided, as well as all major supporting components, such as the sensors and power supplies used. Implementation of the developed CAN-network, its wiring, setup and testing were carried out during this thesis work, and so they are described in detail.

When this work was started, most of the preliminary design work such as component selection and toolchain preparation was already completed by Aalto University in collaboration with Hybria. In addition, the donor vehicle's conversion to a hybrid was planned out and started, involving various driveline and steering components, their batteries and electronics. Work on these systems was carried out in parallel to the direct driven hydraulics by other personnel, and for this reason will be described only cursorily.

3.1 Setup Overview

This is an overview of the systems installed on the mining loader that are relevant for this work.

At the heart of this work are the mining loaders direct drive hydraulics. It consists of two self-contained pump/motor/tank units, each serving a single movement of the bucket/boom assembly. While there are some component sizing differences between the units driving lift and dump cylinders, they are fundamentally similar in construction and purpose. Figure 1 illustrates the physical appearance of the units. The motor is shown in orange, driving submerged pumps in the tank (dark gray) through a belt reduction drive.
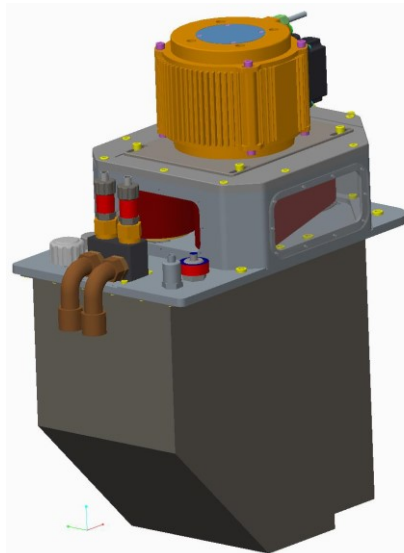

Figure 1 CAD model of a single DDH unit

In a direct drive hydraulic system, the movement of pistons is controlled directly through pump output, without any valves. This arrangement has the possibility to reach exceptional efficiencies, as common sources of loss such as pressure drop in control valves do not exist. This also means that to produce cylinder movement in two directions, the pump/motors must be able to run in reverse and handle the different flow rates required by the piston- and rod sides of the cylinders. These design considerations are

elaborated upon in their own section. Figure 2 illustrates the structure of a single DDH unit, and the most important components used therein.
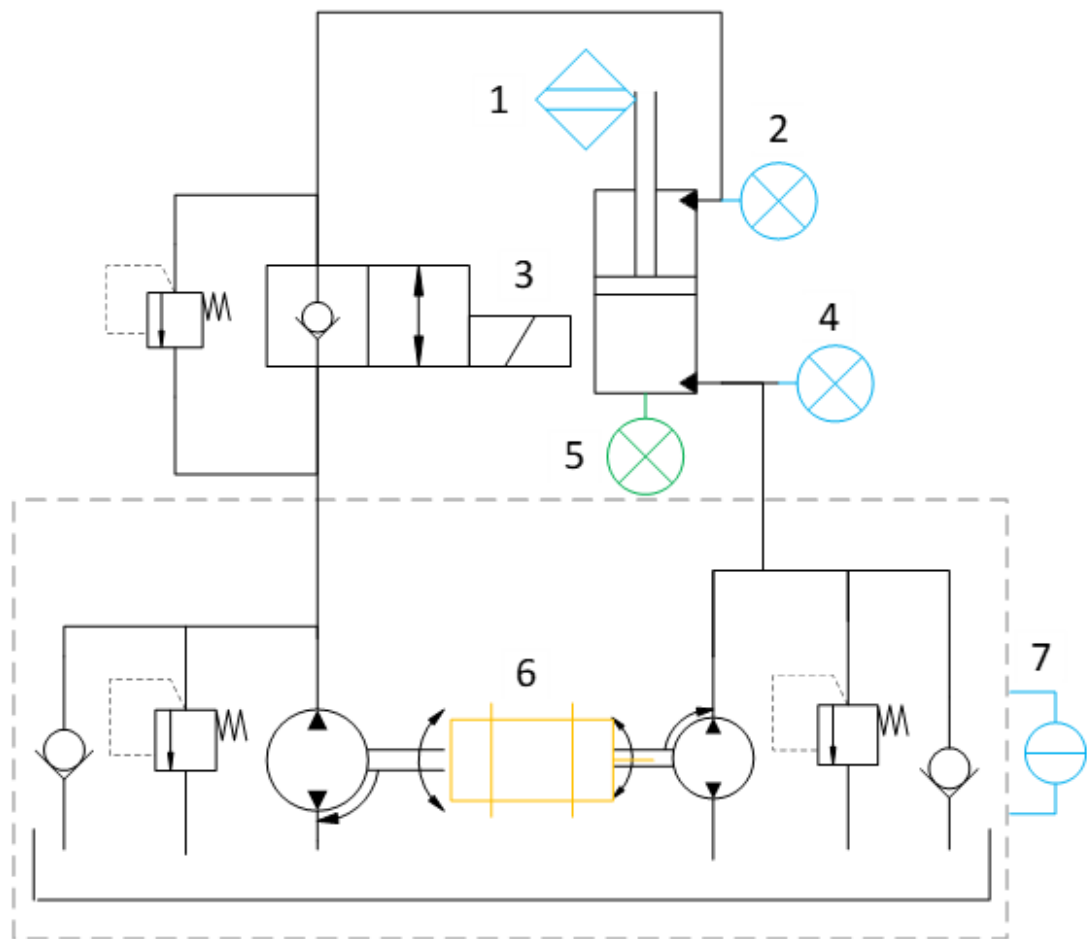
#	Part	Description
1	LM0-CA00B-1212-2C00-PAM	Distance sensor
2	Parker SCPT-CAN	Pressure sensor, lift side on boom
3	TKE CDVD-10	Valve driver (CANbus)
4	Parker SCPT-CAN	Pressure sensor. Lift side on bucket
5	BCM Sensor Model 5718/5798	Load pin
6	SEVCON Gen4 size 6	Motor controller*
7	Hydac HNT 1000	Fluid level measurement

* Measures motor RPM, current torque and temperature

Figure 2 Simplified schematic of the direct drive hydraulic system

All of the pumps in a single DDH (Direct drive hydraulic) unit are powered by a single electric brushless DC motor by means of a toothed belt. The water-cooled motor is mounted on top of the DDH unit, and includes both a temperature- and angle sensor, which are both needed by and connected to the motor controller.

For each of these two motors there is a SEVCON Gen4 controller. They are CAN-connected devices with everything required for the smooth control of the DDH motors. In this application they are configured to receive rpm control instructions through the CAN bus, and control the motor with their inbuilt PI governor. Position control is

implemented with a PID controller running on the DSpace MicroAutoBox unit. Both controllers also communicate their own and the motor's status, so information such as current consumption and power can be recorded.

Parking brakes are an important safety feature on a large machine such as this. They are by default engaged and must be disengaged with hydraulic pressure. This is provided by a small DC motor-pump combo installed between the front wheels under the boom. No special control circuit is needed for the brake system, which is operated by means of a relay and a CAN-controlled proportional valve under control of the main program.

The boom and bucket movement mechanics have load pins on the cylinder attachment points for measuring cylinder forces during operation. These are analog devices, each requiring an amplifier whose output is read by a CAN-connected input/output board. This board is also responsible for actuating the brake pump relay, since it's coil current is far too large to drive directly.

Additional safety hardware includes check valves on the DDH lift lines, which can be opened for normal operation. These valves, found on both the boom and bucket, make sure the load will not drop during power loss or other unwanted situations. They, like every other valve on the loader, are CAN controlled.
User input is provided by a pair of joysticks, again connected to the CAN Bus, and a touchscreen on which the user interface runs.

For additional data gathering the mining loader includes a suite of sensors. There are pressure sensors for the piston- and rod side of both DDH unit outputs and for the parking brakes. DDH units also include fluid level- and temperature monitors. Rotary wire encoders are installed for the boom and bucket movements to accurately determine their position. As with everything else, these sensors are connected to the CAN bus.

There are four discrete CAN buses on the mining loader in order to accommodate devices of different data rates and protocols. Every input device and sensor is connected through these buses except the analog load pins. The buses are handled by a MicroAutoBoxII unit, which is an automotive prototyping system. It hosts all the control logic, user interface, and it also serves as a datalogger. The overall architecture of the mining loader can be thought of as a "star" topology network, with the MicroAutoBoxII at the center.

4 Software

The control software is implemented as a Matlab model, which is compiled to C code that runs realtime on the MicroAutoBoxII controller, with a user interface built in dSPACE control desk version 5.6.

This work included implementing four core areas of the control software: CAN interface definitions for the used devices, the device initialization, configuration and error handling logic, boom and bucket control loop with included automatic cycle support, as well as data gathering using the MicroAutoBoxII build-in flash. This enables the following functionality:

- Initializing all devices on power up
- Enter functional mode, either automatically or after user confirmation
- Run the loader front end, either with operator input or automated cycle
- Alert the user to problems and correct common ones
- Stop system and close safety valves in case of major error

In a separate work, the software was extended to include a facility for sensorless positioning of the boom and bucket. The extension provides an estimate of boom and bucket position based on motor controller feedback and a simulation model of the physical machine. This approach is discussed in [47].

The program can be described as a set of nested state machines, with the highest levels being a normal operating mode and two error levels for critical and non-critical errors. Through monitoring return data from sensors and actuators, the program logic can sense problems in hardware and act accordingly, either resolving the problem or entering the appropriate error mode. At all times, system status is shown to the user on the graphical user interface. As a state machine, the program is best explained through the high level states.

4.1 Graphical user interface

The purpose of this mining loader is twofold. It is intended to be not only a research platform for the new DDH technologies and large scale mobile hydraulics, but also a driveable demonstration. Since the operator might not be familiar with the inner workings of this research device, the mining loader is controlled through a graphical user interface displayed in figure 3.

During normal operation, the program is able to initialize and handle every device on the mining loader automatically, and the user interface plays the same role as a dashboard on a normal car. Remaining battery charge, current consumption and any relevant status indicators are shown. While the interface does hold much more detail, it is there for research and debugging purposes, every necessary action for driving the mining loader is automated.

At all times the current status of the mining loader is displayed in the top bar of the user interface. This bar includes the overall status of subsystems such as parking brakes or DDH drive status, and a breakdown of the most important parts of that system. While these are usually the individual components, such is not always the case. For example,

for brevity, the current status of the DDH drive's battery is represented with a single indicator. In these cases, more detailed data is available elsewhere on the user interface, or either simply overlaid on that indicator.
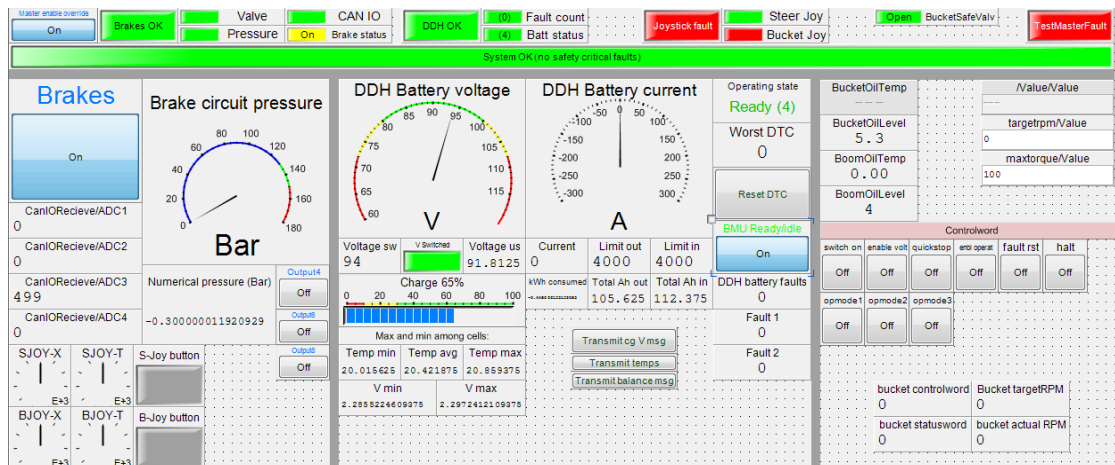

Figure 3 Control dashboard in ControlDesk, the front end of the control system

4.1.1 Usage instructions

The user interface is created in Dspace's "ControlDesk", and a computer running version 5.6 or higher of his program is required to access it. This computer must be connected to the MicroAutoBoxII through an Ethernet cable. Since ControlDesk will attempt to upload the selected program, the user interface must be selected beforehand. After opening the "jarrutesti1" project in ControlDesk, and applying power to the MicroAutoBoxII, pressing "Go online" will access the UI.

If the screen spanning "System OK" indicator is green, everything is in order and the loader can be safely operated. Releasing parking brakes is the only action requiring user input, everything else is controlled through the bucket/boom and steering joysticks, whose actions are displayed on the joystick housing. Current brake status is shown on the status ribbon by the "Brake status" indicator, which is yellow when brakes are engaged, green when disengaged and red in case of a problem. The brakes are toggled by a large on-screen push button labeled "Brakes"

If the "System OK" indicator is red, there is at least one problem significant enough to warrant checking. In nearly every case, more detailed information can be found on the status ribbon, detailing the problematic system and its status. Some common errors include:

- **DDH battery controller (96v) error state.** Anything other than the ready state "4" causes loss of power for the DDH hydraulics. This is a common problem due to there being a noticeable voltage difference in the controller's overall battery terminal voltage measurement and the sum of the individual cell's reading, which causes the device to enter an error state. If clearing the error with the "Reset DTC" button does not work, power cycle the device.
- **Non-critical sensor error.** This error does not prevent operation, but should be checked if data needs to be gathered. These sensors are electrically mounted in a long and branching chain, causing intermittent communication errors. The sensor encountering errors is shown on the status ribbon, and it's cabling should be checked. In case of serious errors locking up the whole CAN bus no device can function, and all devices on the bus will be shown as encountering errors. In this

case the bus in question can be recovered with the "Recover CAN x" button. (This is pretty much resolved with better wiring, if no longer a problem, remove this section)

- **Sevcon motor controller not in a proper state.** These controllers require a specific startup sequence to be given to a "controlword" parameter to achieve operational status. Current status of the controlword is shown on the UI (statusword), and should include the following bits: quickstop disable, enable voltage, switch on and enable operation. If this is not the case, the controller cannot work. Make sure that the devices have no outstanding errors indicated by a blinking green light on the controllers. Also check that they have entered "operational" CAN mode by sending this command with the "Force operational" button. Additional information can be found through the SEVCON DVT program, which requires its own CAN dongle in order to communicate directly with the controllers.

It is good practice to keep track that the control joysticks are operating correctly. For this reason, their current readings are provided in the bottom left part of the UI. While there have been no problems with them, a malfunction of a certain type might not be detected by the mining loaders software if some values are still sent through the CANBus. In this case there is a great risk of uncontrolled and possibly dangerous operation. A large, red safety switch is provided in the cockpit for any such unforeseen situations, which when pressed will issue both a software shutdown command and lock the parking brakes. In non-critical cases the software shutdown command can be issued from the user interface with the "software safety switch" button. Both will cut power to the DDH hydraulics, lock their safety valves, apply brakes and ignore all other user input. This is the same functionality as in the critical error state.

4.2 Normal Operation

During normal operation, the control program interprets user control and acts accordingly. The logic is illustrated in figure 4. No user input is directly sent to actuators, both for safety and practical reasons. Since every device has its own formats and scaling for data, it is advantageous for any control system to operate on abstract data which is then translated for the devices as necessary. The program continuously monitors that the sensors and actuators are both available, sending data and having the correct settings. If this is not the case, an error mode is entered depending on whether the device in question is classified as critical or non-critical. Critical devices include such as parking brake valve relays, charge controllers and position sensors, while non-critical devices are represented mainly by data-gathering pressure temperature and fluid level sensors. The input of these devices is either not required in anything safety critical or does not require immediate action.
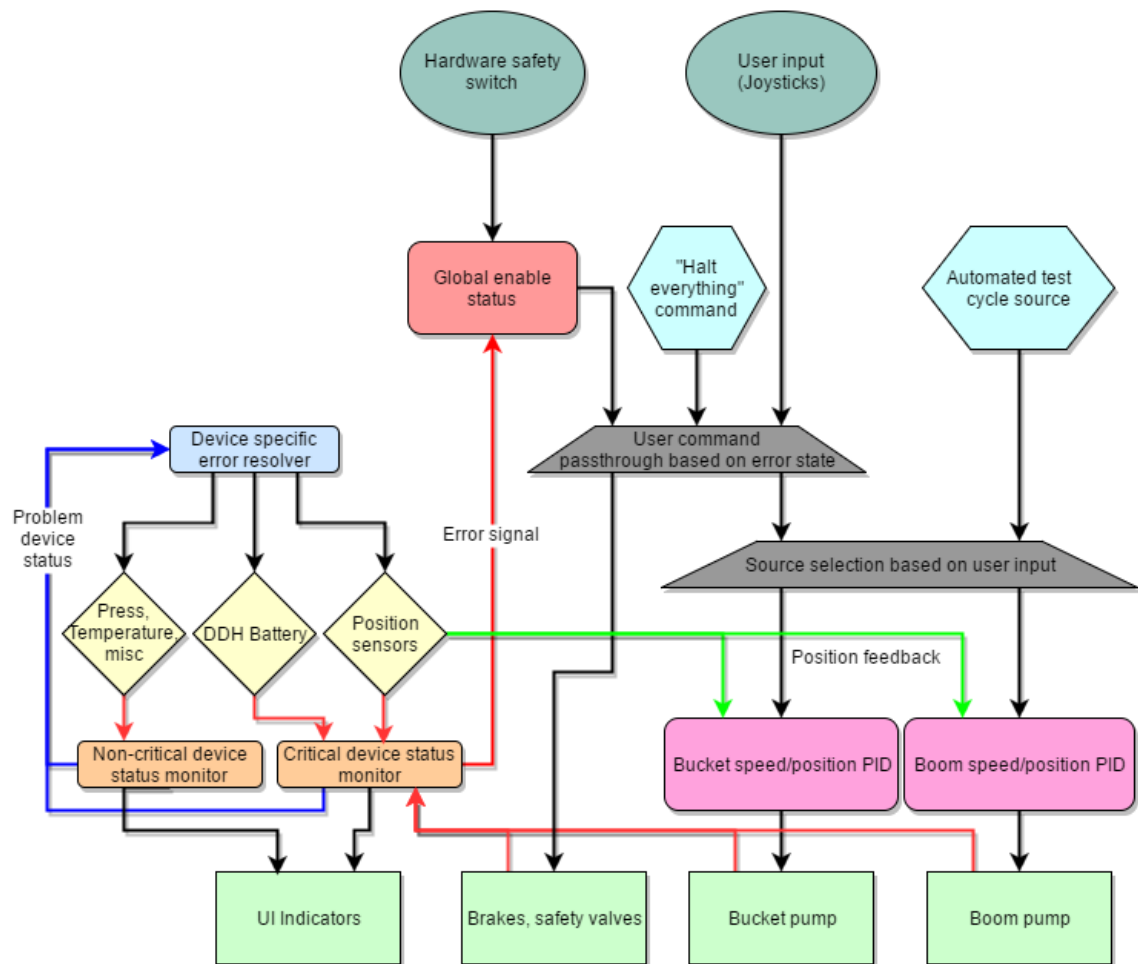
Figure 4 Block diagram of control system fault monitoring logic

4.3 Non-critical error mode

Non-critical errors are those that do not pose immediate risk to either the loader or any personnel. They might still require corrective action or degrade the performance of the mining loader. Examples include faulty oil temperature sensors and incorrect information transmission rates which lead to reduced performance. In applicable cases a simple error resolver is engaged, which attempts to correct the error automatically, bringing the system out of this error mode and back to normal. In those cases where the resolver cannot help, the type of error is displayed in the user interface.

4.4 Critical error mode

A critical error is serious enough to warrant immediate action, locking down the whole machine in order to prevent or minimize any damage. This mode is triggered when any of the safety-critical devices is either not working or missing. Examples include the brake valve relay, without which brake control cannot be assured, DDH motor controllers that are critical in controlling the boom/bucket assembly and the safety locking valves for boom and bucket. In addition, all user input devices such as the steering and boom/bucket joystick count as critical devices. This mode is cleared when the problematic critical device is communicating correctly, or a special override is issued. This override is meant for testing the system when devices are either not connected or experiencing problems and should be used sparingly.

4.5 Error handling

It is possible for common problems to be recovered automatically, especially if such problems are expected due to some permanent feature of the system which cannot be altered. These cases include sensor data rate mismatch, non-initialized state, and a tripped BMS safety check. An example of a data rate mismatch is the data rate setting on pressure sensors, the value of which cannot be saved on the sensor itself. For this reason, every time the sensor is power cycled, it will revert to sending data at every 500 milliseconds, which is too slow for many measurements and especially for the brake system. This condition is automatically detected and corrected. The same logic applies in case the device is not sending any messages. In CANopen devices this condition occurs as a routine part of startup, the devices entering a pre-operational state and requiring explicit initialization. If the sensor cannot be brought out of operational mode, the error will be escalated to critical depending on the sensor concerned. A special case concerns the BMS, which occasionally mistakenly enters a protection mode due to a miscalibrated sensor. This state is automatically detected and cleared. Figure 5 illustrates the logic of the error resolver.
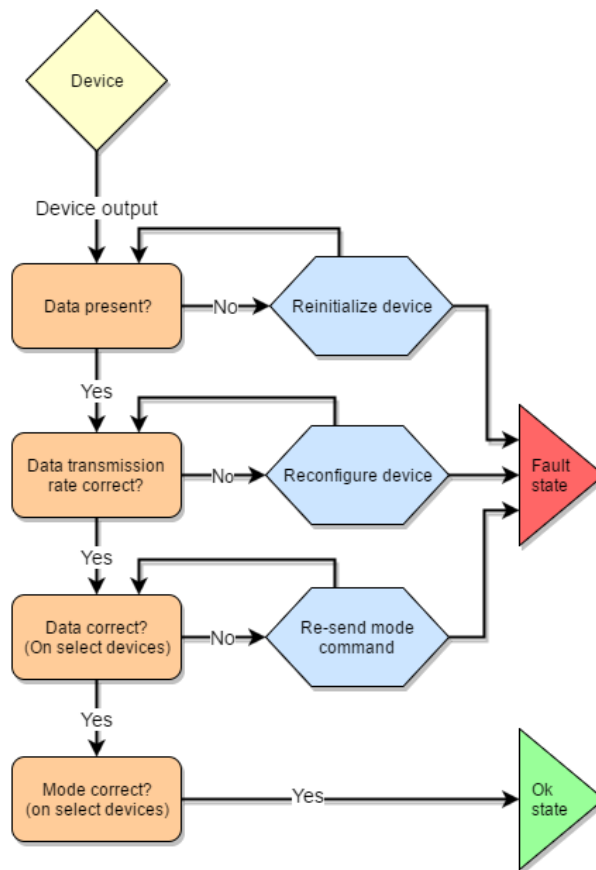
Figure 5 Device troubleshooting and status reporting logic

5 Measurement

In order to have consistent results, the mining loader is driven with repeatable, automatic cycles. This eliminates any inconsistency from manual input and allows for quick testing of different scenarios. As the control software gets direct feedback from the position of the cylinders and uses closed loop PID control, the effects of current battery voltage, oil temperature and such variables are minimized.

When a cycle is running every relevant sensor and data source is continuously sampled and recorded to the flash memory of the MicroAutoBoxII. This data is exported to a Matlab-readable ".mat" format with Dspace's "ControlDesk" software automatically when flash memory content is read. The end result is a set of data formatted as a Matlab struct, which includes the sensor data along with their time axis. This information is called a channel in this work.

For longer cycles, the internal flash memory of the MicroAutoBoxII is not sufficient. In these cases, the measurement data is saved directly on the controller PC, connected via Ethernet. This is done with the ControlDesk record feature, and results in identical .mat files when compared with those saved to the MicroAutoBoxII flash memory.

Two different cycles, simplified and original are used in this work. They have been selected to fulfill different requirements and are introduced in sections 5.1 and 5.2.

5.1 Simplified cycle description

Shown in figure 6 is the simplified working cycle, which aims to simulate a single down-up movement of the boom and bucket assembly. As in a real working cycle, both the boom and bucket movements are used. This cycle does not perfectly correspond to a real working cycle, as that would require the bucket to repeatedly hit the floor and push against it, which is not acceptable here.
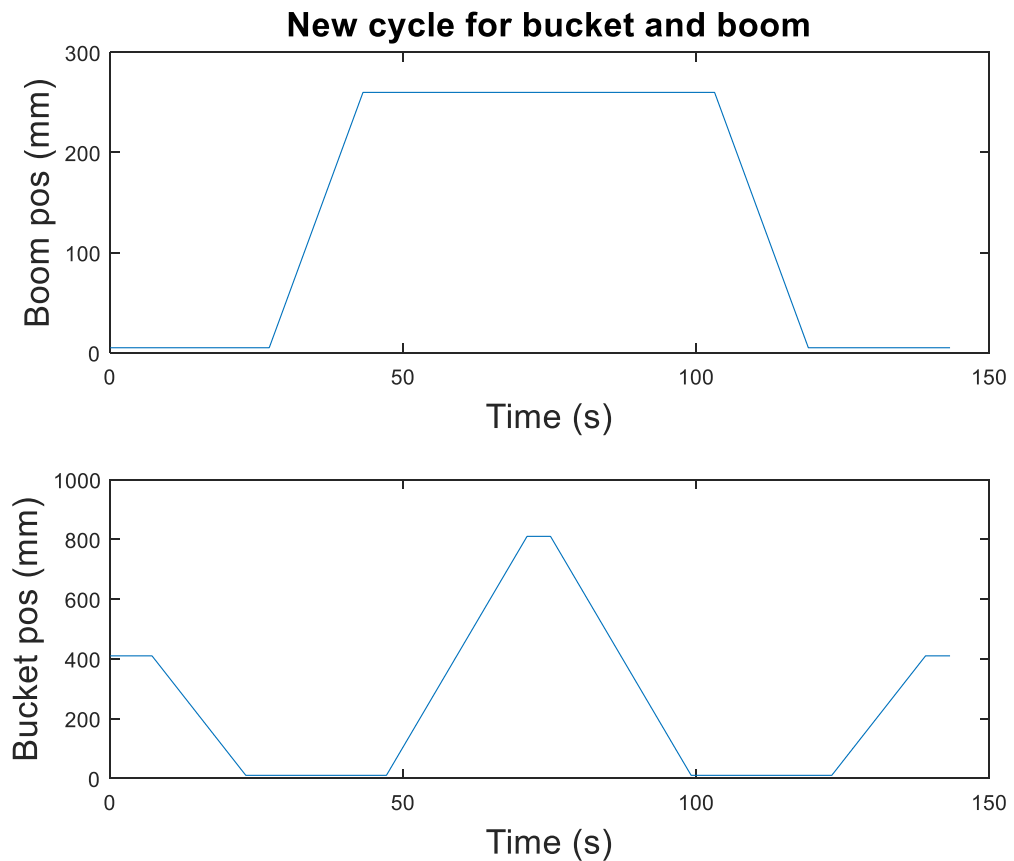
Figure 6 Boom and bucket position commands with the simplified cycle. The cycle is run at several speeds.

It should be noted that the bucket position decreases towards the "up" position, whereas the boom position increases towards it. This is due to the distance measuring draw wire sensor being mounted to the cylinders with the bucket cylinder being reverse acting. The cycle starts with the boom lowered and the bucket in a neutral position. The bucket is pulled to its upper end stops, and the boom lifted to its topmost position. While keeping the boom raised, the bucket is dipped all the way down as if dumping rocks and then raised back up again. The boom is then lowered down. Finally, the bucket is lowered back to its neutral position.

This cycle is run while controlling two variables: the speed at which the cycle is run, and the load mass placed on the bucket. Thus, the results show the DDH units at several different operating points where their ability to perform and efficiency is measured.

There are four different velocities used: 1.5, 3, 5 and 8 cm/s, with the highest velocity being close to the machine's maximum. The velocity of the whole cycle is scaled to these speeds, with the movements being identical but the runtime changing.

Three different loads were selected for testing, 0 kg, 1040 kg and 2205 kg. The load comprises of two sets of weighted metal plates affixed to a frame, of which one or both are used to create the two different loads.

5.2 Original test cycle description

Mirroring one of the tests run with the original, diesel-hydraulic mining loader, the cycle as illustrated in figure 7 includes only boom movement. As the goal is efficiency

measurement, any sources or sinks of power outside that what is measured should be minimized. This precludes the realistic working cycles, as these include action such as driving and steering, all of which are powered by the diesel engine in the original mining loader. To compare the efficiency of the new DDH units to the original setup, a cycle that uses only the boom and bucket movements is needed, as power used by the drive and steering motors cannot otherwise be accounted for. Such a cycle exists in the measurement data, but only for boom movement. Therefore, this cycle is chosen as the only appropriate one for comparison between the conventional and DDH hydraulics.
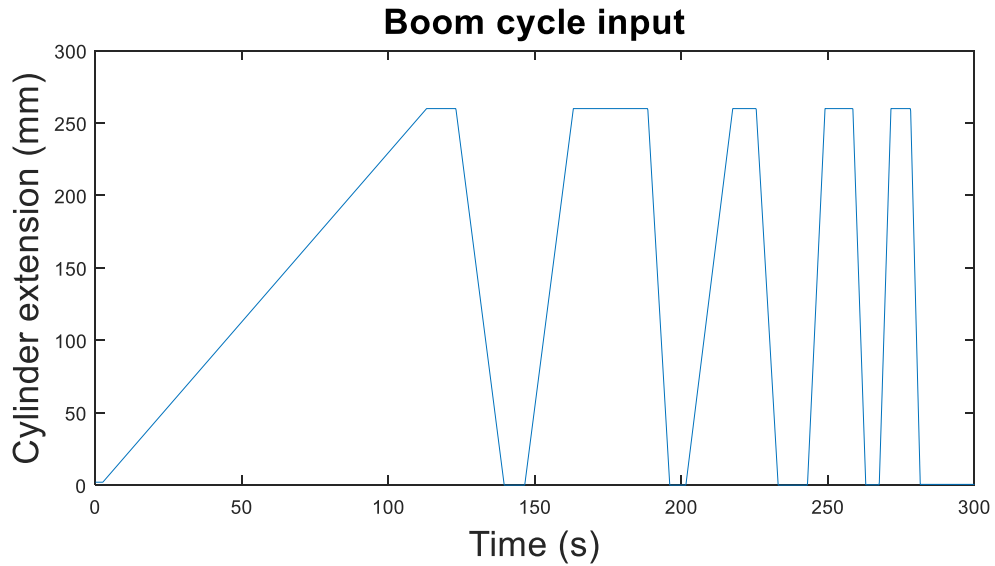
Figure 7 Boom position input

During this cycle the bucket is held in its top resting position. The bucket is loaded with different weights, and the cycle itself incorporates several different velocities ranging from a very slow 2mm/s movement to a maximum of ~78mm/s close of the maximum attainable velocity.

6 Results

This section demonstrates the results from testing with the two cycles defined in sections 5.1 and 5.2.

6.1 Simplified cycle

The measurements from the simplified cycle are shown with the runs with different loads grouped together, with four sets of these results corresponding to the four different velocities. The goal of this investigation is to determine the system's efficiency, with the results being shown with that goal in mind: First the system power input and output with the required data for their calculation and then the actual efficiency that results.

6.1.1 Low speed

The low speed cycle has a velocity of approx. 1.5 cm/s of cylinder extension. As the cycle is the same with all velocities, the low speed cycle takes the most time to complete.

It is clearly visible from figure 8 that the current requirement increases in proportion to the load being lifted, with lifting currents during the lifting portion starting at 25s in the range of 50-130A depending on the load. Regeneration is visible during the lowering portion of the cycle starting after 110s, where the current is negative and being used to charge the battery instead. The current graph for the heaviest 2205 kg load is shaped slightly differently from the lighter loads, with the current ramping up before the actual lifting and not staying constant when the load is held in the up position. This is because the high load placed on the lifting mechanism causes the extension sensor to read a value slightly lower than the normal calibrated starting position, which in turn causes the I term of the PID controller to slowly start ramping up the torque. The inconsistent holding current does not have such a simple explanation. The most likely reasons are motor controller nonlinearity resulting from large temperature swings and PID issues, as the different loads and speeds were all run with the same PID parameters. The results with the highest load all have similar issues, as there is low or no extra power margin left with the 2205 kg load depending on the velocity.
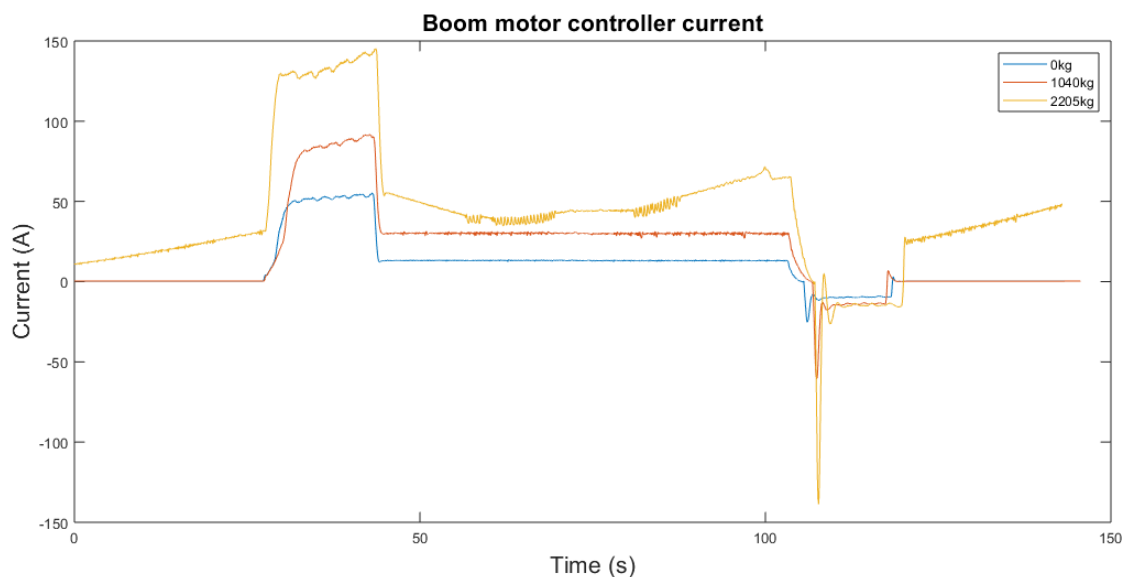

Figure 8 Boom motor controller current, low speed

Figure 9 shows the DDH battery voltage during the cycle. As expected, there is a drop in the voltage during the lifting phase corresponding to the current requirements at that time, with the larger currents required for heavier loads causing more noticeable drops. During the lowering phase regenerated energy from the load is fed back to the battery, causing a jump in voltage as the battery accepts charge.
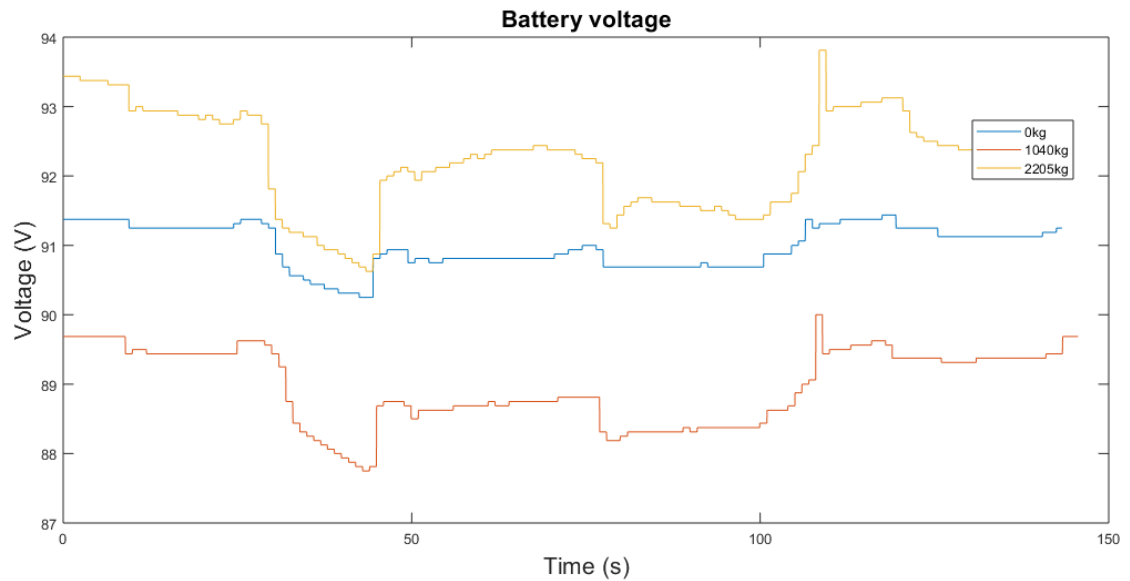

Figure 9 Battery voltage, low speed

The power graph of figure 10 is not measured directly, but instead calculated from the current and voltage measurements. Since both the voltage and current measurement points are before the motor controller this data includes controller losses, which must be taken into account when determining efficiency. Both the lifting and lowering phases can be clearly seen in the data, with a peak lifting power of ~13kW for the highest load. The negative values seen correspond to energy regeneration, this is the power used to charge the battery.
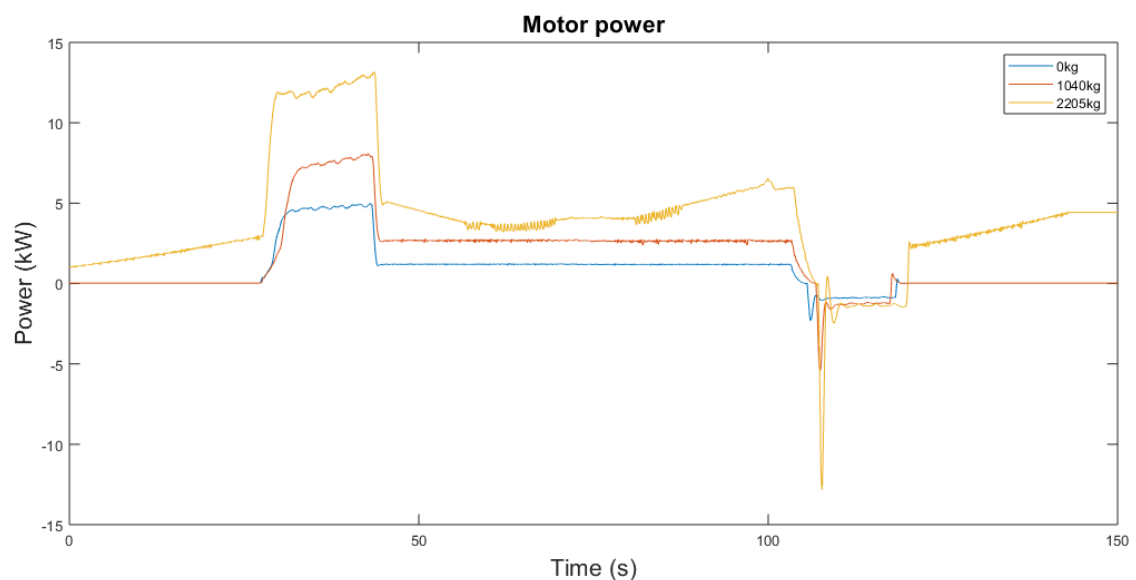
Figure 10 Motor power, low speed

The force shown in figure 11 is measured directly with load pins mounted to each cylinder. The lifting motion has two parallel cylinders, therefore the combined load on the cylinders is the sum of measurements from both load pins. Usually when the boom is lowered most of the load is taken by the frame end stops, which is seen in the data as very

low force on the cylinders. With the load lifted the value remains quite stable with small variations due to geometry, and in the middle, movement of the bucket. In the case of the highest load the PID controller has started ramping up motor power early, most likely due to the increased load forcing the boom below the zero position setpoint either due to slop or bending in the mechanism itself. Since both the load and the velocity at which this load is moved is measured at the cylinders, there is no need to take into account the geometry of the machine when calculating the efficiency, as the calculation only depends on the force and velocity.
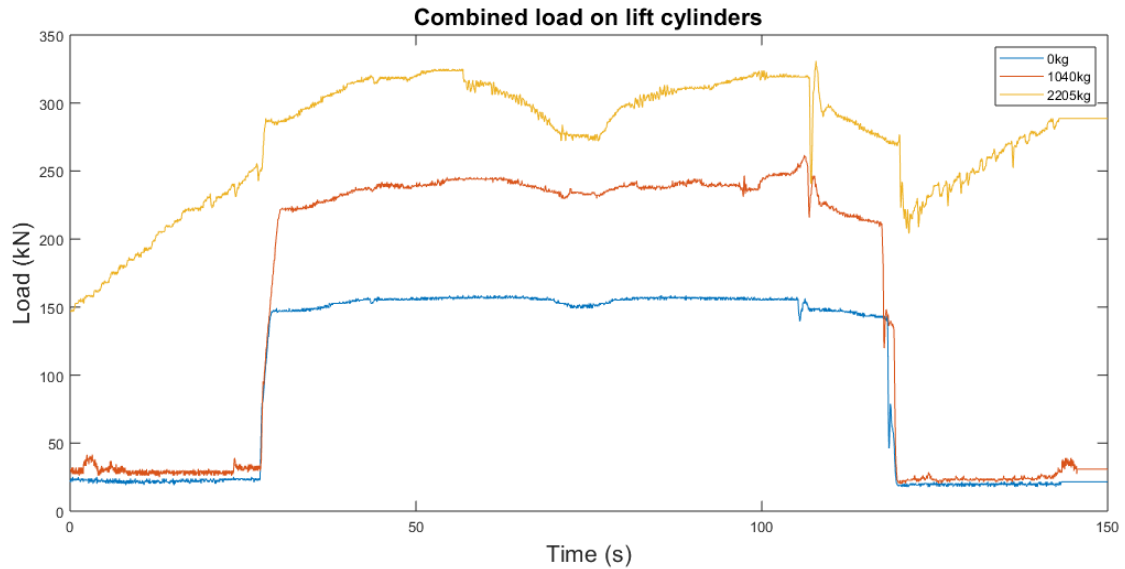
Figure 11 Combined lifting force, low speed

Velocity shown in figure 12 is measured with a distance sensor mounted on the lifting cylinders. It shows how the increased load slows acceleration, as the highest value is close to the machine's maximum. The PID controller has difficulties starting load lowering smoothly, as both the motor controller and the mechanism itself conspire to produce a considerable stick-slip like effect which it does not explicitly take into account. The narrow spikes occurring when the load is stationary result of the position sensor crossing a quantization point due to shaking as the machine works and can be ignored.
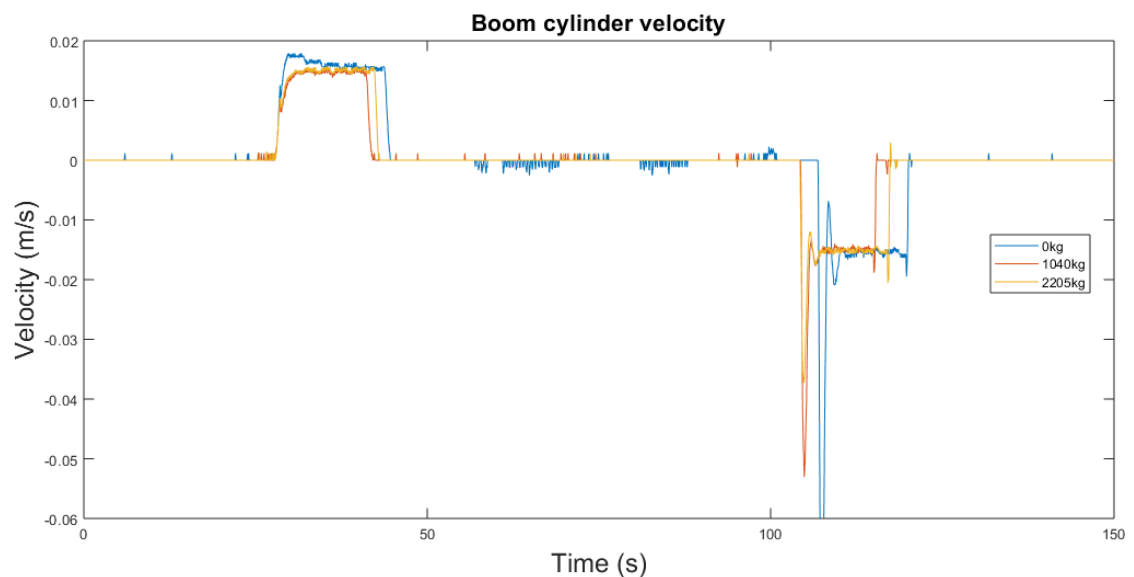
Figure 12 Boom cylinder velocity, low speed

26

Lifting power is calculated from lifting velocity and the load being lifted, with the results shown in figure 13. Due to the spikes in velocity when the lowering starts, there are corresponding spikes in the power as well.
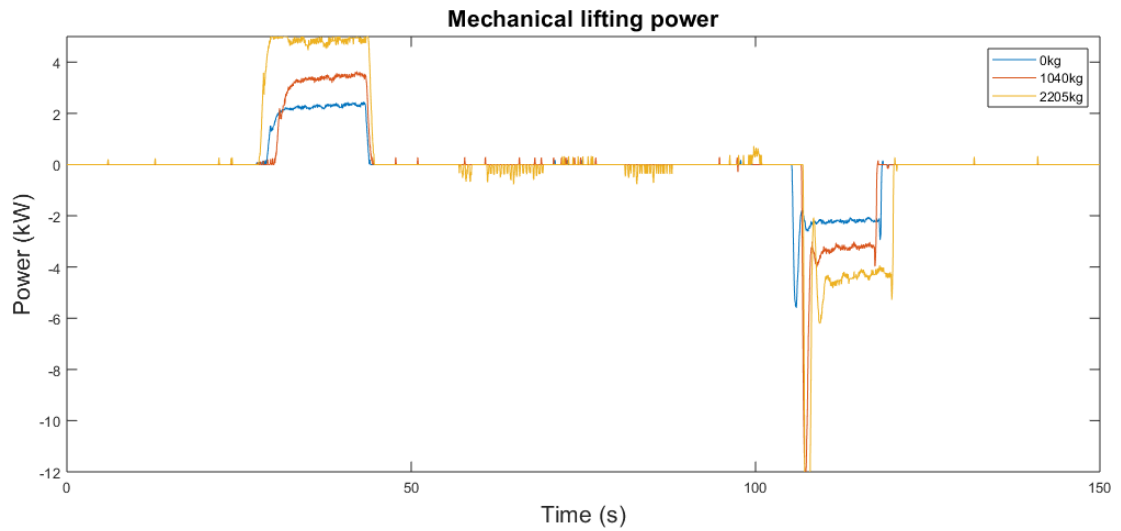

Figure 13 Mechanical lifting power, low speed

6.1.2 Medium speed

The measurements are the same for the medium speed, with a boom velocity of 3 cm/s. In figure 14 it can be seen that the current required to lift the load is larger as expected.
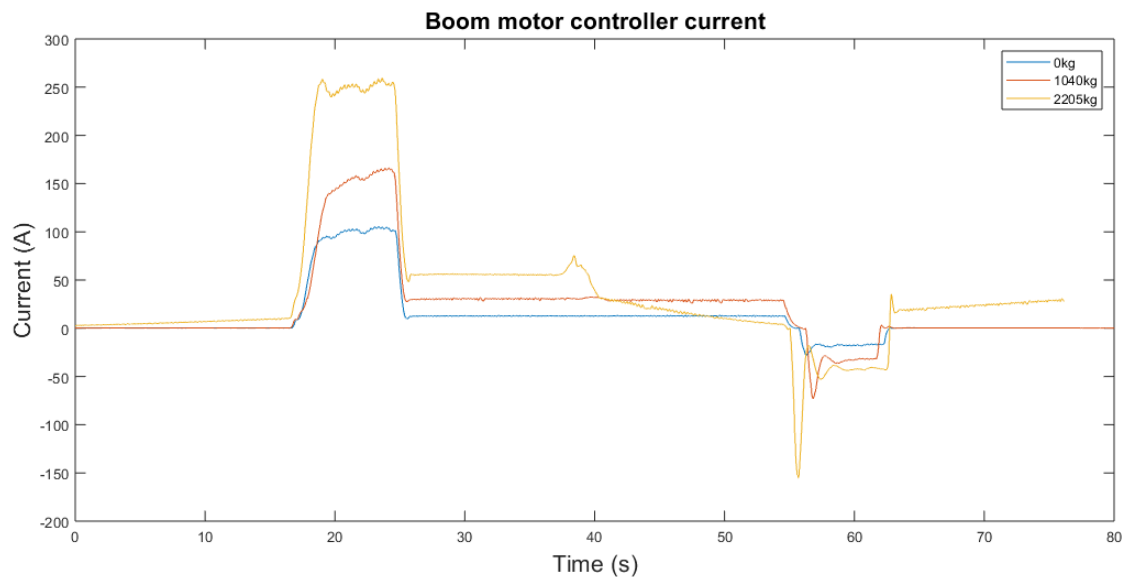

Figure 14 Motor controller current, medium speed

In figure 15 the battery voltage drops more under the increased current. It should be noted that the battery level itself varies due to the exact state of charge during the measurement, and it is the drop in the voltage under load, which is more interesting.
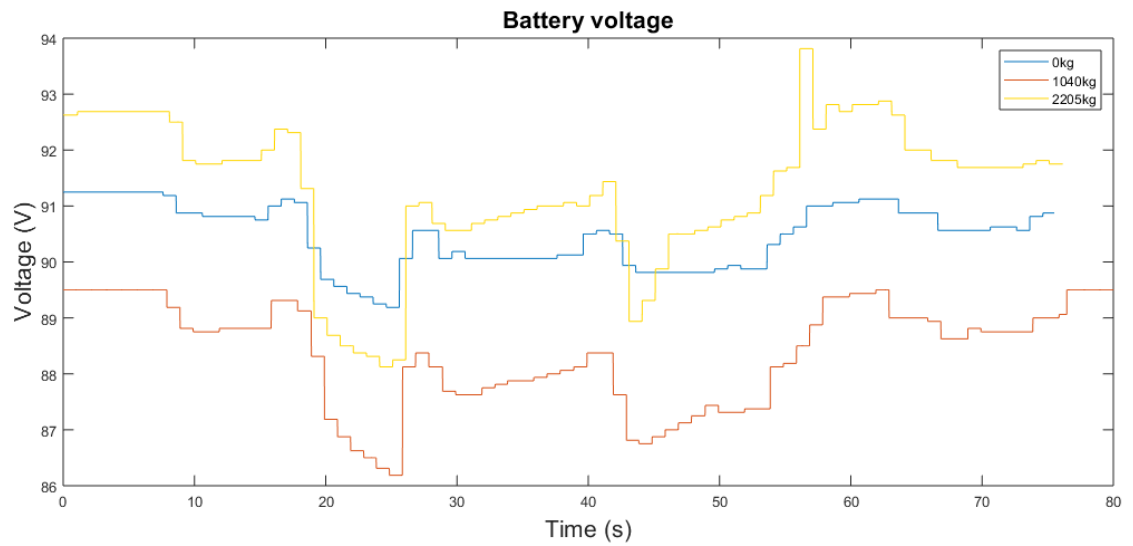
Figure 15 Battery voltage, medium speed

Figure 16 shows the increased motor power to cope with the higher load.
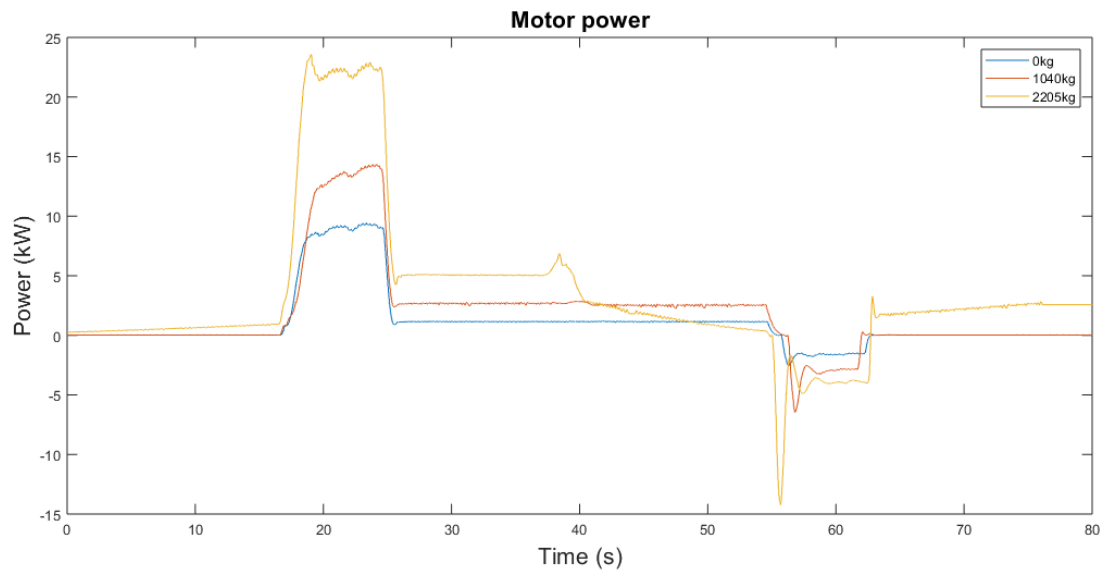
Figure 16 Motor power, medium speed

The load on the cylinders is almost identical to the slow speed measurement as expected, but as seen in figure 17 the highest load level is starting to show jumps and unevenness, mainly caused by the PID jerks as it attempts to stabilize the high load.
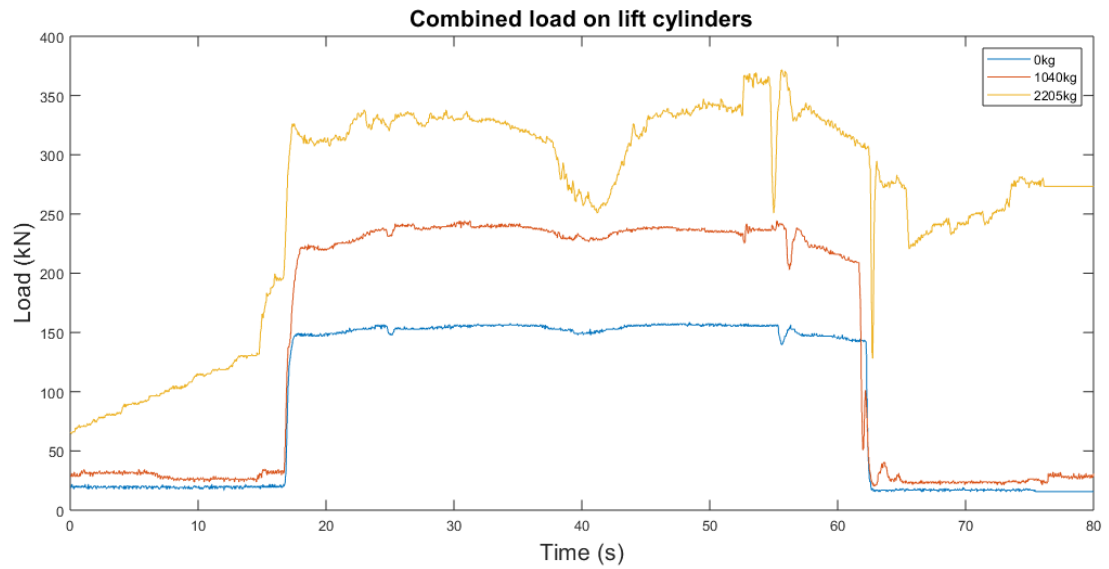
Figure 17 Combined load, medium speed

The velocity measurement in figure 18 shows increased overshoot at the beginning of the lowering phase, this results from the increased cycle speed.
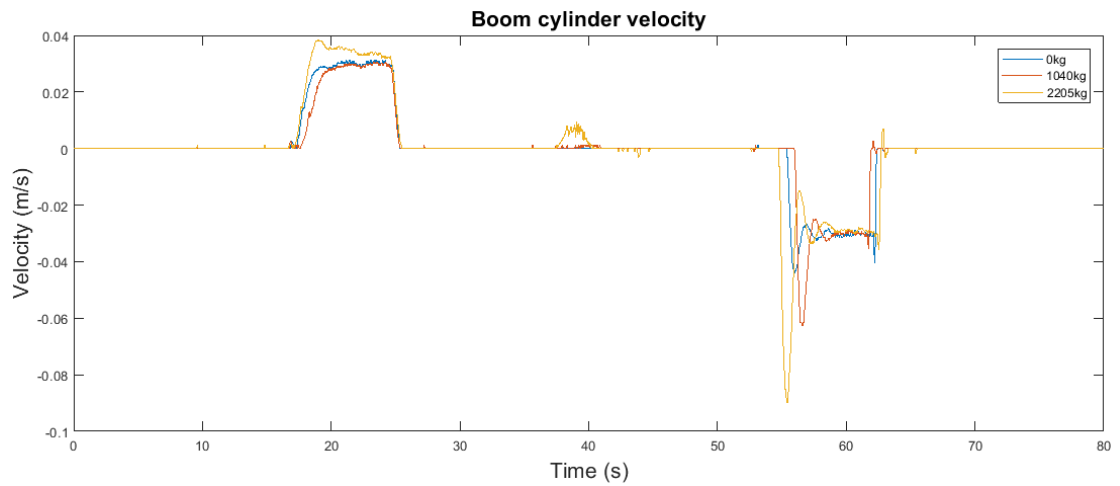
Figure 18 Boom cylinder velocity, medium speed

Figure 19 shows the lifting power, increasing as expected with load.
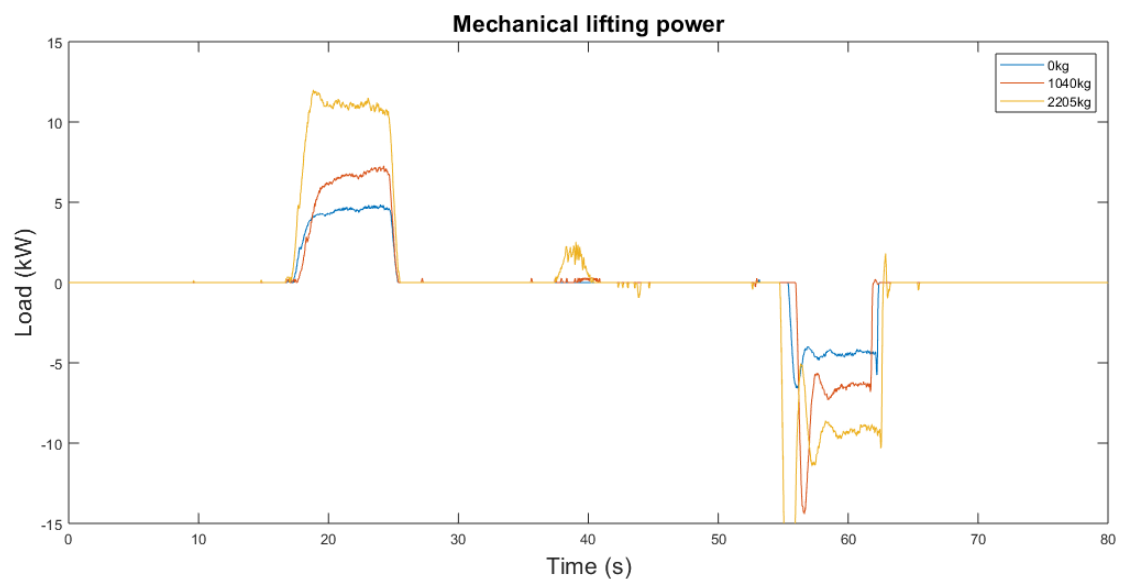
Figure 19 Mechanical lifting power, medium speed

6.1.3 High speed

With the "high" speed cycle corresponding to a maximum cylinder velocity of 5 cm/s the electric drive is starting to reach its limits, with current saturating to a value of ~375A when lifting the heaviest load as seen in figure 20. Lower loads still have some headroom left at this speed. At the higher load levels a PID artifact is visible, the load does not completely reach the upper setpoint, but is held slightly under it until being jerked into position. This is visible in almost every figure with the highest load.
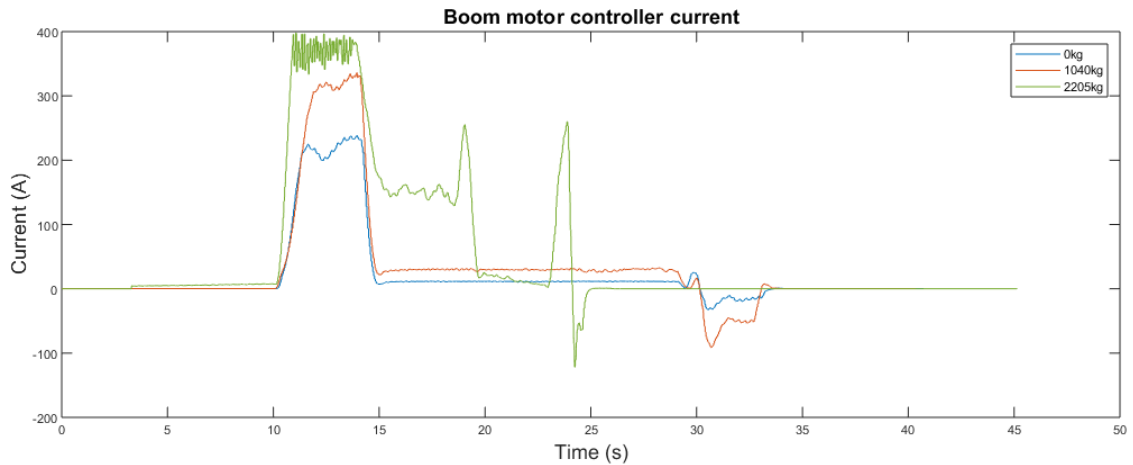
Figure 20 Motor controller current, high speed

Figure 21 illustrates the noticeably larger battery voltage drops during lifting.
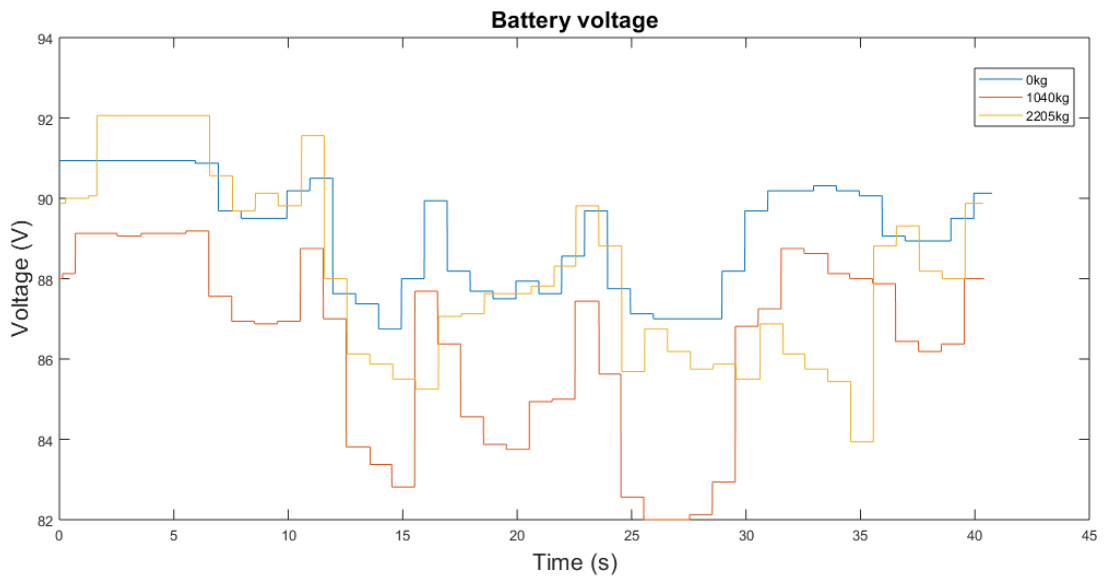

Figure 21 Battery voltage, high speed

In figure 22 the yet higher motor power is shown. Motor power is limited to 35 kW, this limit was reached during the fast cycle with the heaviest load. At this speed, the power available for regeneration starts to suffer, especially with the lower loads due to friction and pumping losses taking up a larger portion of the lowering energy.
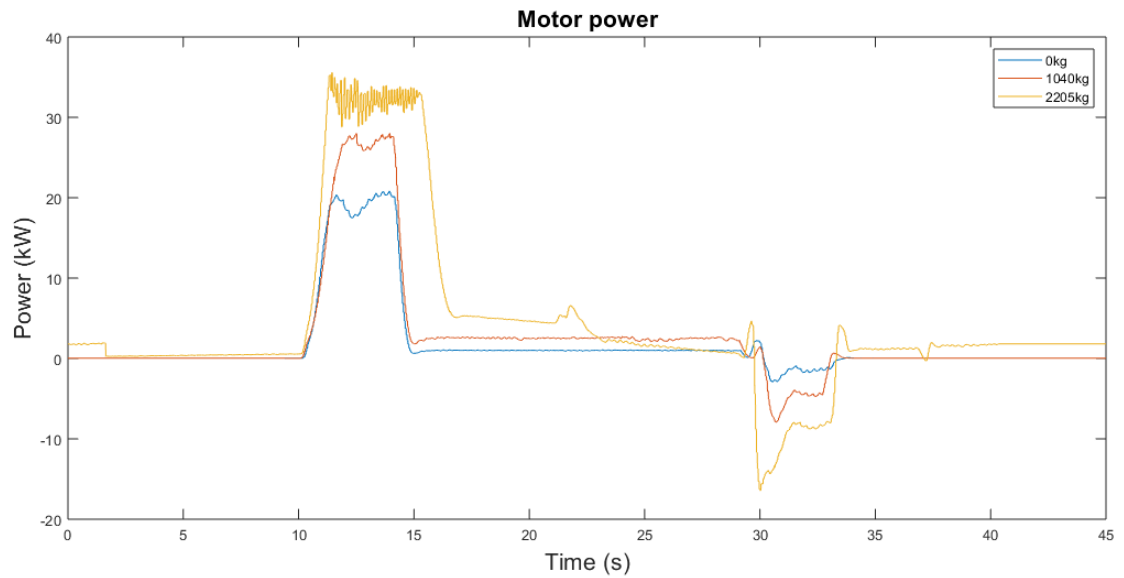
30

Figure 22 Motor power, high speed

In figure 23 the load is nominal for the 0 kg and 1040 kg load, but there is significant jumpiness with the 2205 kg load.
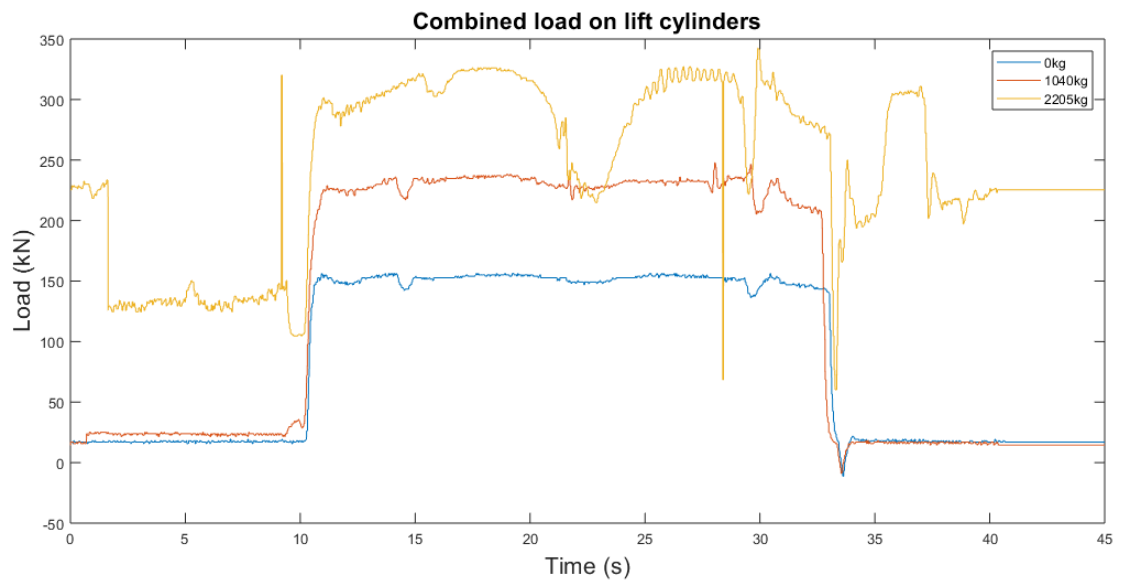

Figure 23 Combined force, high speed

From figure 24 the result of reaching the motor power limit is visible, the highest load cannot be lifted fast enough to match the cycle. Both the 0 and 1040 kg load are still within the machine capabilities.
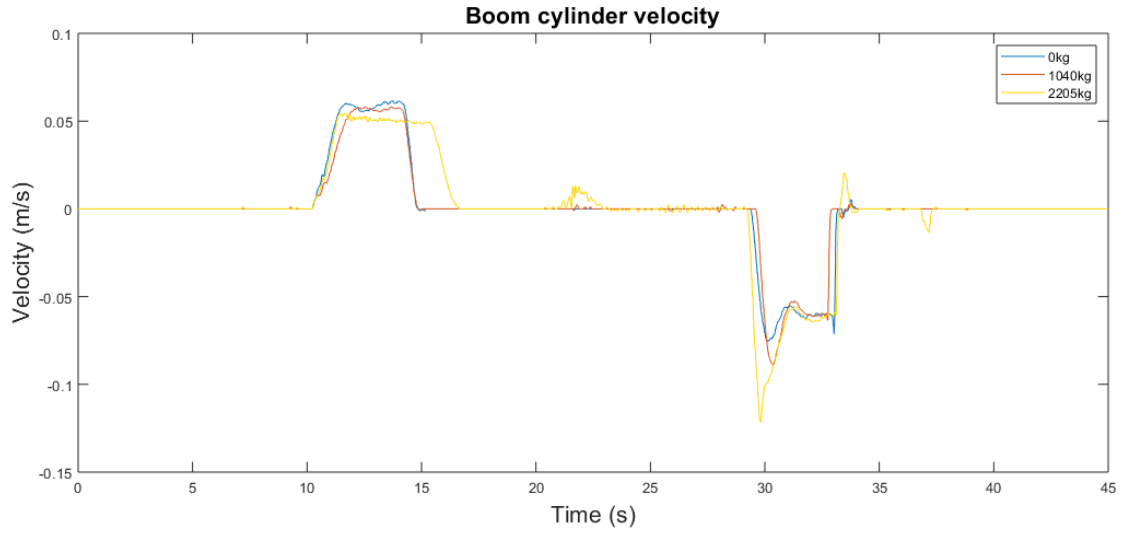
Figure 24 Boom cylinder velocity, high speed

As expected, figure 25 shows the increased power required to lift the load. Since the maximum power is reached, lifting takes more time.
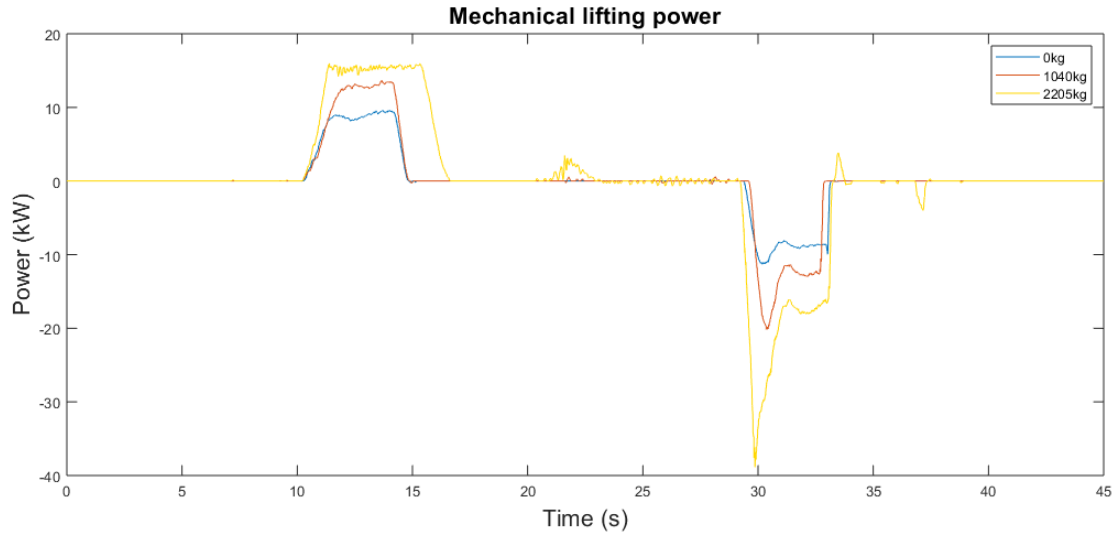

Figure 25 Lifting power, high speed

6.1.4 Highest speed

The fastest cycle uses a reference cylinder movement velocity of 8 cm/s. This is high enough that it can only be cleanly accomplished without load, with both loads the machines power limit is reached and lifting speed is thus lower. In figure 26 this can be seen as saturation of the controller current and the corresponding increase in lifting time. The figure also shows how close to saturating the current is without external load at this speed, which was selected to showcase the fastest movement the machine is capable of.
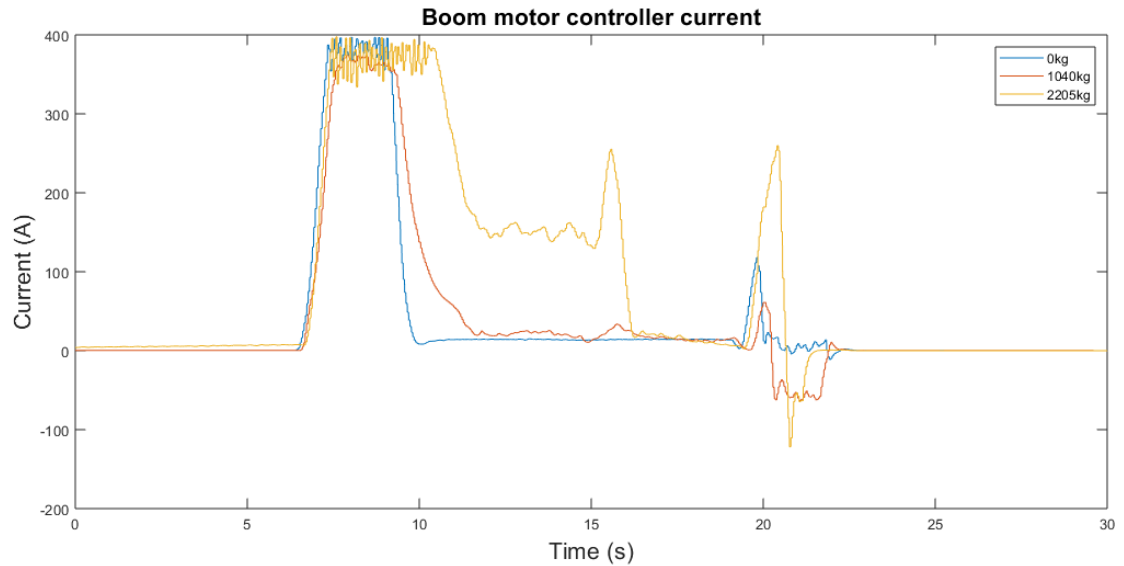
Figure 26 Motor controller current, highest speed

The battery voltage droops nearly 10 volts at this load and speed as shown in figure 27. This is because the capacity of the battery is fairly small in comparison to the currents delivered. The lithium titanate pack is sized mainly as a buffer, and it can easily support the load.
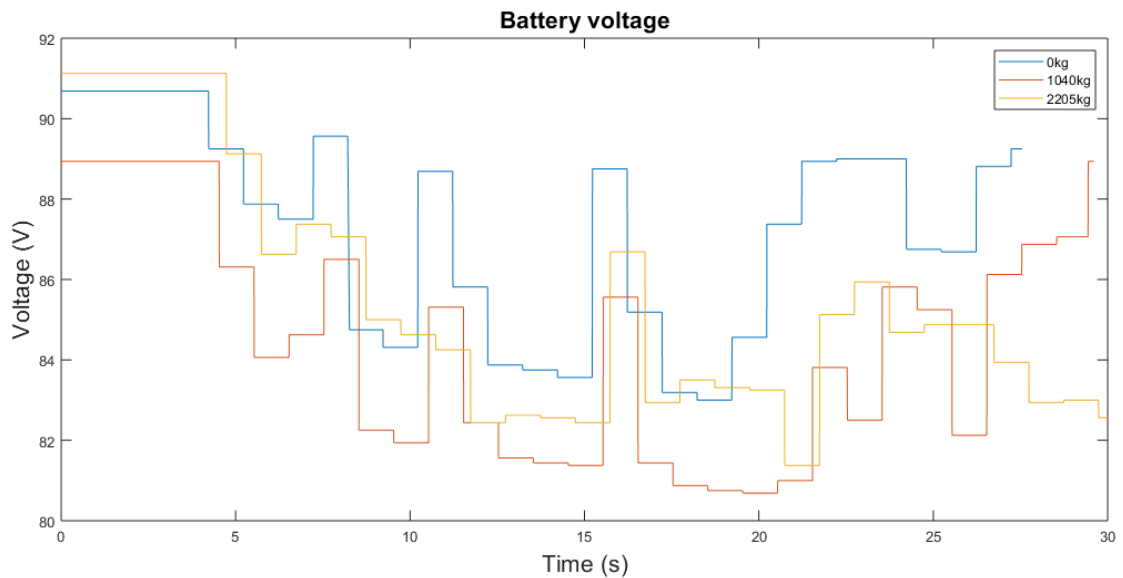

Figure 27 Battery voltage, highest speed

As with controller current, figure 28 shows motor power saturation in all but the zero load cases. In the 2205kg case, the achieved movement speed is slow enough to cause significant integrator windup in the PID controller, resulting in the lift cylinders pushing against the end stop for a while after the move is finished as seen in figure 28.
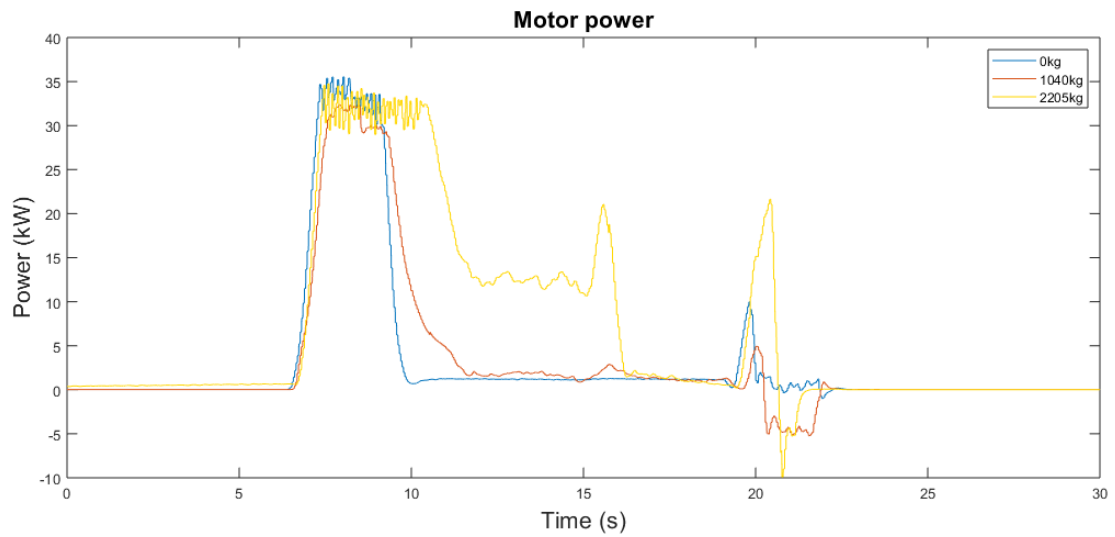
33

Figure 28 Motor power, highest speed

Figure 29 shows there are some anomalies in the load pin measurements of the highest load case right before the lowering movement starts. This is assumed to be caused by the forced end stop contact.
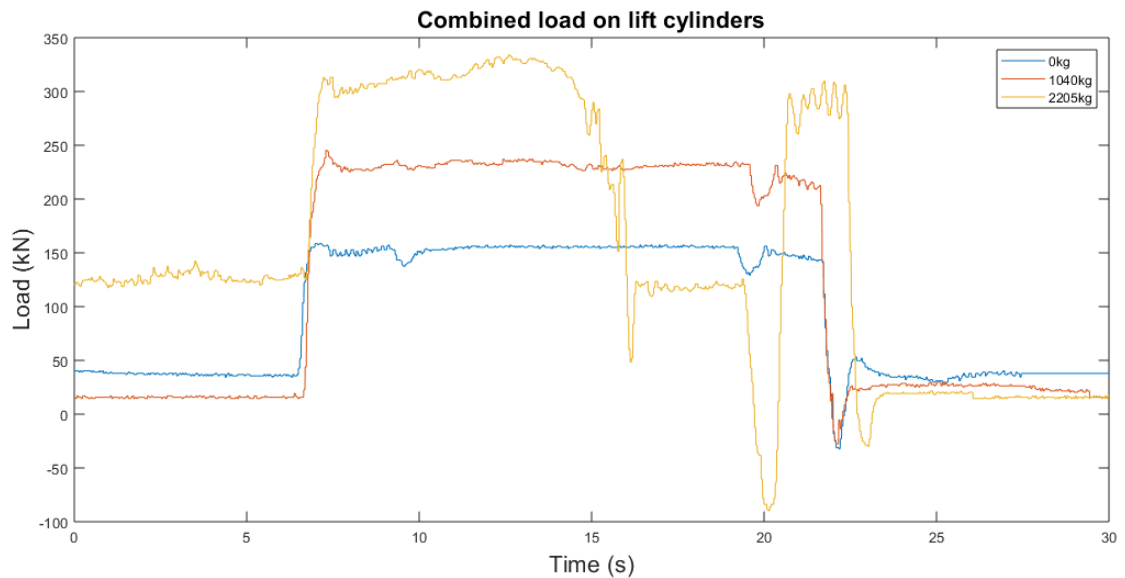

Figure 29 Combined load, highest speed

The lifting velocities in figure 30 clearly show the effect of increased load, the set speed is only reached without any load.
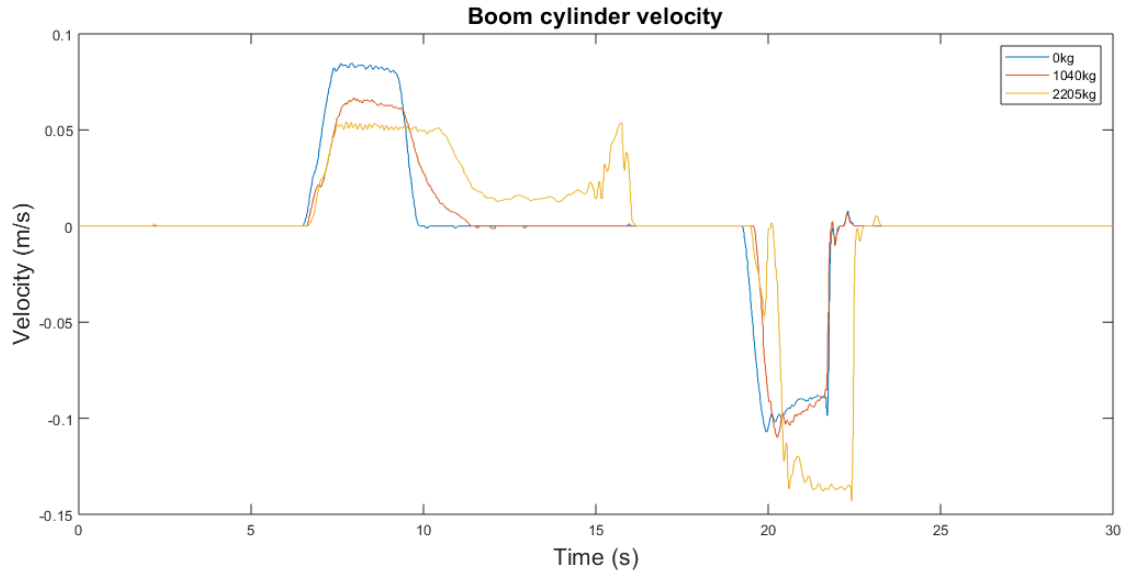
Figure 30 Cylinder velocity, highest speed

In figure 31 the lifting power does not change much due to the power limitation, with time to complete the movement being the main difference.
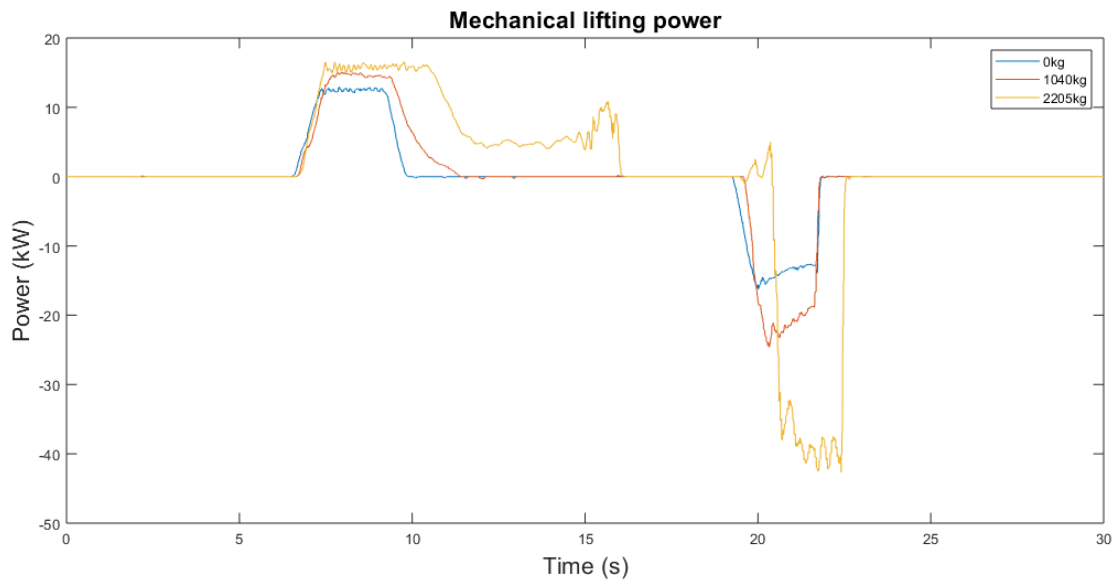

Figure 31 Lifting power, highest speed

6.2 *Original test cycle*

Results from this measurement are split in two categories: work done by boom movement, and power input to the system. Data from the conventional load sensing setup is presented first in 6.2.1, followed by the DDH setup in 6.2.2.

6.2.1 Load sensing setup

To calculate efficiency, system output and input power is needed. The output can be calculated through the actual mechanical work performed by the lifting cylinders. Figure 32 illustrates boom movement, which is exactly as shown in the cycle description as this is the reference signal.
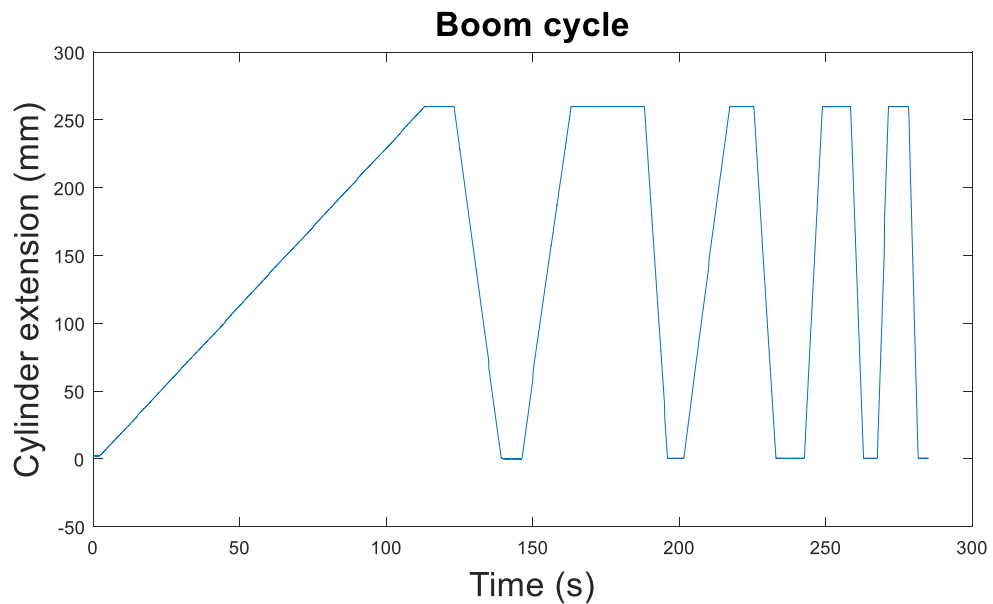
Figure 32 Boom movement during the cycle

It can be seen from figure 33 that the only bucket movement is slight leak-induced creep, the bucket is not used during this cycle.

Figure 33 Bucket movement during the cycle. This movement is due to gravity induced creep

The large load spikes visible in figures 34 and 35 result from the cylinders being driven against their end stops. The actual lifting and lowering happens during the mildly sloping parts. Due to how the load pins are set up, the load acting to compress the cylinders is shown as negative.

Figure 34 Load acting on the right side cylinder load pin
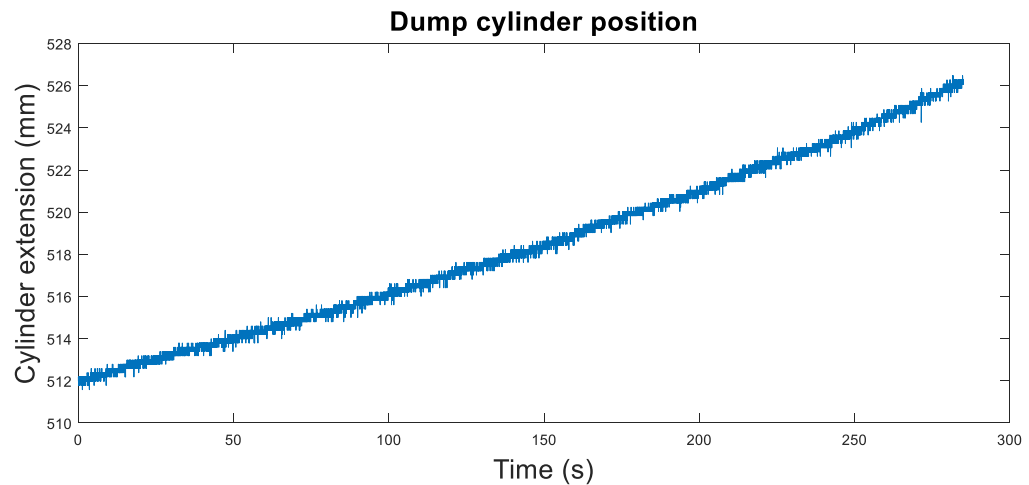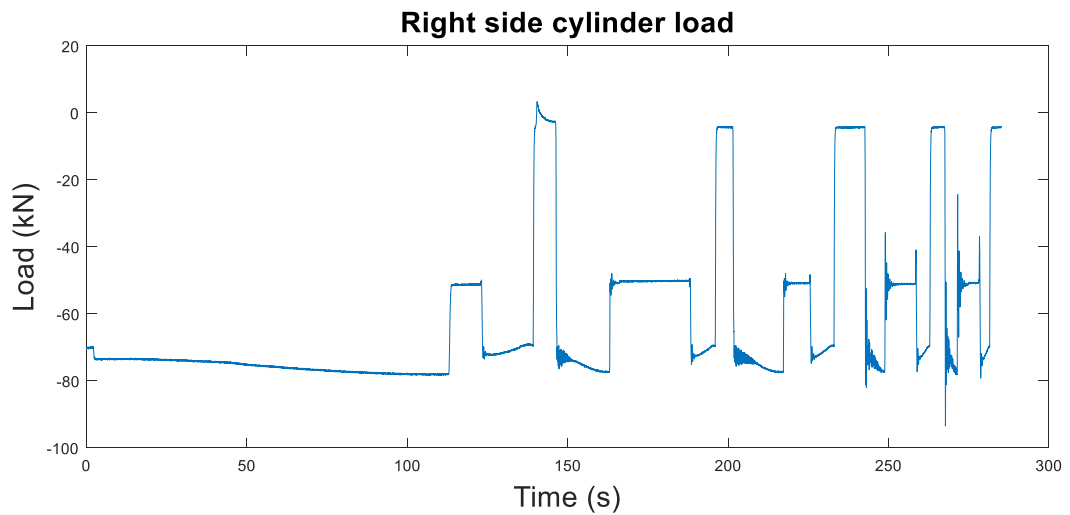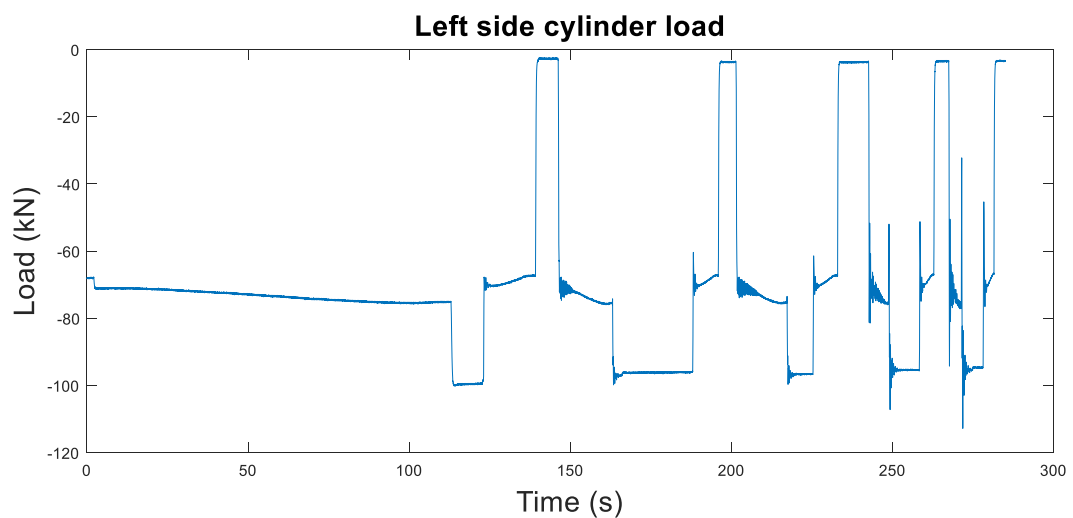

Figure 35 Left side, load on both cylinders is measured independently

The spikes are also visible on the left side cylinder load, but it can be seen that the ones corresponding to the top limit are inverted when compared to the right side load. This is because there is a very slight difference in the cylinder stroke lengths, causing the right side cylinder to reach the end of its travel first. At that point, its force acts only against its own end stop, causing no response to the load pin. However, since the left cylinder has not reached the end of its travel, it can still exert force on the cylinder's common mounting point. This is shown as an increase in the load reported by its load pin, and also as a corresponding but opposite load change on the right cylinder load pin, as this cylinder, already at the end of its travel, is being pulled by the left side cylinder. Adding the cylinder loads together will largely remove these spikes as they are equal and opposite of each other, as shown in figure 36.
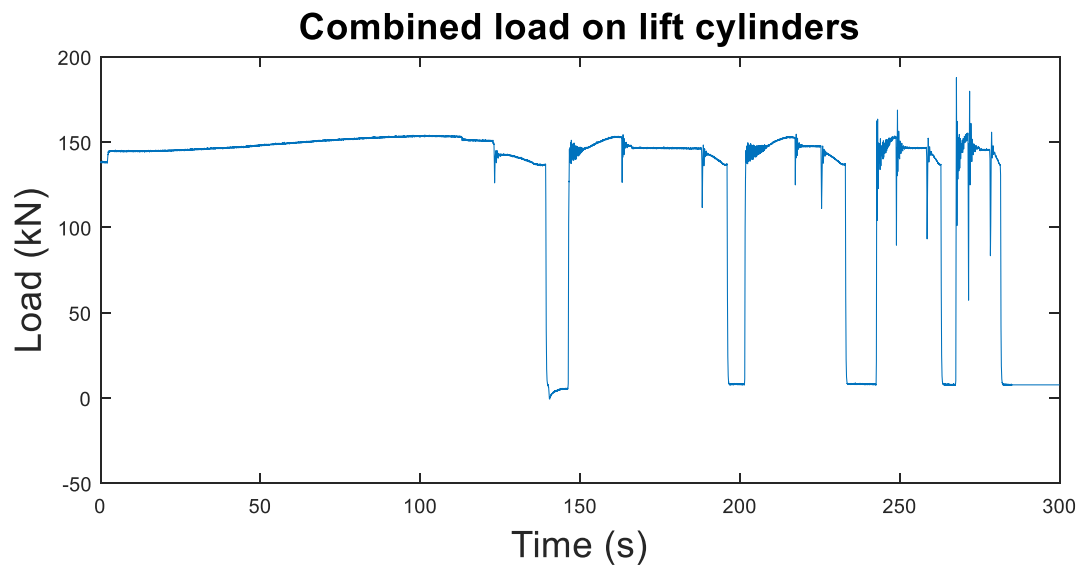
Figure 36 Combined load of the lifting cylinders

Note the absence of spikes caused by driving the mechanism against its endpoints. When the mechanism is sitting in the "down" position on the mining loader, the cylinders are unloaded and do not support the load. This can be also seen at the points where load is near zero.

Movement speed is derived from position measurements. Due to noise, the speed profile shown in figure 37 is a result of deriving a fitted curve instead of the data itself, the procedure is detailed in the analysis section.
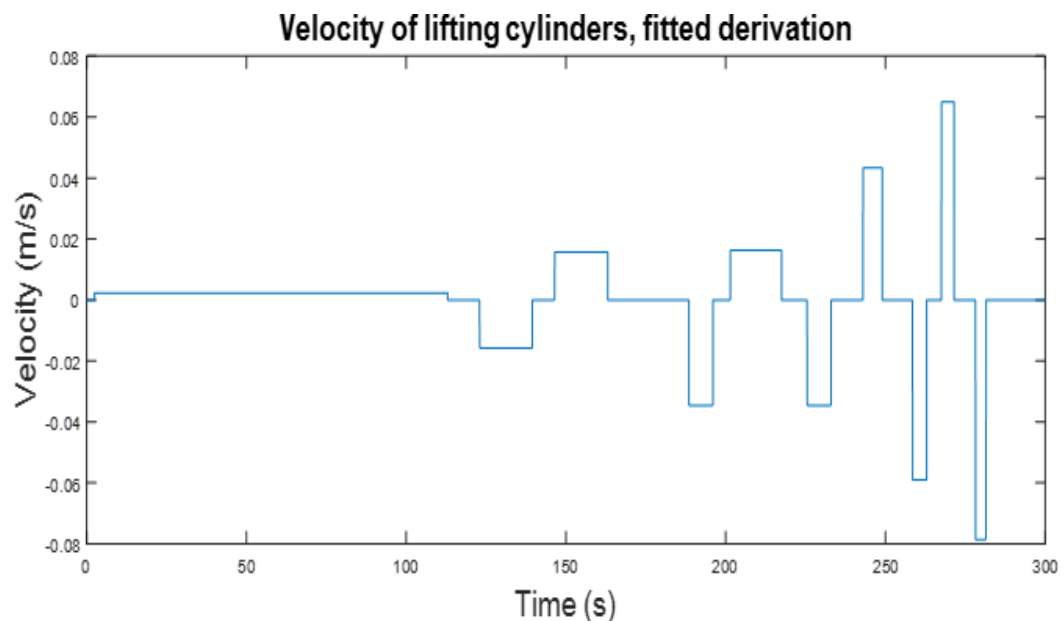
Figure 37 Velocity of lifting cylinders

Combined with cylinder load, this information can be used to calculate work performed by the lifting movement as presented in figure 38. When the load is lowered, work is being done into the system as shown in the negative power. However, since this power is not being regenerated in any way, it is wasted with the conventional load sensing setup. Therefore, this power is disregarded as shown in the figure.

38
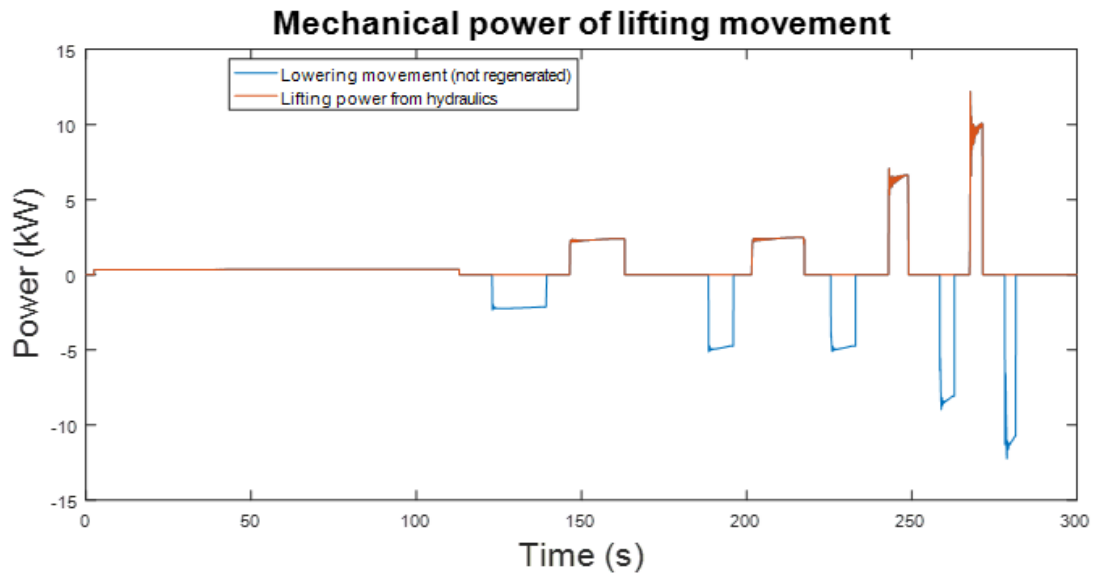
Figure 38 Mechanical output power, with wasted power from lowering shown in blue

Input power is provided by the ICE and can be found from the measured torque and RPM. The raw torque measurement in percentage of maximum is shown in figure 39.
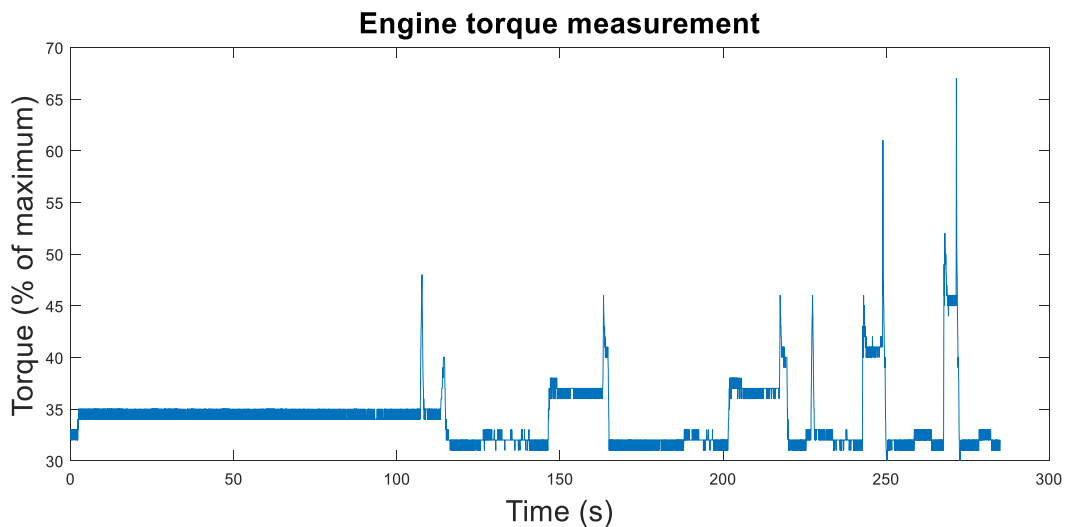
Figure 39 Measured torque of the ICE, in percent of its maximum

Since the engine torque measurement is recorded as a percentage value of its rated maximum, it is useful convert this into the actual values in Newton-meters. As the rated torque of the engine is listed as 470 Nm, the results are as shown in figure 40. In the load sensing setup, the engine torque responds to power demand, this can be seen as torque increases during the lifting phases of the cycle.
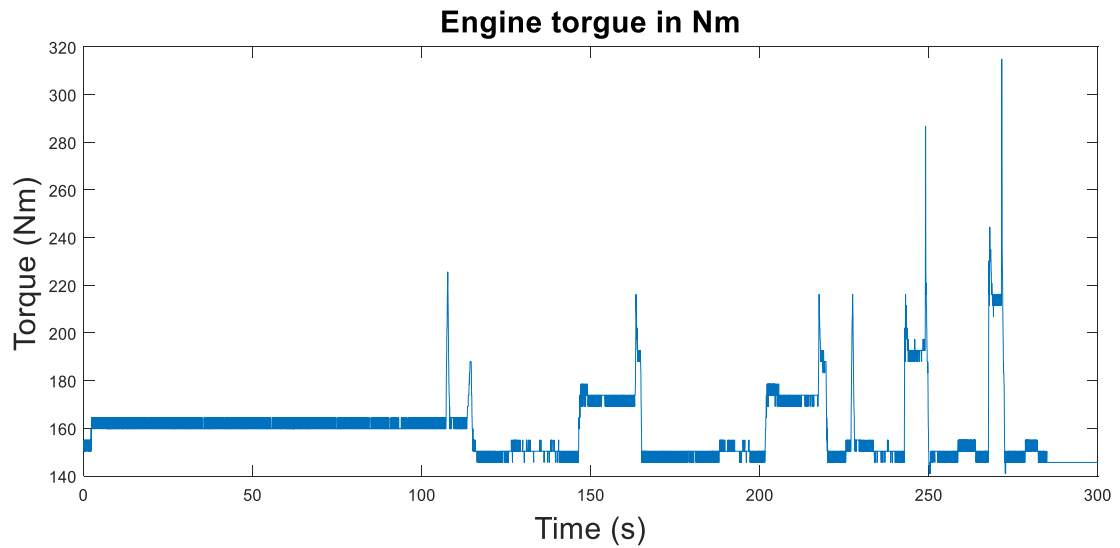
Figure 40 Engine torque in Nm

During work, the ICE attempts to maintain a constant RPM. Engine speed is controlled to around 2200 rpm, with sudden spikes induced by load changes visible as shown in figure 41. The governor introduces overshoot when compensating for the sudden drop in RPM caused by load.
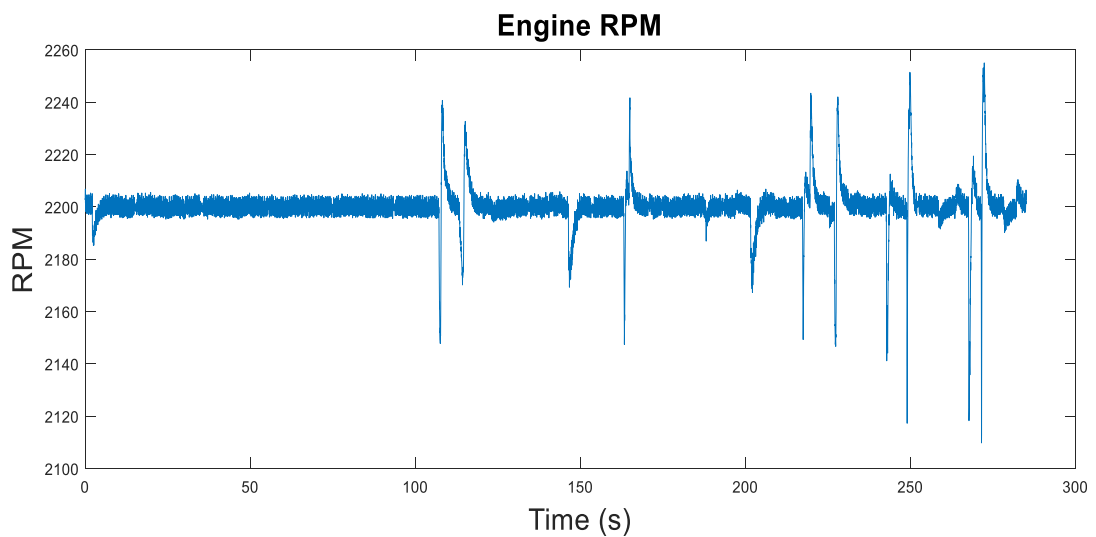
Figure 41 ICE RPM during the cycle

Figure 42 shows that due to the nearly constant RPM power follows the torque closely. During the transient spikes power is taken from the rotational inertia of the flywheel, visible as spikes in power. This behavior is good for a fast response, since the ICE cannot increase its power output nearly as fast as the valve-controlled hydraulics can demand. As the ICE maintains constant RPM during the cycle, energy for the quick accelerations is available from the rotational mass of the flywheel and the engine itself. This is observable in the RPM graph as a quick drop when a movement is started.

40
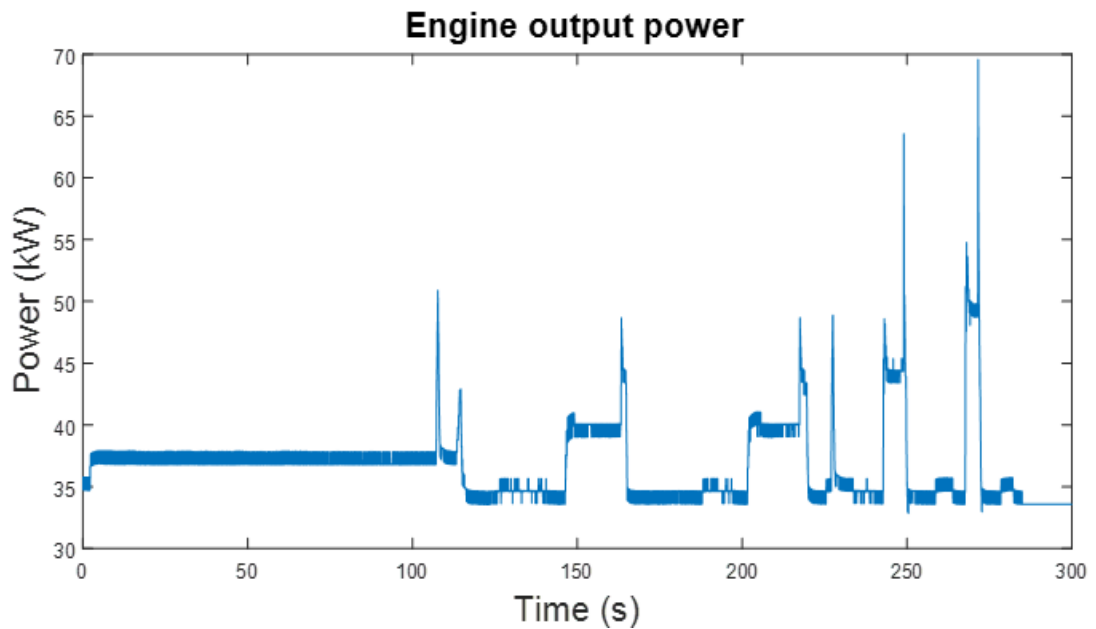
Figure 42 Engine power during cycle

6.2.2 DDH setup

Measurements differ slightly for the DDH setup, with current and voltage having the key role in the input power. The output power is found in the same way as the conventional setup, from the speed and load of the movement. With the DDH setup, the original measurement cycle was used as an input, which the PID controller tries to approximate to the best of its ability. The actual result is shown in the figure 43. Overshoot can be seen with the faster velocities. In addition, some speed error during the first, slow start due to stick-slip effect overcoming the controller's P term contribution, requiring the integrator to spool up to start the motion. Nevertheless, the cycle can be seen to be quite faithful to the original.
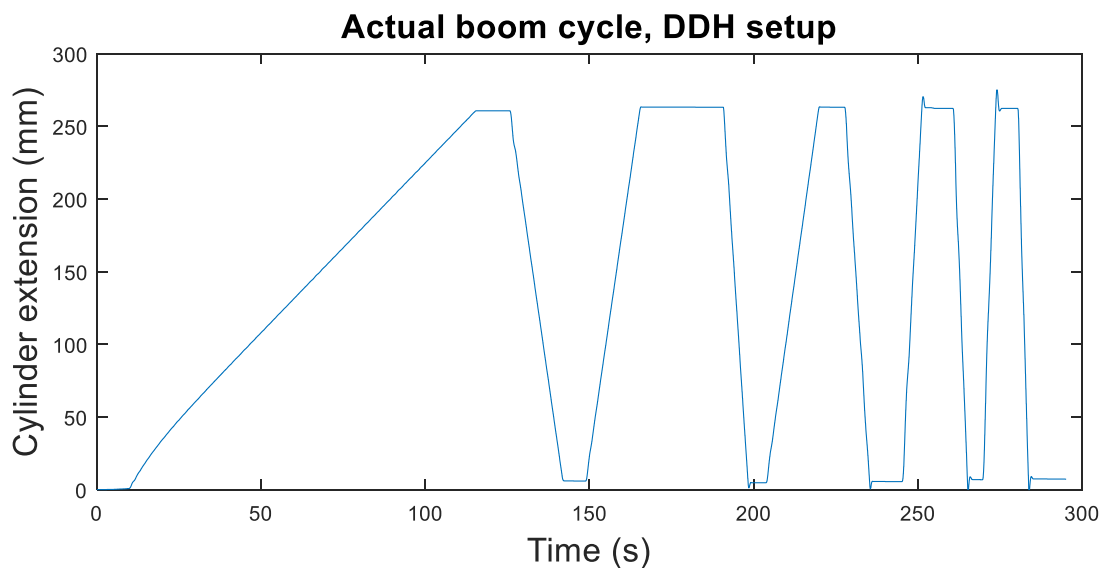
Figure 43 Realized boom position during the cycle

Velocity of the movement is found in the same way as with the load sensing setup, through fitting a line to the noisy position derivation. The result is shown in figure 44.

41
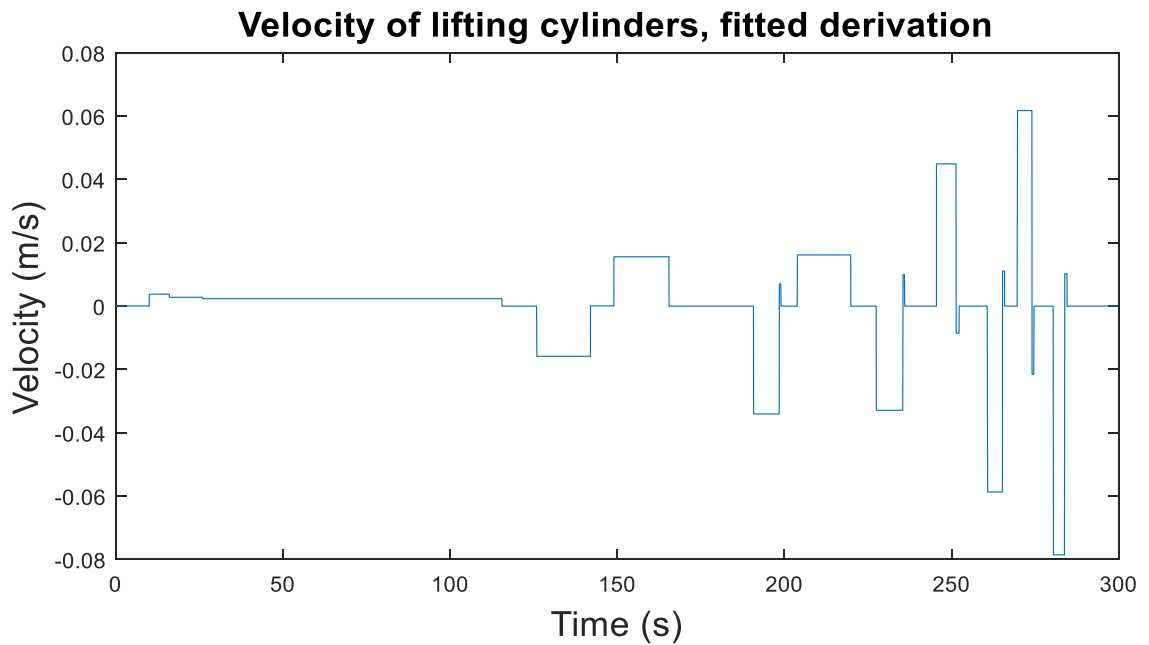
Figure 44 Velocity of the lifting cylinders of the DDH setup

The measured cylinder loads are shown in figures 45 and 46. It can be seen that the mechanism does not quite reach the bottom, since the cylinders are supporting the weight at all times. This was done in order to not confuse the PID controller, and since only the lifting and lowering actions are factored into the calculations, the comparison stands.
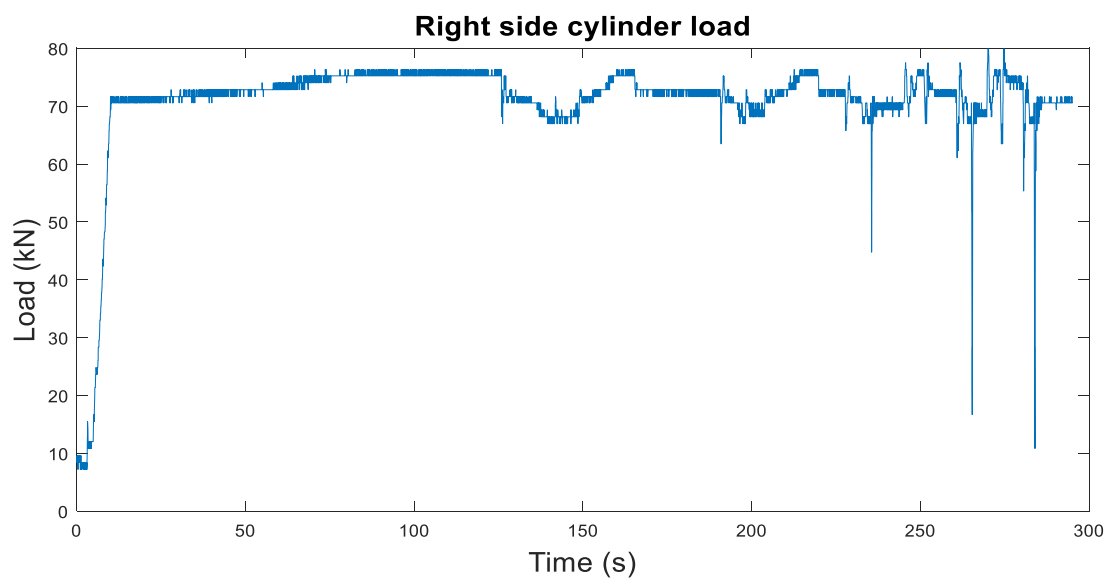
Figure 45 Load acting on the right side cylinder load pin
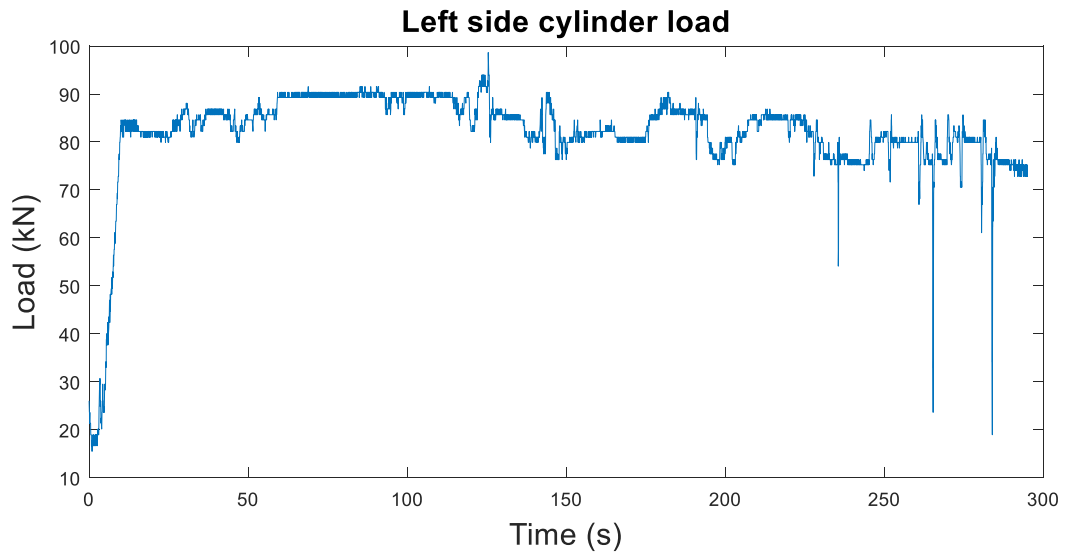
Figure 46 Load acting on the left side cylinder load pin

The total load resulting from adding both cylinder loads together is shown in figure 47.
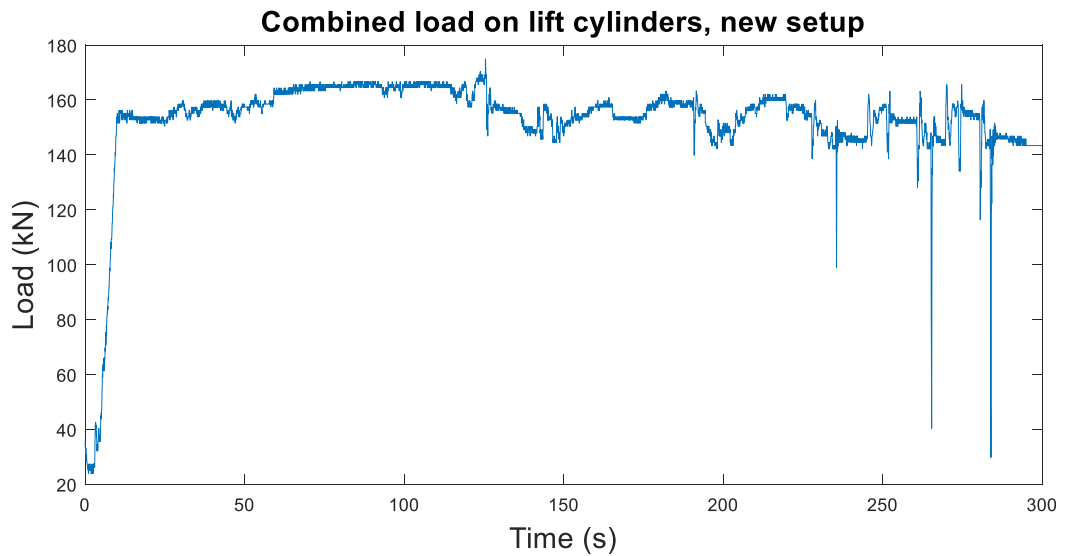
Figure 47 Total load of the lifting movement

The input power depends on the current and voltage, which can be seen in figures 48 and 49. Highest transient current of 400A was measured at 270 seconds, this peak is outside the range of figure 48 to better visualize normal operation.
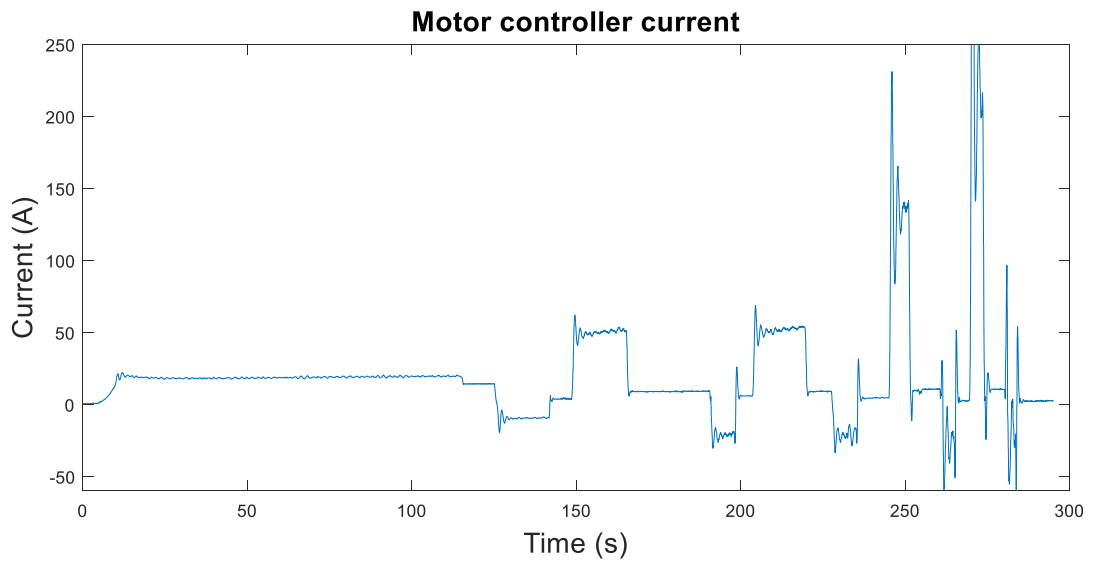
Figure 48 Motor controller current, scale clipped to 250A

The inaccuracy of the voltage sensor can be seen in figure 49, this issue is partly fixed in the newer simplified cycle measurements.
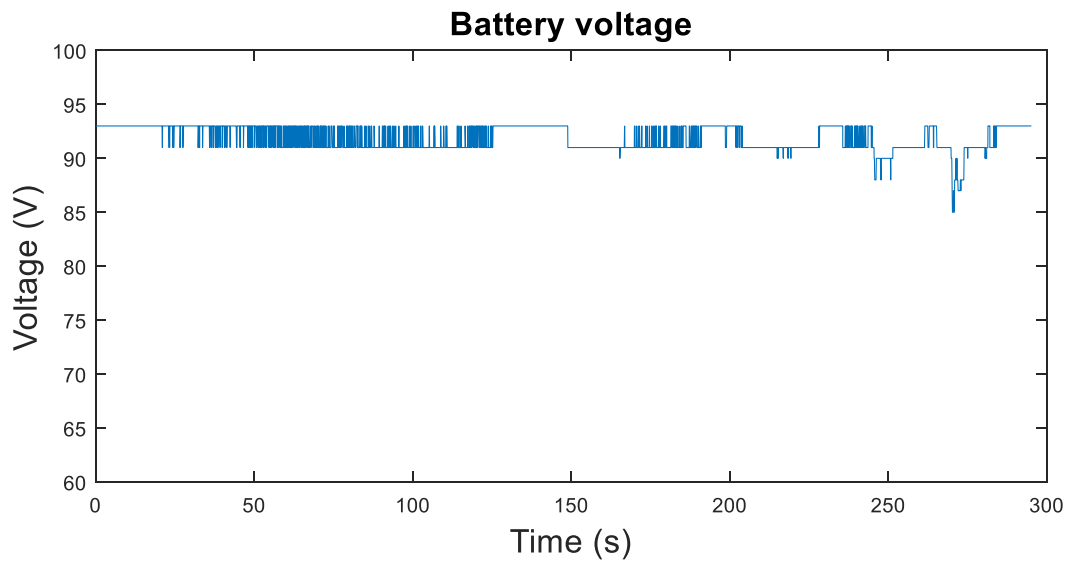
Figure 49 Battery voltage as seen by the lifting movement SEVCON controller

Figure 50 shows both the system input (motor) power, as well as the achieved physical output.
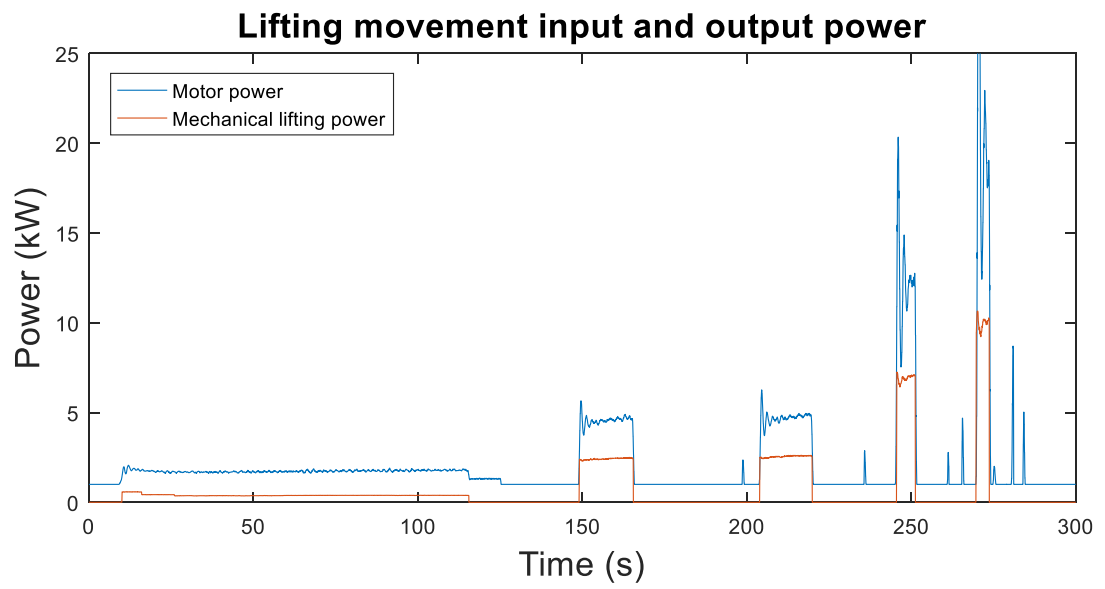
Figure 50 Lifting movement input and output power.

7 Analysis

This section demonstrates the equations used in calculations.
Efficiency is defined as the ratio of output power to input power.

$$\eta = \left(\frac{P_{out}}{P_{in}}\right) \cdot 100 \tag{1}$$

Here, the output power is work done by the boom and bucket movements, and input power is the power either produced by the ICE or taken from the battery.

Output power calculations are the same for both the new DDH setup, and the old ICE-powered one. Power can be expressed as a product of velocity and force.

$$P = F \cdot v \tag{2}$$

Force is directly available from load pins installed on the cylinders. Newer data gathered with the simplified cycle includes direct velocity measurement, a feature of the position sensor used. For older data, it can be derived from the raw position measurement:

$$v(t) = \frac{ds}{dt}, \tag{3}$$

where s is the position.

Engine power can be calculated from the product of torque T in Nm and angular speed ω in rad/s.

$$P = \tau \cdot \omega \tag{4}$$

It is advantageous to present the energy expended and regenerated during the cycle directly as joules to better visualize the situation. From the above data, energy can be found with

$$E = P \cdot t \tag{5}$$

7.1 Simplified cycle

Efficiency is calculated with (1) from the input and output power. In figure 51 both the lifting and lowering efficiencies are shown for all three tested loads. The lowering efficiency is calculated in the same manner, except with the lowering power as input and power accepted by the battery as output. The aforementioned velocity measurement quantization noise is visible here in the stationary parts of the cycle and can be ignored.

Figure 51 shows that for the low speed case, the efficiency starts at around 50% for the no load case, the highest value of the measurements for this speed. Regeneration efficiency likewise peaks with no load, reaching 40%. At this speed, increased load causes a loss in efficiency for both lifting and regeneration (lowering), with higher loads reaching progressively lower numbers. At the maximum 2205 kg load, lifting efficiency has dropped to roughly 40% and regeneration to 30-35%. Although they trend similarly, regeneration efficiency behaves differently compared to lifting in that the gap between the no load and 1040 load scenarios is much smaller.

Such a slow speed is not optimal for efficiency. The efficiency curve of the average BLDC motor indicates lower efficiencies at very low RPM, and since the load is at all times borne by the motor, there is a loss of efficiency simply due to the long time spent holding the load against gravity.
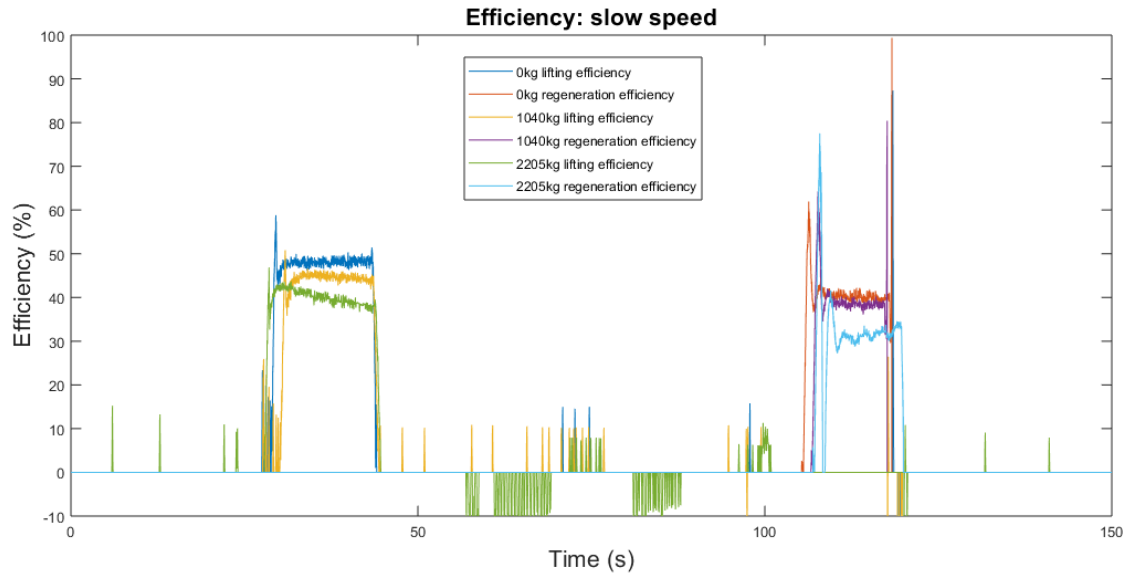
Figure 51 Lifting and lowering efficiency, low speed

Figure 52 shows the net energy taken from the batteries during the cycle. Regeneration lowers the total due to recovering the energy. Completing the cycle at this velocity requires 170 kJ, 82 kJ and 55 kJ respectively for the 2205kg, 1040kg and 0kg load cases.
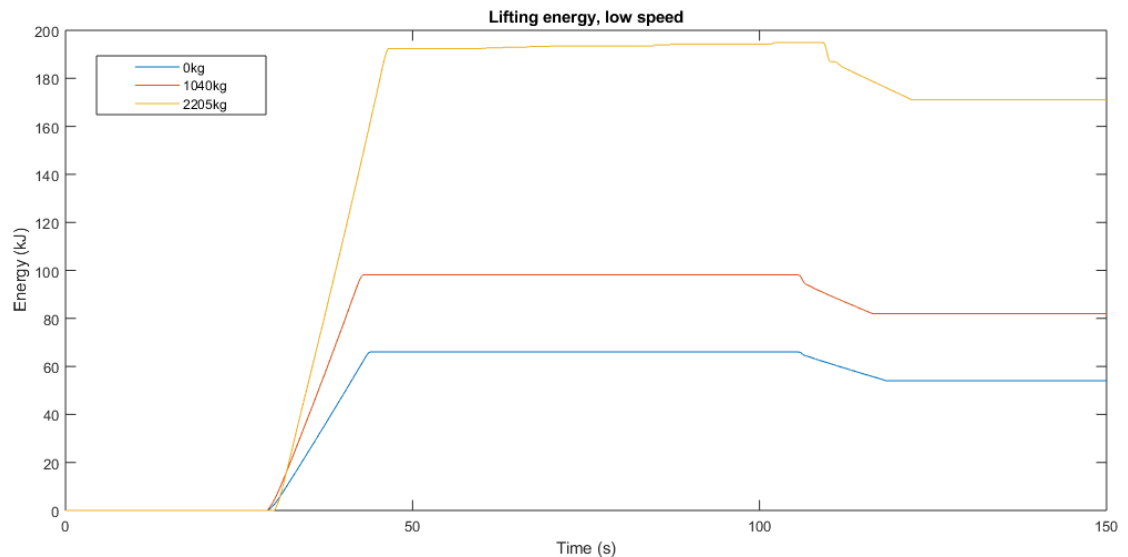
Figure 52 Energy used for lifting and lowering, low speed

It can be seen from figure 53 that at medium velocity, higher lifting efficiencies of 53% are achieved. Furthermore, the addition of load has a minimal impact in this case, with only the heaviest 2205 load suffering a very slight 1-2% loss. The situation with regeneration efficiency is different, the point of peak efficiency has shifted to higher loads. A continuous value of 45% is achieved with the 1040 kg load, followed by 40% with 2205kg and 35% with 0 kg. This is because resistance to movement from friction and hydraulic losses increases with speed, and the force caused by these losses on the lowering boom cylinder is subtracted from the force available for spinning the motor when regenerating. The peak efficiency point to move to higher and higher loads as the speed increases.
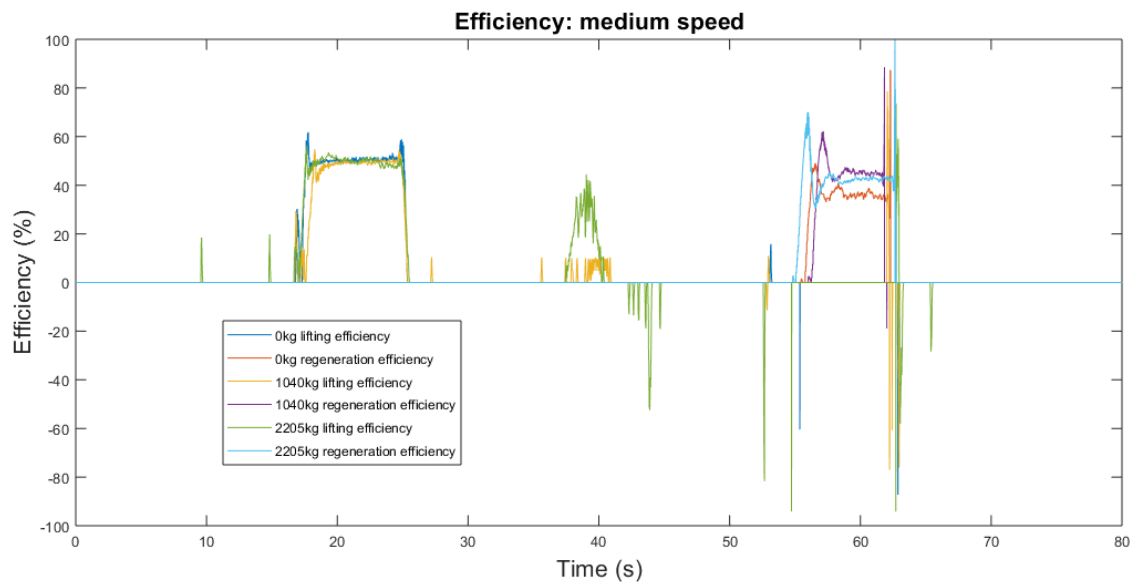
Figure 53 Efficiency, medium speed

Figure 54 illustrates the increase of efficiency, energy required for the cycle at highest load has lowered from 170 kJ to 141kJ. A decrease of 20% in energy requirements was achieved due to slightly higher lifting efficiency and regeneration efficiency. The result is a good illustration on how seemingly small fractional increases in efficiency can result in noticeable energy cost decreases. The total energy for the 1040 kg case has likewise reduced from 82 to 70 kJ, with only the 0 kg load staying the same at 55 kJ. The 0 kg case suffers from less regeneration, which balances out the increased lifting efficiency at this velocity. It is clear that in a machine capable of it, regeneration efficiency plays an important role in the net energy usage. Figure 54 also shows the result of the boom not reaching target position right after the first lift, and the correction later at 40s to reach it. Beyond start-stop transients, this does not affect the energy balance.
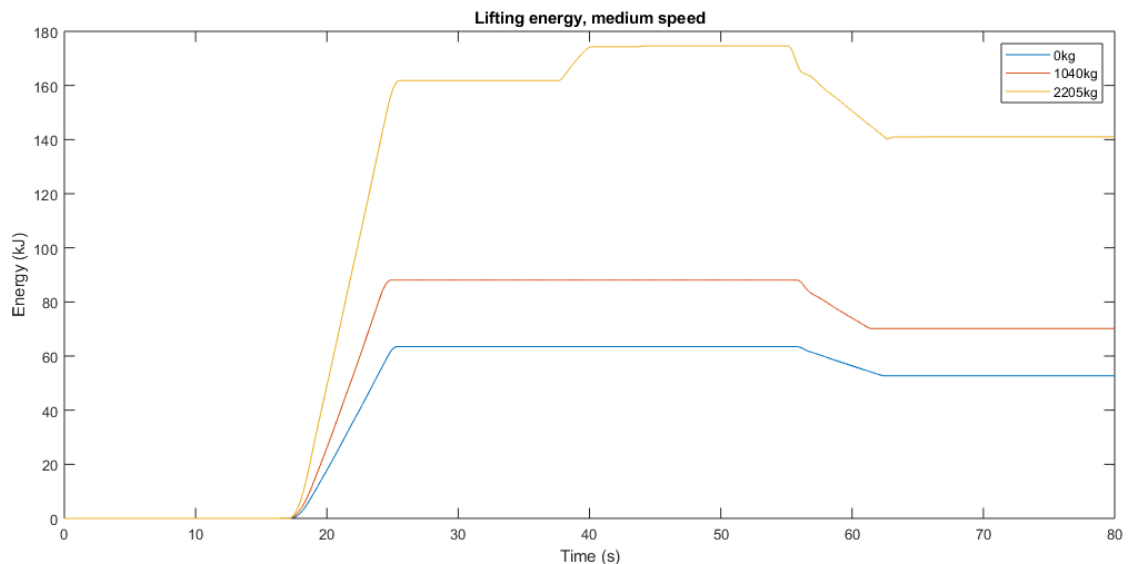
Figure 54 Energy used for lifting and lowering, medium speed

With the high velocity case illustrated in figure 55, lifting efficiency again remains a nearly constant 48%, slightly lower than with the medium velocity case. The lifting time is increased at the highest load due to that case reaching the limits of machine capability, resulting in a lower actual lifting velocity. In a real world working situation, this would

be the likely operating point of the mining loader. As observed in previous results, the peak regeneration efficiency point has shifted further towards higher loads, with the 2205 kg case showing the highest efficiency of ~50%. At lower loads the efficiency is much lower, under 40% for 1040kg and under 20% with 0 kg. Higher lowering velocities simply require more load on the cylinder to overcome losses and generate useful power. It should be noted that the highest regeneration efficiency measured was achieved with this velocity and the highest measured load of 2205 kg.
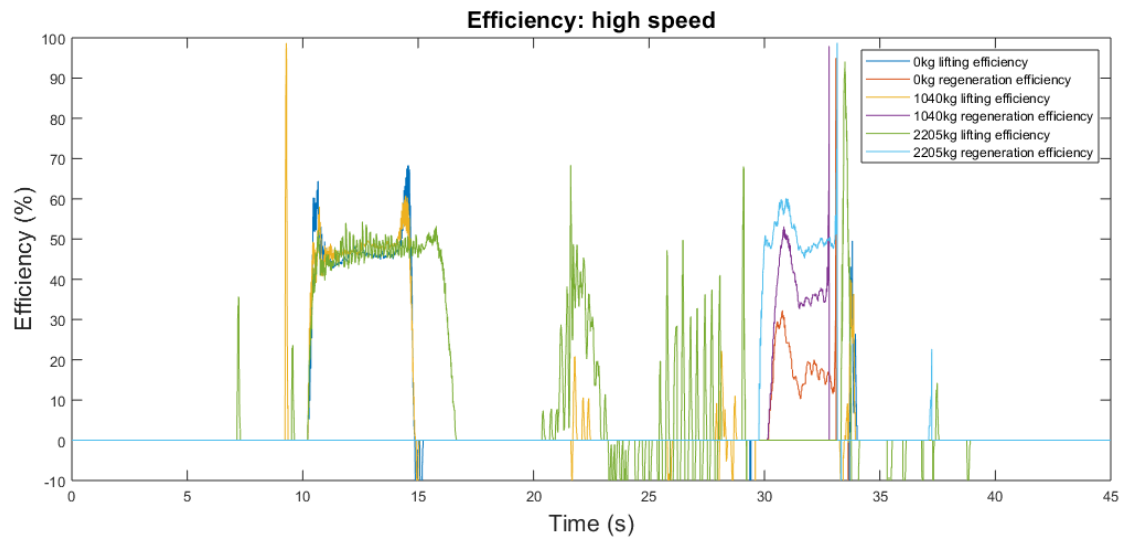
Figure 55 Efficiency, high speed

As seen from figure 56, cycle energy for the 2205 kg load has remained virtually unchanged at 141 kJ. The slight loss of lifting efficiency is compensated by the gain in regeneration efficiency. With the 1040 kg and 0 kg loads, energy requirements have risen to 78 kJ and 66 kJ respectively. It can be said that at the 2205 kg load, both the 3 cm/s and 5 cm/s velocities lie within the machines optimal operating point, due to minimal differences in efficiency around that area. In contrast, the lower loads are seeing a loss in efficiency at this point when compared to the 3 cm/s velocity. This is good behavior with regards to the mining loader case, as they are often operated at maximum achievable lifting velocities.
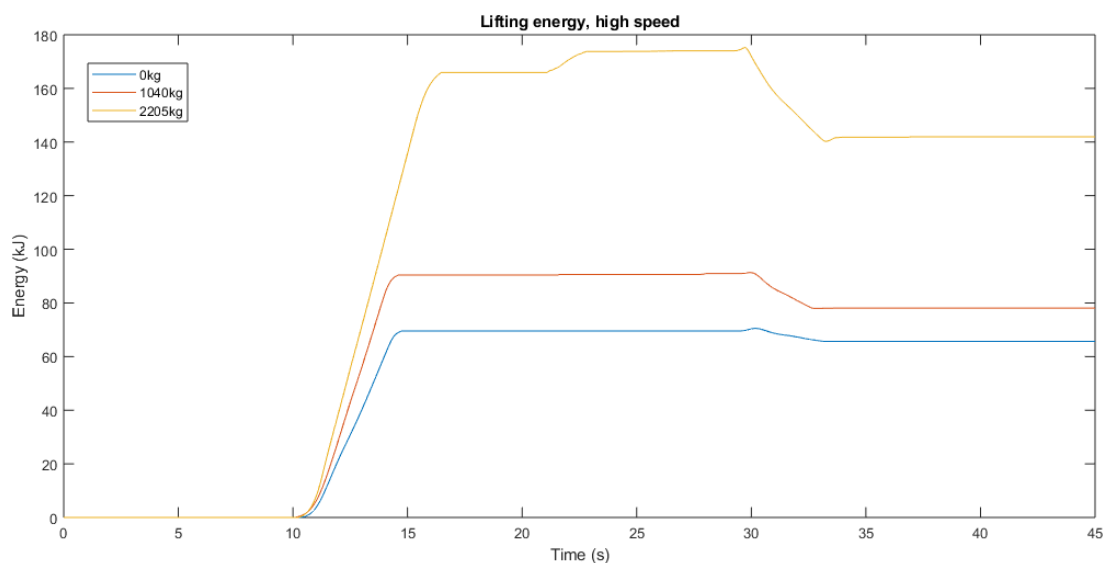
Figure 56 Energy used for lifting and lowering, high speed

There are noticeable differences to previous cases in the highest 8 cm/s speed illustrated in figure 57. Lifting efficiency is noticeably lower at 40% for the 0 kg load case, caused by increased losses at this velocity. Lifting velocity for both the 2205 and 1040 kg loads has saturated as maximum machine power is reached, making the 2205 kg measurement redundant in everything except duration. In both of these saturated cases lifting efficiency is maintained at or slightly below 50%, with the lower load simply reaching a higher lifting velocity. Regeneration at this speed is limited, with the 0 kg load achieving effectively no regeneration. 1040 kg load regeneration has dropped to roughly 20%. Curiously, the 2205 kg load shows poor regeneration as well. This is an unexpected result, as there should be more energy available for regeneration after subtracting movement-related losses.
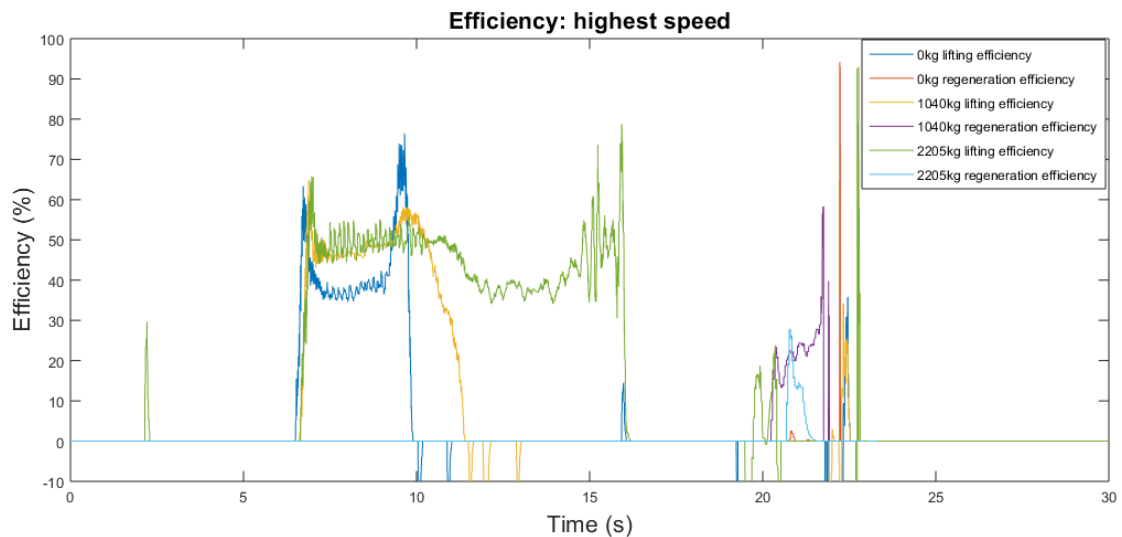
Figure 57 Efficiency, highest speed

As seen in figure 58, lack of regeneration combined with lower lifting efficiency raises the energy costs for the 2205 kg load to 200 kJ. At 1040 kg and 0 kg the energy costs are similar at ~82-85 kJ. The lack of regeneration is clearly visible.
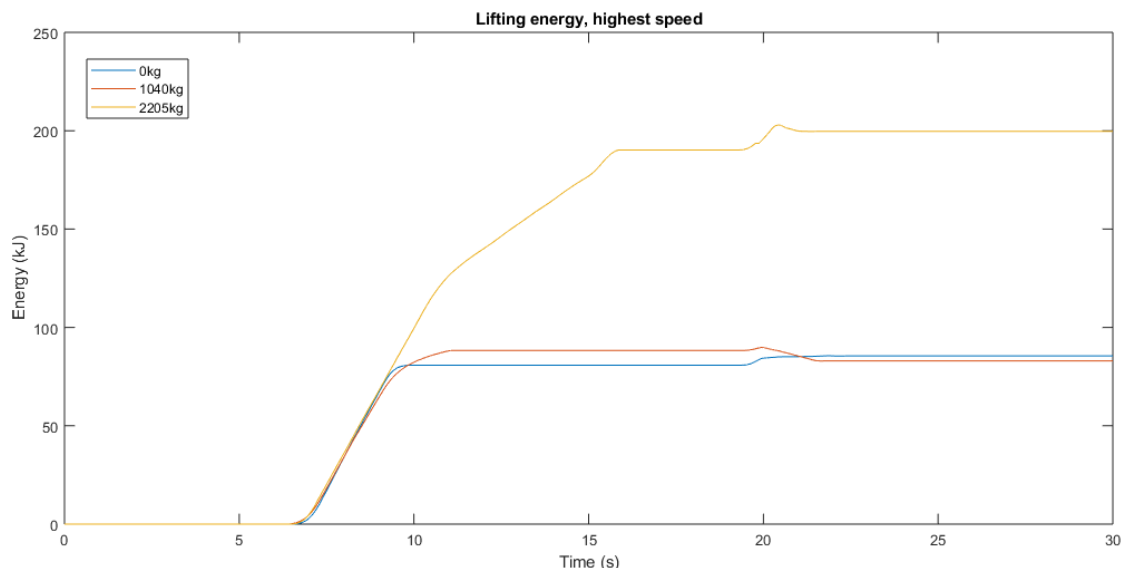
Figure 58 Energy used for lifting and lowering, highest speed

The results suggest an optimal operating point between 3 and 5 cm/s when loaded. The DDH setup maintains a good efficiency up to maximum achievable speed with load, with fast unloaded movements and slow movements in general resulting in somewhat lower efficiencies. Even then, the difference is low, around 5%. Regeneration has a lower

50

optimal operating point, which is strongly dependent on the load. Higher loads require higher speeds to achieve good regeneration, with significant losses at high speed and low load as well as low speed, high load ones. This trend does have its limits, at maximum load and speed regeneration begins to suffer again.

7.2 Original test cycle

Results from this measurement are split in two categories: work done by boom movement, and power input to the system. Data from the conventional load sensing setup is presented first in 7.2.1, followed by the DDH setup in 7.2.2.

7.2.1 Load sensing setup

It is required to derive speed from the movement's position in order to find its power. Simple derivation is not enough however, as the measurement is too noisy. By using a Chebyshev II 8th order lowpass filter with a stopband edge frequency of 7 rad/s and stopband attenuation of 40 dB (Matlab implementation), it is possible to arrive at a much better result as illustrated in figure 59.
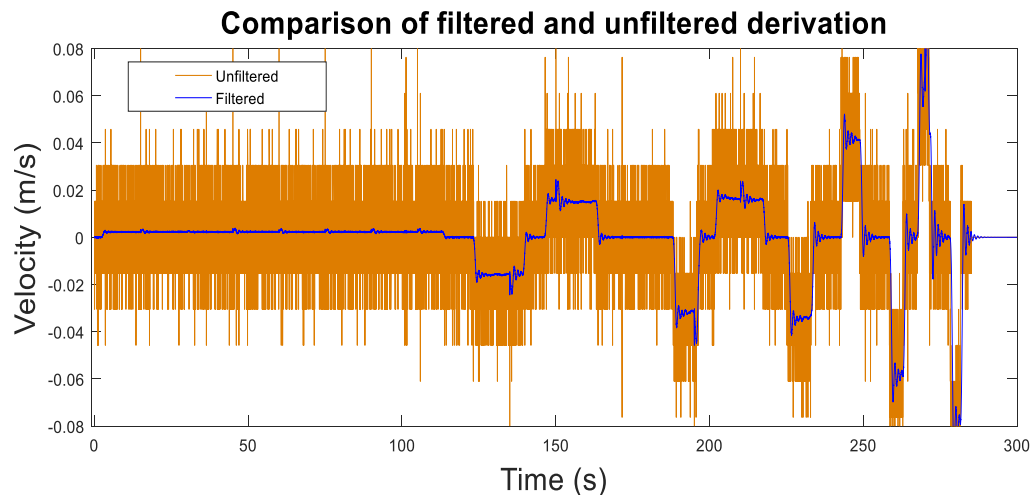
Figure 59 Derivation of boom velocity from its position, filtered and unfiltered

This approach has several drawbacks, though. The filtering introduces artifacts such as delays and overshoot, which are not present in the data. As the intention is to calculate power with respect to time, the delays especially are harmful. By shifting quick changes in speed away from the corresponding engine power spike, the result gets distorted. While these issues could be mitigated by applying the exact same filter to the power data, an easier and more accurate solution is available.

Since the test cycle only includes constant speed movements with very quick accelerations and decelerations, it is possible to fit a curve on the measurement consisting only of straight lines. Since the curve is completely smooth, deriving it causes no problems. Such a curve was constructed in Matlab Simulink's signal generator, and the error between this approximation and the real measurement is as shown in in figure 60. The actual measured cycle corresponds well to the fitted curve, reaching a maximum error of 10 mm only briefly.
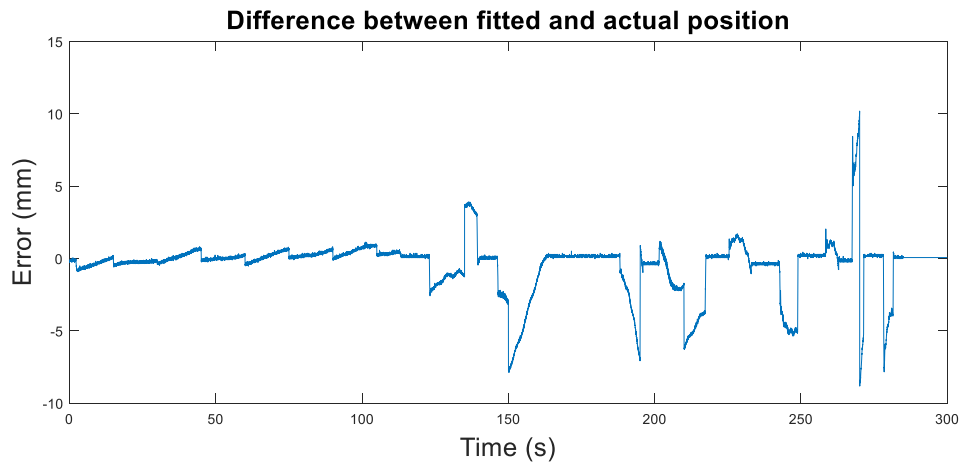
Figure 60 Position difference between actual measurement values and the fitted curve

It can be seen from figure 61 that the derived velocity is far smoother.
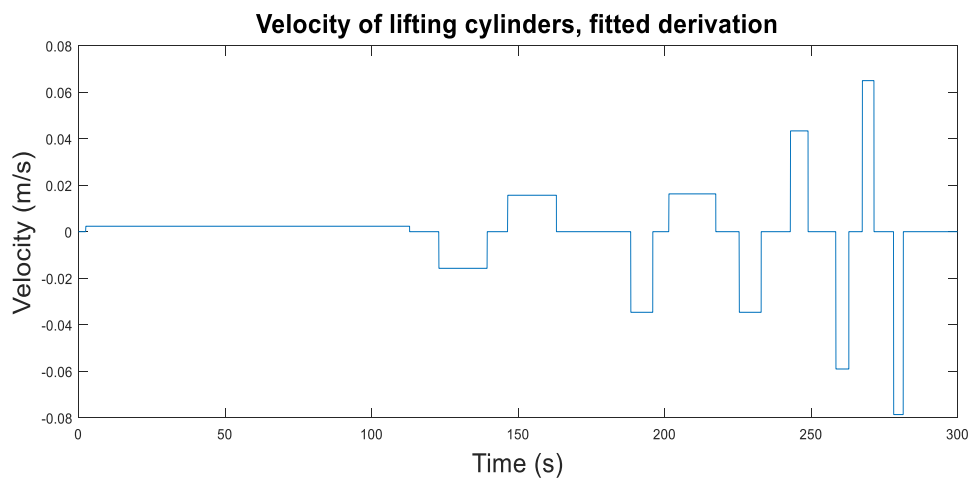
Figure 61 Velocity as derived from the fitted position curve

This simplification assumes instant accelerations and constant velocity during movement, and by looking closer at the position graph, it seems to be a reasonable assumption. Figure 62 shows a detail from the position measurement.
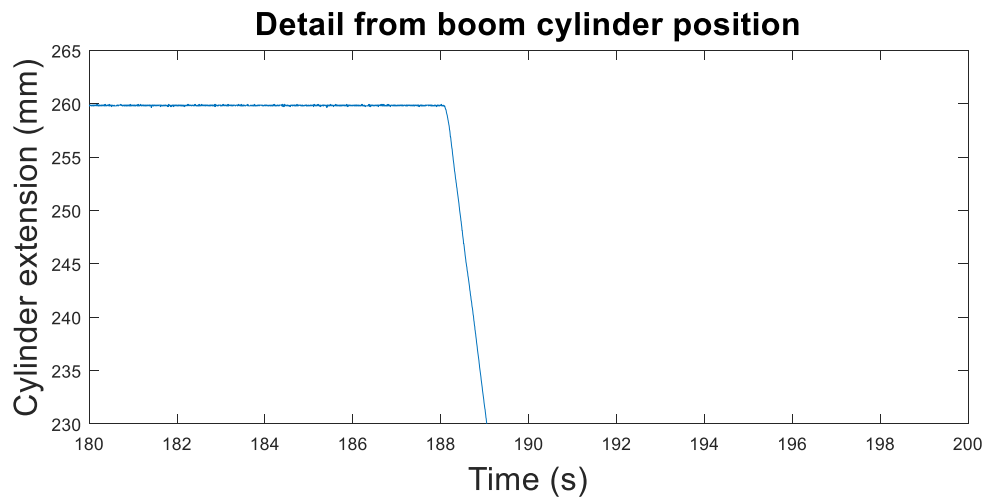
Figure 62 Detail from the boom cylinder position graph, showing a typical quick acceleration and stable velocity from Figure 43

52

Efficiency during the cycle is simply the output power divided by input power calculated with (1) and illustrated in figure 63.
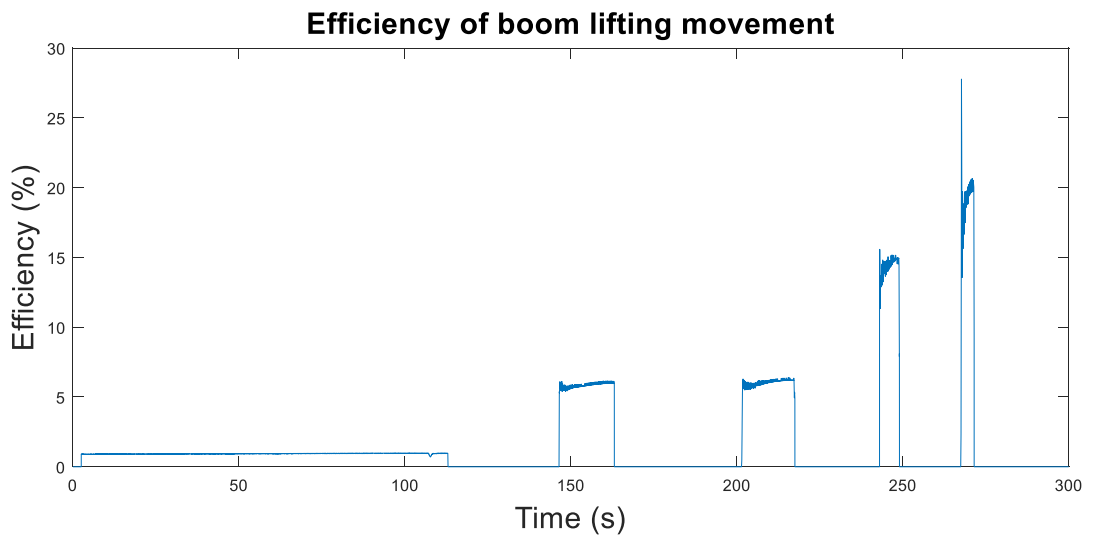
Figure 63 Efficiency during cycle

A clear trend is that the efficiency of the conventional cycle correlates positively with the cycle's speed. This is a result from the load sensing hydraulic system, which is not able to ramp down to very low power levels. Since the engine is always running, and wasting power, the percentage of power going to the actual movement improves with higher power levels.

During this cycle, the highest efficiency recorded was ~20% from the engine to lifting power. Running the cycle with higher load, maximum recorded efficiency reached ~40% with the fastest movement.

The wasted power here comes from how the load sensing system is set up. The variable displacement pump appears to have some minimum displacement, since even at zero actual load, ~35 kW engine power is required to keep the pump and accessories running. Since the engine maintains full speed during work, power loss is not reduced by simply running the pump slower.

With the DDH setup, much higher efficiencies were reached. After the slow initial lift, the efficiency reaches approximately 53%, and stays roughly constant with increasing speed. This is consistent with an electric motor with a fairly constant efficiency across much of its operating range mounted in a direct drive configuration. At the very low speed of 2 mm/sec during the initial lift, hydraulic leakage along with reduced controller and motor performance impact the efficiency negatively, lowering it to around 21%

The measurements from the DDH system are quite noisy, however. This is attributable to the modified PID-control used, which is tuned very aggressively to closely approximate the original testing cycle, becoming prone to micro-oscillations. The controller must contend with delays mainly caused by the motor controller's response time, starting performance and stick-slip movement, which lower its performance. Along with the noisy voltage sensor, this is the main source of error in these measurements.

7.2.2 DDH setup

Calculating efficiency with (1) yields Fig. 64. With the DDH setup, much higher efficiencies were reached. After the slow initial lift, the efficiency reaches approximately 53%, and stays roughly constant with increasing speed. This is consistent with an electric motor with a constant efficiency across much of its operating range mounted in a direct drive configuration. At the very low speed of 0.002m/sec during the initial lift, hydraulic leakage along with reduced controller and motor performance impact the efficiency negatively, lowering it to around 21%
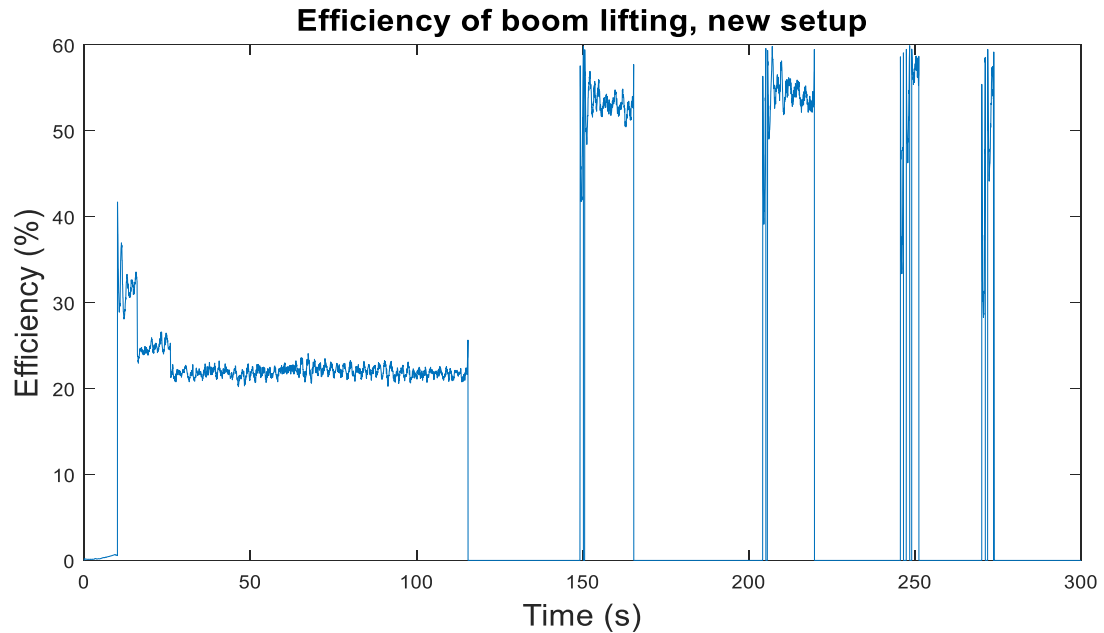
Figure 64 Boom lifting efficiency,   DDH setup

Due to aforementioned reasons, the starting velocity of the slowest 0.002 m/s movement is somewhat higher than the reference. This shows up as a noticeably higher efficiency of 37% in the beginning, dropping to 21% after the movement slows down. The DDH system is shown to have velocity dependent efficiency in this cycle, but only at the extremely low end of the speed range.

The following section presents an estimate for the economic feasibility of putting the described system into practical use.

8 Economic considerations

For any new technology to be commercially adopted, there must be a financial incentive to do so whether through direct savings or savings through lower long term operational costs. Currently, the specialized electrical equipment required by a hybrid working machine are more expensive than their analogues in conventional machines. While some of these components, especially batteries driven by increasing demand and maturing technology [48] are rapidly becoming more economical, a hybrid machine does come with higher upfront costs than a conventional one. Therefore, the financial appeal of such a machine depends on its ability to pay back the difference of purchase price through savings from operational costs.

8.1 Time to return of investment

A return of investment (ROI) analysis takes into account the difference of purchase price and through estimating operating cost savings, gives an indication of when the product has paid for itself and starts generating profit when compared to the conventional option. A lower ROI time is clearly better, as it allows the company to reap benefits from its investment sooner, and often significantly affects whether the investment is made in the first place. In this case, a hybrid mining loader with DDH is compared against its conventional counterpart with the intention of estimating how long it takes for the technology to pay for itself.

8.2 Sources of uncertainty

This analysis is an estimate with two main sources of uncertainty. Firstly, several values used in the calculations are estimates or not directly comparable. As a one-off prototype, the DDH mining loader does not benefit from economies from scale as serially produced machines do. In addition, it is not optimized for cost savings. Conversely, the price of those parts made in house at the university will be lower than a comparable industrial ones, as profit margins and work cost are not included.

Secondly, the exact lifetime and maintenance costs of these machines are not commonly available, as mining companies have not published this internal data. There exist estimated breakdowns for usage costs for mining equipment [49] which will be used for these calculations. For fuel consumption there exist measurements from the particular loader this work concerns before its hybrid conversion, but as the conversion has not progressed far enough to complete full working cycles, estimates will draw from simulations of this hybrid machine [50] and other similar hybrid installations [51].

8.3 Calculation method

The two main components of a ROI calculation are the initial cost difference at purchase time, and monthly savings during operation. Since there currently exists in production a very close analogue of the EJC90 used here, the LH204, its purchase price will be the comparison point. The difference of that when compared to the hybrid loader will be obtained by removing the cost of the conventional hydraulic and automotive components replaced from the total cost of the equipment it was replaced by. As proven by this conversion, a viable hybrid mining loader can be built on a standard frame by only

55

changing the relevant components. While not optimal with regards to performance, this construction allows easy cost and performance comparisons with the conventional version.

The basic form of the equation calculating time to full return of investment is

$$t_{ROI} = \frac{C_{hyb} - C_{conv}}{R_{conv} - R_{hyb}} \tag{6}$$

Where
t_{ROI} = Time to return of investment (payback time) in months
C_{hyb} = Capital costs of the hybrid mining loader
C_{conv} = Capital costs of the conventional option
R_{conv} = Monthly running costs of the conventional loader
R_{hyb} = Monthly running costs of the hybrid loader

8.4 Capital costs of conventional loader

This hybrid mining loader prototype was converted from an EJC90 loader. This model is no longer available, meaning there is no current price for it. However, an extremely close analogue in every way is offered by Sandvik, the LH204, which is thus used as the baseline. These loaders have a tramming capacity of 4082 and 4000 kg respectively, and very similar weights and dimensions.

Based on weight, the purchase price (C_{conv}) of a new LH204 is 350 000€.

8.5 Capital costs of hybrid loader

To estimate the capital costs of a hybrid mining loader, any additional equipment used for hybridization is added to the list price of the conventional one, and removed conventional equipment removed from it. For components used in hybridizing the EJC 90 loader, the cost breakdown is shown in table 1.

Table 1 Additional components required for the DDH frontend wrt the original setup

Hybrid case	Component	Price	Quantity
DDH motor	Motenergy me1304	768 €	2
DDH controller	SEVCON Gen4 Size 6	1 173 €	2
Boom pumps	PGL100-008 x2 (set)	1 813 €	1
	PGL100-013+001x1 (set)	1 077 €	1
Bucket pumps	PGL100-016 x2 (set)	1 078,20 €	1
	PGL100-022 x2 (single)	661,70 €	2
Drive motors	1PV5135	1 104 €	2
Inverter	HES880	6 000 €	1
Battery Week 29	Week 29	5 000 €	1
Battery 96v (3x 24v 60ah)	ALTAIRNANO 24V 60Ah	3 000 €	3
Battery management+ 60ah 96v	BMS+CCU + 24v60Ah cell	5 000 €	1
Slew drive	IMO WD-H 0300	3 000 €	1
Slew drive electrics	-	4 000 €	1
Volksvagen genset TDI 2.0 - 475 NE		5 000 €	1
Generator	Siemens	2000	1
	Total	50 382 €	

The conventional components that are no longer needed are listed in table 2.

Table 2 Components that are no longer needed by the DDH frontend (estimate)

Conventional case	Price
Frontend pump	400,00 €
Drive pump	400,00 €
Centerjoint torque motor	2 000,00 €
Deutz 2012 engine	3 000,00 €
Frontend lift motor	400,00 €
Frontend dump motor	400,00 €
Total	6 600,00 €

The net cost for the conversion is therefore 43 782€ This brings the total cost of the hybrid mining loader, C_{hyb}, closer to 400k€ That difference of price between the conventional and hybrid loader is what affects investment recouping time and is used in the following calculations.

8.6 Working cycle used for running cost calculations

The stock configuration of the EJC90 loader was tested in 2009 at an experimental mine in Tampere [52]. This data forms a baseline of performance and efficiency against which the proposed hybrid mining loader is compared. Figure 65 presents a two-dimensional simplification of the path of the loader within the mine, including grade and distance information.
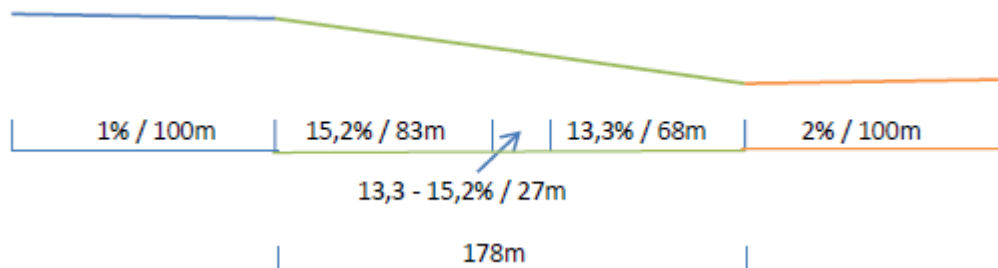
Figure 65 Grades and distances of the working cycle

Figures 66 and 67 show the path from above, with color coding corresponding to the projection of figure 65. This cycle is the "long route" for testing the mining loader underground in [52] and measures a total of 378 m one way.

The terrain is not as uniform as figure 65 might lead to believe, as is often the case in the real world. The HIL simulation model used in [52] uses motor load and engine output, so this should not adversely affect the simulation.

UPPER LEVEL

DUMP
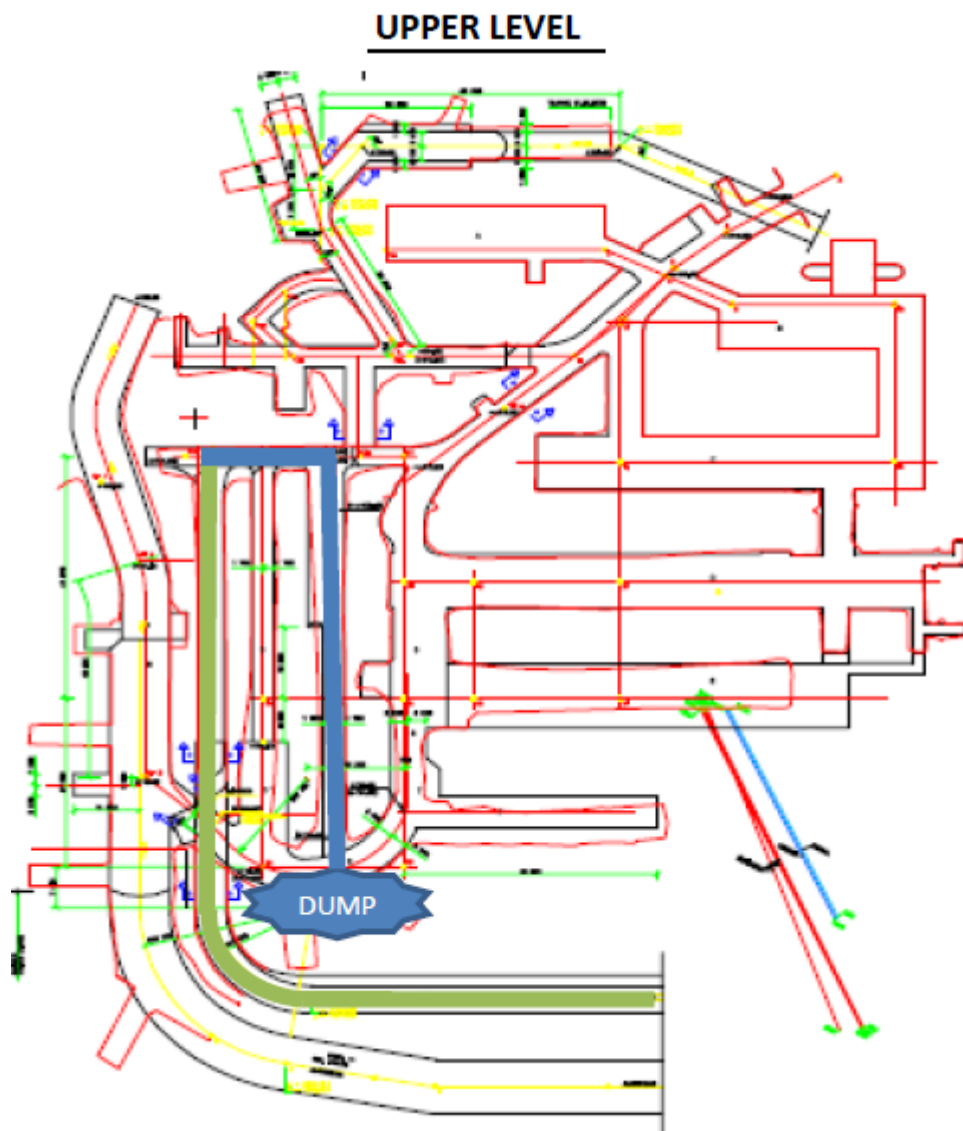
Figure 66 Upper level of research mine, path of the loader colored
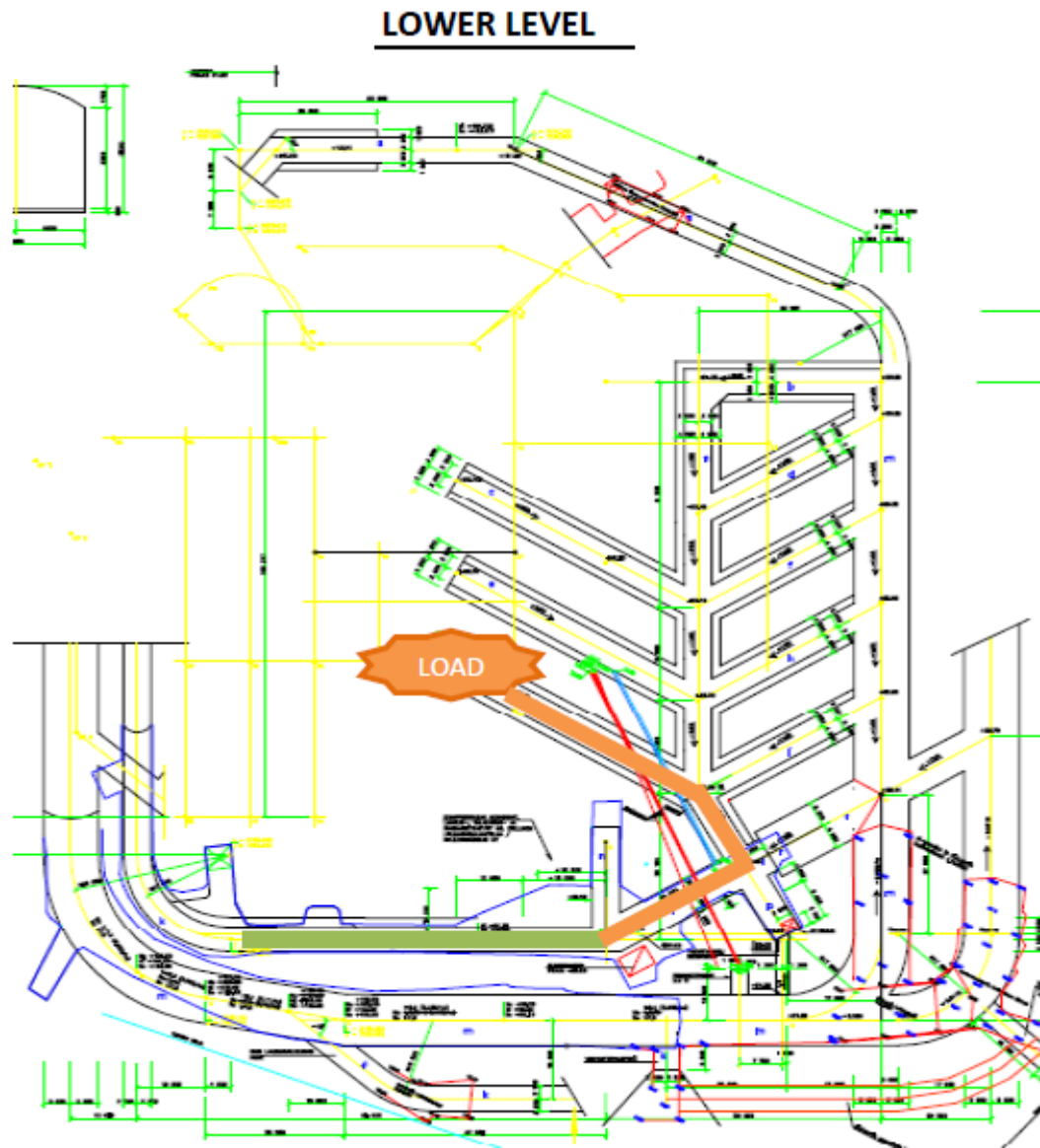
Figure 67 Lower level of the research mine, path of the loader colored

8.7 Monthly running costs of conventional loader

The running costs of a mining loader consist of more than fuel costs. Tires, lube and replacement parts combined with overhaul labor contribute a significant portion of total running costs. These costs are estimated using data from infomine.com, scaled to the size and weight to the EJC 90 as well as the working cycle it was used with. This data, shown in table 3, will not be a perfect fit but does provide a reasonable approximation.

Table 3 Monthly running cost estimate for a 109 000-pound LHD, scaled from Infomine data

2014 $ to € exchange rate		1,33		
Running cost, generic 109k lbs ldr	Raw hourly running costs	In Euro	Wt scaled	Monthly
Overhaul parts	4,83	3,63 €	1,02 €	341,70 €
Overhaul labour	3,9	2,93 €	0,82 €	275,91 €
Maintenance parts	8,97	6,74 €	1,89 €	634,59 €
Maintenance labour	7,25	5,45 €	1,53 €	512,91 €
Diesel fuel	48,12	36,18 €	10,13 €	3 404,30 €
Lube	7,18	5,40 €	1,51 €	507,96 €
Tires	28,02	21,07 €	5,90 €	1 982,31 €
Wear parts	0,74	0,56 €	0,16 €	52,35 €
Total	109,01	81,96 €	22,95 €	7 712,03 €

8.8 Monthly running costs of hybrid loader

Although a hybrid mining loader might facilitate extra methods for running cost reductions in other areas, such as anti-skid controls for reducing tire wear or reduced maintenance needs due to less moving and wearing parts, these are outside the scope of this thesis. According to [52], the simulated hybrid loader uses roughly 50% of the fuel the conventional loader does when performing the working cycle used in testing. The modified running costs based on reduced fuel consumption are found in table 4.

Table 4 Montlhy running costs for a hybrid LHD, based on fuel consumption only

Running cost, hybrid 109k lbs ldr	Raw hourly running costs	In Euro	Wt scaled	Monthly
Overhaul parts	4,83	3,63 €	1,02 €	341,70 €
Overhaul labour	3,9	2,93 €	0,82 €	275,91 €
Maintenance parts	8,97	6,74 €	1,89 €	634,59 €
Maintenance labour	7,25	5,45 €	1,53 €	512,91 €
Diesel fuel	24,06	18,09 €	5,07 €	1 702,15 €
Lube	7,18	5,40 €	1,51 €	507,96 €
Tires	28,02	21,07 €	5,90 €	1 982,31 €
Wear parts	0,74	0,56 €	0,16 €	52,35 €
Total	84,95	63,87 €	17,89 €	6 009,88 €

According to this estimate, monthly running costs decrease 1702€. Calculated with (6), this results in a ROI time of ~25.72 months, approximately 2.1 years. The useful life of a mining loader varies, with reported values ranging from 12000 to 20000 hours depending on maintenance, equipment quality and operator ability. The source includes comments on these being traditional values that are expected to be exceeded with modern machinery with advanced diagnostics. Depending on the way the loader is used, yearly utilization can range from 3500 to 6000 hours, giving a lifetime range from 2 to 5.7 years [12]. It should be noted that the Infomine source [49] does not specify loader utilization, therefore a direct comparison is impossible. Nevertheless, most of the cost accrues from sources linked to running hours and not calendar life (such as fuel, tires and maintenance), thus giving roughly equivalent benefits regardless of how hard the LHD is run. Due to the difficulty of finding first-hand information on vehicle running costs and lifetimes the range of best and worst-case scenarios suggests the presented hybrid LHD is economically viable, but not in all use cases.

9 Discussion

The presented DDH setup was able to achieve a higher efficiency than the conventional load sensing setup with all measured loads and velocities. Notably, the lifting efficiency of the DDH setup was nearly constant across all loads and all but the very slowest speeds, contrasting with the strongly load-dependent efficiency of the conventional setup. Highlights include a twentyfold efficiency difference of 1% vs 21% in favor of DDH at the lowest measured speed, with the gap closing to ~20% vs 53% with higher loads and velocities. This is disregarding the potential for energy regeneration during lowering, capable of recovering ~20-50% of the potential energy. Regeneration is an important benefit of DDH technology, however it was intentionally left outside the raw lifting efficiency comparisons due to it being not representative of the work the DDH units do as installed on a mining loader due to limited operation of a fully loaded bucket. Nevertheless, it is an advantage completely absent in the load sensing system it replaces and can be a highly useful addition to any number of different DDH applications. For example, the many emerging swing energy recovery systems for excavators could also be implemented with DDH. The strongest argument for DDH this research provides is that it comfortably exceeded the conventional system in efficiency with all operating regimes, even with conservative estimates without regeneration. Any system which achieves this without compromise in power, working ability or usability shows considerable promise. The value proposition of DDH as proposed in this work therefore hinges on the economic side, weighing these advantages against the increased equipment up-front cost.

The mining loader test case proved to be a rather good fit for DDH technology. All of the efficiency improvements were achieved without negatively affecting lifting capacity or speed. Operator feel in manual mode was good, and the machine was capable of sub-centimeter bucket positioning accuracy, more than enough for the intended work. It is the author's belief that this prototype, when completed, will prove up to the task of real world work. The biggest drawback, or rather an unused opportunity, is the regeneration ability. The electric drive used in DDH is intrinsically capable of regeneration without any additional components or software. The same technology could provide greater benefits applied to a system that lends itself better to regeneration, such as the traction drive of the loader. In that case, regeneration could be used to recoup energy on the nearly ubiquitous downhill section of the working cycle.

There are issues requiring future attention with the prototype DDH units, which are detailed here. The most significant of these is the disposal of motor waste heat. Due to the high efficiency, the DDH units do not generate as much heat as a conventional hydraulic system of same capacity, and thus were able to operate some time without any active cooling. For extended work, the units were provisioned with water cooling by means of an integrated cooling jacket in the motors. This proved to be thermally weakly coupled to the motor's coils, allowing only for a slight reduction of operating temperature even with a strong flow of cool water from an external source. For heavy-duty work, a motor with better thermal characteristics will be required. A smaller issue was the control performance of the SEVCON motor controller. The simple PID controller provided is not up to the task of handling the stick-slip effect, highly variable load and non-linear response caused by the boom and bucket geometry. Implementing more advanced control outside the SEVCON is tricky due to the non-real-time nature of CAN communications. While this will be of no concern in the standard mining loader application with open-loop human operated controls, any automation application should take this in account.

A notable limitation of this research was the comparative lack of data on the conventional load sensing system originally installed in the loader. While a good set of thorough

measurements was available, these could not be replicated or adapted to this particular research due to the machine in its original configuration no longer existing. The greatest drawback was a lack of directly comparable data at higher loads. All such measurements were from the real working cycle of a mining loader, and thus included prodigious use of the traction and center joint motors. Since there is only a single point of system power input measurement (the engine) and no way to determine the power split between traction, boom and the bucket, these measurements could not be used.

There is uncertainty in the conventional hydraulic component valuations, since these are sold business-to-business and are challenging to find accurate estimations for. The same applies for mining loader operating costs, for which a good source was found but required some extrapolation to account for different machine size. Nevertheless, the values chosen should be significantly on the conservative side, especially regarding conventional hydraulic components. These are standard components bought in bulk, for a significantly lower price than the often customized single units used for this research.

The control system created as part of this work, beyond its role as a simple machine operating interface and data gathering tool, had a few notable advantages and disadvantages. The prototype mining loader incorporates a large number of CAN devices, which are split between separate CAN buses with different protocols (J1939 and CANopen) and bitrates. Putting the control and diagnostics of all these on a single screen proved invaluable in the commissioning of the system, after which the automatic initialization, configuration and error handling on both device and bus level was extremely useful.

A disadvantage was the use of a simple PID controller for controlling the boom and bucket movements. This was not optimal due to the various nonlinearities and delays present in the system. Even though this controller was modified with a simple velocity dependent adaptive P-factor that improved the control performance, there still were cases where the controller was insufficient. A more advanced controller, such as fuzzy PID implemented in [53] or a model predictive controller can improve this.

9.1 Future outlook

Electrification of mining equipment and other heavy machinery is on the rise. Whether it takes the form of pure battery-electric vehicles, hybrids, trolley line, umbilical power or other, this new generation of vehicles will use electricity to drive actuators and traction motors. This presents a favorable environment for DDH adoption. Such vehicles by definition have a powerful source of electricity available, negating much of the additional cost of implementing such for DDH only. In every case except umbilical and trolley power, efficiency is paramount in order to maintain good range and autonomy, incentivizing the use of high efficiency options such as DDH. Using pure electric actuators in heavy machines to solve the same problems is troublesome due to the shock loads encountered, a problem that is also solved by DDH systems.

Modern motor controllers allow for highly precise and fast control of the PMSM/BLDC motors, as seen in their use in demanding applications such as camera stabilization gimbals, multicopters and self-balancing robots. This ability could theoretically extend the DDH use case to servo hydraulics such as vehicular power steering, an application that traditionally has had difficulties balancing the feel of hydraulics and efficiency of electrics.

The broader trend for higher efficiency in machinery is undeniable, with the driving economic, political and environmental causes unlikely to abate.

10 Conclusions

This work demonstrated that DDH can replace conventional mining loader front end hydraulics, providing notably higher efficiency without compromise in working ability or operator feel. Lifting efficiency was found to reach its highest value of 50-53% at cylinder speeds from 3 to 5 cm/s, corresponding to boom lifting time of 5 to 8 seconds. This includes those cases when the power limits of the machine are reached with high loads. Such behavior is a good fit for the mining loader case, as the loaders often operate near to or at their maximum power, where the DDH units achieve their good efficiencies.

A distinguishing feature of the DDH system is the flat efficiency curve. At cylinder extension speeds ranging from 1.5 to 8 cm/s, reaching maximum attainable pump RPM, the efficiency variation was only 13 percentage points (40-53%), most of which at the very edges of the operating envelope. Discounting the outlier of the high speed unloaded movement, this drops to only 4 percentage points. The wide range of efficient operating points makes DDH a good choice for dynamic applications that encounter diverse operating conditions and allows for easier design optimization for more single purpose applications.

The proposed system is economically viable. The estimated difference between purchase prices of a conventional and hybridized LHD is 43 782€, which with monthly operating costs 1 702€ lower results in a return of investment time of 2.1 years. LHD's in most cases have working lives longer than this, making the hybrid LHD a valid investment. It should be noted that this is a fairly pessimistic evaluation valid only mines which do not directly benefit from a reduction of ICE exhaust gases. Closed mines with a ventilation-on-demand system will see a faster return of investment time, with every liter of diesel saved is likewise saved from ventilation costs, which tend towards 40% of total mine operating costs. In addition, electric machinery in LHD's is cheaper to maintain, whereas the ROI estimate assumes identical maintenance costs. Therefore, the DDH equipped hybrid mining loader is likely even more attractive than this estimate indicates.

References

[1] Explaining road transport emissions, European emissions agency, 31 p. ISBN 978-92-9213-723-6

[2] EUR-Lex, Commission Regulation (EU) 2017/1151 of 1 June 2017 (Light passenger and commercial vehicles).
https://eur-lex.europa.eu/eli/reg/2017/1151/oj. Visited on 23.11.2018

[3] The 13th five-year plan or economic and social development of the People's Republic of China.
http://en.ndrc.gov.cn/newsrelease/201612/P020161207645765233498.pdf. Visited on 23.11.2018

[4] Comparative study on the differences between the EU and US legislation on emissions in the automotive sector. Directorate-General for Internal Policies of the Union, 2017. 100 p. ISBN 978-92-846-0330-5

[5] Natalia Szymlet, Piotr Lijewski, Paweł Fuć, Barbara Sokolnicka, Maciej Siedlecki. Comparative analysis of passenger car and non-road machinery specific emission in real operating conditions. 2018 International Interdisciplinary PhD Workshop (IIPhDW), 2018. DOI: 10.1109/IIPHDW.2018.8388362

[6] Hitachi ZH210LC-5 capacitor electric hybrid excavator.
https://hitachicm.com.au/products/excavators/medium-excavators/zh210lc-5. Visited on 24.11.2018

[7] Cat 366E H hydraulic hybrid excavator.
https://www.cat.com/en_AU/articles/solutions/gci/get-the-facts-onthenewcathybridexcavator.html. Visited on 24.11.2018

[8] Sandvik DD422iE electric mining jumbo.
https://www.rocktechnology.sandvik/globalassets/products/underground-drill-rigs-and-bolters/pdf/dd422ie-brochure-english.pdf. Visited on 24.11.2018

[9] Volvo EX2 electric excavator. https://www.scimag.news/en/2018/02/21/volvo-ex2-the-fully-electric-excavator-wins-intermat-innovation-awards/. Visited on 24.11.2018

[10] Euler De Souza. Cost saving strategies in mine ventilation. CIM Journal, Vol. 9, No. 2, 2018, 2018. The Robert M. Buchan Department of Mining, Queen's University. Kingston, Ontario, Canada. DOI: 10.15834/cimj.2018.9

[11] Wisam Farjow, Mohamed Daoud, X. N. Fernando. Advanced diagnostic system with ventilation on demand. 34th IEEE Sarnoff Symposium, 2011. DOI: 10.1109/SARNOF.2011.5876449

[12] Jack de la Vergne. Hard rock miner's handbook, p. 174. ISBN: 0-9687006-1-6

[13] EUR-Lex, Commission Regulation (EU) of 18 May 2018 (Non-road mobile machinery). https://eur-lex.europa.eu/eli/reg_del/2018/989/oj. Visited on 24.11.2018

[14] EPA Emission Standards for Nonroad Engines and Vehicles, Nonroad Compression-Ignition Engines: Exhaust Emission Standards. http://nepis.epa.gov/Exe/ZyPDF.cgi?Dockey=P100OA05.pdf. Visited on 24.11.2018

[15] Yong Jiang, Jianguo Li, Zhi Jiang, Ou Wang, Simulation and analysis of obstacle control strategy for electric driven seabed mining vehicle. 2017 Chinese Automation Congress (CAC). DOI: 10.1109/CAC.2017.8243157

[16] Jacek Paraszczak, Kostas Fytas, Marcel Laflamme, Feasibility of Using Electric Trucks in Deep Metal Mines. Departement of Mining, Metallurgical and Materials Engineering, Université Laval, Quebec City, Canada, 2014. DOI: https://doi.org/10.1007/978-3-319-02678-7_122

[17] Metin Özdoğan, Hakkı Özdoğan, Diesel-Electric Mining Loaders - A Case Study. 25th Turkish Mining Congress, April 2015 Antalya, At Antalya, 2015. DOI: 10.13140/RG.2.1.4714.4728

[18] Jacek Paraszczak1, Erik Svedlund, Kostas Fytas, Marcel Laflamme, Electrification of Loaders and Trucks – A Step Towards More Sustainable Underground Mining. International Conference on Renewable Energies and Power Quality, Cordoba, 8th to 10th April, 2014. ISSN 2172-038 X, No.12

[19] D. Jannuzzi, Use of Supercapacitors, Fuel cells and Electrochemical Batteries for Electric Road Vehicles: A Control Strategy. The 33rd Annual Conference of the IEEE Industrial Electronics Society (IECON) Nov. 5-8, 2007, Taipei, Taiwan. DOI: 10.1109/IECON.2007.4460412

[20] William Jacobs, Thomas Bräunl, Melinda Hodkiewicz, Electric LHDs in Underground Hard Rock Mining: A Cost/Benefit Analysis. School of Mechanical and Chemical Engineering University of Western Australia, 2013.

[21] Vladimir Radev, Simmons-Rand Company. United States patent 5,163,537. Battery charging system for electric battery powered vehicles, 1992.

[22] Björn Nykvist, Måns Nilsson, Rapidly falling costs of battery packs for electric vehicles. Nature Climate Change, 2015. DOI: 10.1038/NCLIMATE2564

[23] Artisan vehicles Z40, https://www.artisanvehicles.com/z40/. Visited on 24.11.2018

[24] Li Li, Jing Ge, Renjie Chen, Feng Wua, Shi Chen, Xiaoxiao Zhang, Environmental friendly leaching reagent for cobalt and lithium recovery from spent lithium-ion batteries. Waste Management, volume 30, issue 12, December 2010, Pages 2615-262. DOI: https://doi.org/10.1016/j.wasman.2010.08.008

[25] Duncan Kushnir, Björn A.Sandén, The time dimension and lithium resource constraints for electric vehicles. Resources Policy, volume 37, issue 1, March 2012, Pages 93-103. DOI: https://doi.org/10.1016/j.resourpol.2011.11.003

[26] Linda Gaines, The future of automotive lithium-ion battery recycling: Charting a sustainable course. Sustainable Materials and Technologies, volumes 1–2, December 2014, Pages 2-7. DOI: https://doi.org/10.1016/j.susmat.2014.10.001

[27] RHD-Scharf Muckmaster 600EB electric LHD.
http://www.rdhminingequipment.com/wp-content/uploads/2018/08/MM600EB-Muckmaster-Evolution-Battery-LHD-2018.pdf. Visited on 24.11.2018

[28] Artisan vehicles A10 electric LHD. https://www.artisanvehicles.com/a10/. Visited on 24.11.2018

[29] Artisan vehicles A4 electric LHD. https://www.artisanvehicles.com/a4/. Visited on 24.11.2018

[30] Atlas Copco Scooptram ST7 electric LHD. https://www.epiroc.com/en-fi/products/loaders-and-trucks/electric-loaders/scooptram-st7-battery. Visited on 24.11.2018

[31] RHD-Scharf Haulmaster 800 electric truck.
https://www.rdhscharf.com/product/haulmaster-800-26-30-35-40/. Visited on 24.11.2018

[32] Volvo HX2 autonomous electric load carrier.
https://www.volvoce.com/united-states/en-us/about-us/news/2017/volvo-ce-unveils-the-next-generation-of-its-electric-load-carrier-concept/. Visited on 24.11.2018

[33] Electric truck haulage in north America. http://www.womp-int.com/story/2009vol09/story027.htm. Visited on 24.11.2018

[34] Dave Willick, ABB Inc. Underground Electric Haulage Trucks Introduction and Benefits. 16th Annual MDEC Conference – Toronto, Ontario Canada, 2010.

[35] Hitachi EH5000AC-3 mining truck with trolley option.
https://www.hitachiconstruction.com/wp-content/uploads/2016/10/DKE5000HT_16-10.pdf. Visited on 24.11.2018

[36] Kiruna brochure, old equipment. http://static.ito-germany.de/docs/datenblatt/Used-Kiruna-Dumper-Tunneldumper-gebraucht-tunneling.pdf Visited on 24.11.2018

[37] Atlas Copco EMT-50 trolley electric truck.
http://www.miningchina.com/uploads/attachment/path/146/Technical_specification_Electric_Minetruck_EMT50_9851_3226_01_tcm818-3525768.pdf. Visited on 24.11.2018

[38] Debdatta Das, Puja Chowdhury, Truong B. N. M, KyoungKwan Ahn, A novel energy recuperation system for hybrid excavator using hybrid actuator. 15th International Conference on Control, Automation and Systems (ICCAS), 2015. DOI: 10.1109/ICCAS.2015.7364681

[39] Antti Lajunen, Improving the Energy Efficiency and Operating Performance of Heavy Vehicles by Powertrain Electrification. Aalto University publication series DOCTORAL DISSERTATIONS, 125/2014. ISSN: 1799-4942

[40] Paula Immonen, Energy efficiency of a diesel-electric mobile working machine. Acta Universitatis Lappeenrantaensis 518, Lappeenranta University of Technology, 2013. ISBN: 978-952-265-414-4

[41] Ehsan Esfahanian, John A. Meech. Hybrid Electric Haulage Trucks for Open Pit Mining. 16th IFAC Symposium on Automation in Mining, Mineral and Metal

Processing, San Diego, California, USA. August 25-28, 2013. DOI: https://doi.org/10.3182/20130825-4-US-2038.00042

[42] Komatsu Joy-22 diesel-electric hybrid mining loader. https://mining.komatsu/product-details/joy-22hd. Visited on 25.11.2018

[43] Olli Matikainen, Hybrid underground loader. 2010 Project Update, MDEC Conference, Oct 2010. http://mdec.ca/2010/S3P1_matikainen.pdf. Visited on 25.11.2018

[44] ALHA5140 Hybrid LHD. http://www.miningmes.com/underground-mining-load-haul-dump-lhd/ALHA5140-Hybrid-LHD.html. Visited on 25.11.2018

[45] Logset 12H GTE Hybrid harvester. https://www.logset.com/fi/harvesterit/logset-12h-gte-hybrid. Visited on 25.11.2018

[46] Komatsu HB205-1 capacitor hybrid excavator. http://www.komatsu.com/ce/products/pdfs/HB205_215LC-1_CEN00450-00.pdf. Visited on 25.11.2018

[47] Tom Sourander, Sensorless position control of direct driven hydraulic actuators. Aalto University School of Engineering, Department of Mechanical Engineering, 2017. http://urn.fi/URN:NBN:fi:aalto-201710307329

[48] Gert Berckmans, Maarten Messagie, Jelle Smekens, Noshin Omar, Lieselot Vanhaverbeke, Joeri Van Mierlo, Cost Projection of State of the Art Lithium-Ion Batteries for Electric Vehicles Up to 2030. MOBI Research Group, Vrije Universiteit Brussel, Pleinlaan 2, 1050 Brussels, Belgium, 2017. DOI: https://doi.org/10.3390/en10091314

[49] InfoMine, Mine cost estimating. Mining Equipment Fleet - 10,000 tonne per day (ore + waste) open pit mine. http://costs.infomine.com/costdatacenter/miningequipmentcosts.aspx. Visited on 25.11.2018

[50] Lasse Laurila, ECV2-LUT / Tubridi –project. Electric Commercial Vehicles – ECV 3. national seminar, 2015. https://ecv-fi-bin.directo.fi/@Bin/5f5ed0d6818dafe08c6df8fac7a900c4/1543182790/application/pdf/212259/07_Laurila_Lasse_ECV_Tubridi_2015_10_08.pdf. Visited on 26.11.2018

[51] Yanbiao Feng, Zuoming Dong, Jue Yang, Rui Cheng, Performance modeling and cost-benefit analysis of hybrid electric mining trucks. 12th IEEE/ASME International Conference on Mechatronic and Embedded Systems and Applications (MESA), 2016. DOI: 10.1109/MESA.2016.7587102

[52] Jarkko Nokka, Energy efficiency analyses of hybrid non-road mobile machinery by real-time virtual prototyping. Acta Universitatis Lappeenrantaensis 785, Lappeenranta University of Technology, 2018 ISBN: 978-952-335-192-9

[53] Tatjana Martinovski, Tom Sourander, Aleksi Turunen, Tatiana Minav, Matti Pietola, Control strategy for a direct driven hydraulics system in the case of a mining loader. 11th International fluid power conference, Aachen, 2018. http://publications.rwth-aachen.de/record/724001/files/724001.pdf. Visited on 26.11.2018